

Diversity of Voltage Activated Calcium Currents
in Identified Olfactory Interneurons

In a u g u r a l - D i s s e r t a t i o n

zur Erlangung des Doktorgrades
der Mathematisch-Naturwissenschaftlichen Fakultät
der Universität zu Köln

vorgelegt von

Andreas Husch

aus Prüm

Köln 2007

Berichterstatter: Prof. Dr. P. Kloppenburg
PD Dr. J. Schmidt

Tag der mündlichen Prüfung: 28.11.2007

Contents

Abbreviations.....	6
Zusammenfassung.....	7
Abstract.....	9
1 Introduction.....	11
1.1 The insect olfactory system.....	11
1.2 Variety of voltage gated calcium channels.....	13
1.3 Objectives of this thesis.....	15
2 Materials & Methods.....	16
2.1 Animals and materials.....	16
2.2 Cell culture.....	17
2.2.1 Cell culture dissection.....	17
2.2.2 Dissociation of olfactory interneurons.....	17
2.3 Intact brain preparation.....	18
2.4 Electrophysiological recordings.....	20
2.4.1 Whole cell patch clamp recordings.....	20
2.4.2 Data aquisition.....	21
2.4.3 Data analysis.....	21
2.5 Odor stimulation.....	23
2.6 Histology.....	25
2.6.1 Whole mount preparation of biocytin filled neurons.....	25
2.6.2 Slice preparation of the stained neurons.....	25
2.6.3 Confocal laser scanning microscopy.....	26

3 Results	27
3.1 Voltage activated calcium currents in vitro and in situ.....	28
3.1.1 Voltage activated inward currents.....	28
3.1.2 Charge carrier.....	31
3.1.3 Calcium currents in vitro.....	33
3.1.4 Inorganic ions as calcium channel blockers.....	35
3.1.5 Calcium currents in situ.....	38
3.2 Identification of different olfactory interneuron types.....	41
3.2.1 Odor responses	43
3.2.2 Uniglomerular projection neurons (uPNs).....	45
3.2.3 Type I local interneurons (type I LNs).....	47
3.2.4 Type II local interneurons (type II LNs).....	49
3.2.5 Comparison between uPNs, type I LNs and type II LNs.....	50
3.3 Voltage activated calcium currents in identified neuron groups.....	53
3.3.1 I/V-relationship of calcium current activation.....	53
3.3.2 Tail current analysis.....	57
3.3.3 Steady state inactivation.....	59
3.3.4 Characterization of calcium currents in type II LN subpopulations.....	62
4 Discussion	71
4.1 Voltage activated calcium currents in vitro and in situ.....	71
4.1.1 General parameters of voltage activated calcium currents.....	72
4.1.2 Rundown during whole cell voltage-clamp recordings	75
4.2 Identification of olfactory interneurons.....	76
4.3 Diversity of voltage activated calcium currents in identified neuron types.....	78
4.3.1 Analysis of calcium currents in identified neurons.....	79
4.3.2 Functional significance of voltage activated calcium currents.....	80
4.4 Diversity of other voltage activated ion currents.....	82
4.5 Conclusions.....	83

List of Figures.....	85
References.....	87
Acknowledgments.....	96
Erklärung.....	98
Teilpublikationen.....	99

Abbreviations

4-AP	4-aminopyridine
AL(s)	antennal lobe(s)
AP(s)	action potential(s)
HVA	high voltage activated
I_A	transient potassium current
I_{Ba}	barium current
I_{Ca}	calcium current
I_h	h-current; activated by hyperpolarization
$I_{K(V)}$	sustained potassium current
$I_{K(Ca)}$	calcium dependent potassium current
I_{max}	maximum current
I_{Na}	sodium current
LN(s)	local interneuron(s)
LVA	low-voltage activated
M-LVA	mid/low-voltage activated
MWRS	Mann-Whitney rank sum
ORN(s)	olfactory receptor neuron(s)
PN(s)	projection neuron(s)
s	slope factor
SD	standard deviation
TEA	tetraethylammonium chlorid
TTX	tetrodotoxin
uPN(s)	uniglomerular projection neuron(s)
$V_{0.5(act)}$	potential at half-maximal activation
$V_{0.5(inact)}$	potential at half-maximal inactivation
VGCC	voltage-gated calcium channel

Zusammenfassung

Innerhalb des Antennallobus (AL) der Insekten projiziert jede Rezeptorzelle zu einem Glomerulus und viele Rezeptorneuronen konvergieren innerhalb jedes Glomerulus, wo sie lokalen Interneuronen (LNs) und (Ausgangs-) Projektionsneuronen (PNs) synaptische Eingänge liefern. Die Verzweigungen der LNs beschränken sich auf den AL. Die Projektionsneurone hingegen projizieren ihre Axone in höherrangige Neuropile des Protocerebrums, einschließlich der Pilzkörper und dem lateralen Lobus des Protocerebrum. Insbesondere Projektionsneurone waren im Fokus intensiver Studien, da sie zahlreiche Funktionen erfüllen und eine Schlüsselrolle im zentralen olfaktorischen Verarbeitungsweg spielen. Im Gegensatz dazu sind die Rolle und funktionellen Eigenschaften der LNs noch unklar. Zum besseren Verständnis der biophysikalischen Parameter, die die olfaktorische Informationsverarbeitung auf zellulärer Ebene vermitteln, wurden spannungsaktivierte Kalziumströme (I_{Ca}) in olfaktorischen Interneuronen des Antennallobus von adulten Schaben wie folgt analysiert: 1) in akut dissoziierten Zellen (in vitro), 2) in einer intakten Hirnpräparation (in situ) und 3) in eindeutig identifizierten und intakten Neuronen.

Die Kombination von *whole cell patch-clamp* Ableitungen in Strom- und Spannungsklemme mit Einzelzellmarkierungen ermöglichte es, uniglomeruläre PNs (uPNs) und LNs verschiedener Untergruppen zu studieren. Anhand ihrer

physiologischen und morphologischen Eigenschaften konnten zwei Hauptgruppen von LNs identifiziert werden, die im Folgenden als Typ I LNs und Typ II LNs bezeichnet werden. Duftstimulation und depolarisierende Strominjektionen lösten in Typ I LNs TTX-sensitive Aktionspotentiale aus. Ableitungen in der Spannungsklemme lösten spannungsaktivierte Natriumströme, transiente und gleichrichtende Kaliumströme und Kalziumströme aus. Im Gegensatz dazu lösten Duftstimulationen und Strominjektionen in Typ II LNs zwar Membrandepolarisationen, jedoch keine TTX-sensitiven Aktionspotentiale aus. In wenigen Ableitungen saßen kleine (2 mV) „spikelets“ auf den duftevozierten Depolarisationen auf. Spannungsaktivierte Natriumströme waren in Typ II LNs nicht messbar. Die spannungsaktivierten Kalziumströme hingegen waren signifikant größer als in Typ I LNs und die Eigenschaften der Aktivierung waren signifikant unterschiedlich. In Typ I LNs lag die Spannung der halbmaximalen Aktivierung ($V_{0.5(akt)}$) des I_{Ca} bei -11.1 ± 6.5 mV, was im Bereich der $V_{0.5(akt)}$ von uPNs ($V_{0.5(akt)} = -10.6 \pm 3.4$ mV) lag. Im Gegensatz dazu war $V_{0.5(akt)}$ in Typ II LNs zu signifikant negativeren Potentialen verschoben ($V_{0.5(akt)} = -19.4 \pm 4.7$ mV). Diese Ergebnisse deuten darauf hin, dass die durch Duftstimulation hervorgerufenen Depolarisationen in Typ II LNs vor allem durch Kalzium Ströme getragen werden könnten und dass die spannungsaktivierten Kalzium Ströme eine Rolle in graduiertes synaptischer Übertragung zwischen Typ II LNs und anderen olfaktorischen Interneuronen spielen könnten.

Abstract

In the insect antennal lobe (AL) each olfactory receptor cell projects to one glomerulus and many receptor axons converge in each glomerulus, where they provide synaptic input to local interneurons (LNs) and projection (output) neurons (PNs). The arborizations of LNs are confined to the AL. In contrast, the PNs extend axons to higher order neuropiles of the protocerebrum, including the mushroom bodies and the lateral lobus of the protocerebrum. In particular PNs have been in the focus of intensive studies, because they serve multiple functions and play a key role in the central olfactory pathway. However, the role and functional properties of LNs are less well understood. Towards the goal to better understand the biophysical parameters that mediate olfactory information processing on the cellular level, voltage activated calcium currents (I_{Ca}) in olfactory interneurons of the AL from adult cockroach were analyzed: 1) in acutely dissociated cells (in vitro), 2) in an intact brain preparation (in situ), and 3) in unequivocally identified and intact neurons.

Using whole cell patch-clamp recordings in current and voltage-clamp mode in combination with single cell staining, uniglomerular PNs (uPNs) and two major types of LNs could be identified by their physiological and morphological properties, which in the following are referred to as type I LNs and type II LNs. In type I LNs odor stimulation and depolarizing current injection elicited overshooting TTX-sensitive action potentials. Voltage-clamp recordings revealed a voltage-activated

sodium current, a transient and a sustained potassium current and a calcium current. In contrast, in type II LNs odor stimulation and current injections induced membrane depolarization, but no TTX-sensitive action potentials. In some recordings small (~ 2 mV) 'spikelets' were riding on the odor evoked depolarization. In type II LNs voltage activated sodium currents were not detectable. However, I_{Ca} was significantly larger compared to type I LNs and the activation characteristics were significantly different. For type I LNs the voltage for half maximal activation ($V_{0.5(act)}$) of I_{Ca} was -11.1 ± 6.5 mV, which is in the range of $V_{0.5(act)}$ for uPNs ($V_{0.5(act)} = -10.6 \pm 3.4$ mV). In contrast to this, in type II LNs the $V_{0.5(act)}$ of I_{Ca} is significantly shifted to more negative potentials ($V_{0.5(act)} = -19.4 \pm 4.7$ mV). These results suggest that the odor-evoked depolarization in type II LNs might be carried largely by I_{Ca} and that I_{Ca} might play a role in graded synaptic release between type II LNs and other olfactory interneurons.

1 Introduction

Odor discrimination is crucial for the survival of most animals. The first-order synaptic relay in olfactory systems of vertebrate and invertebrate animals have striking similarities in physiology and neuronal organization, suggesting that olfactory information is processed through similar mechanisms in these evolutionary remote animals (Eisthen 2002; Hildebrand and Shepherd 1997; Strausfeld and Hildebrand 1999; Wilson and Mainen 2006). One experimental system that has served very successfully as a model to understand olfactory information processing is the first order olfactory relay or antennal lobe (AL) of insects (Keene and Waddell 2007; Laurent 1999; Vosshall and Stocker 2007). As an important step towards the long term goal to better understand the cellular mechanisms that mediate olfactory information processing I characterized the biophysical properties of voltage activated Ca^{2+} currents in identified olfactory interneurons from the ALs of adult *Periplaneta americana*.

1.1 The insect olfactory system

Inside the insect antennal lobe each olfactory receptor cell projects to one glomerulus and many receptor axons converge in each glomerulus, where they provide cholinergic synaptic input to local interneurons (LNs) and projection neurons (PNs). The arborizations of local interneurons are confined to the antennal lobe, whereas the

projection neurons extend their axons to higher order neuropiles of the protocerebrum, including the mushroom bodies and the lateral lobe of the protocerebrum. Studies in the fruit fly, *Drosophila melanogaster*, using genetically encoded activity sensors (Ng et al. 2002; Wang et al. 2003), proposed that olfactory information proceeds along a straight and simple path (*labeled-line*), with minimal interaction among receptor-specific tracks: receptor → glomerulus → output neuron → higher brain regions. For some odors of particular biological significance such as CO₂ straight processing tracks may exist (Suh et al. 2004), but recent work shows that the general picture is more complex (for review see Stopfer 2005). With in vivo patch-clamp recordings in the antennal lobe of the fruitfly, Wilson et al. (2004) have shown, that a given PN can respond to odors of many different chemical classes. The authors compared explicitly the odor sensitivities of olfactory receptors and their immediate postsynaptic PNs. Surprisingly the electrophysiological results indicated that PNs are more broadly tuned than their presynaptic ORNs (Wilson et al. 2004). They concluded that PNs not only receive direct input from ORNs, but also input from neighboring glomeruli, possibly mediated by local interneurons. As already described in other insects, especially in the american cockroach, many antennal lobe LNs are GABAergic (Boeckh and Tolbert 1993; Distler 1989; Distler 1990; Malun 1991b), providing inhibitory input to the PNs (Christensen et al. 1993; MacLeod and Laurent 1996; Waldrop et al. 1987). As expected, also in *Drosophila* many LNs contain the inhibitory transmitter GABA. Blocking GABA-mediated inhibition reduced the temporal variability in odor evoked PN firing patterns (Wilson and Laurent 2005), demonstrating that olfactory information is dramatically restructured within the antennal lobe. However, inhibitory local interneurons alone can not generate the complex response patterns, observed in PNs. Recent work from Shang et al. (2007) described that some of the apparent complexity in the antennal lobes output rises from a previously unidentified population of excitatory cholinergic local

interneurons. These data indicate the presence of at least two or even more completely different physiological and morphological types of local interneuron populations. In the bee antennal lobe at least two morphologically different types of local interneurons have been described (Fonta et al. 1993). Immunohistochemical data from insect antennal lobe suggest an even more complex role of local interneurons. Some LNs are histaminergic (Gebhardt and Homberg 2004; Loesel and Homberg 1999; Nassel 1999) and other subpopulations are immunoreactive for other neuropeptides, amines or nitric oxide (Berg et al. 2007). However, even basic questions regarding the physiology of different types of LNs are not completely understood. For example in the locust (*Locusta migratoria*) olfactory system only non-spiking local interneurons are reported (MacLeod and Laurent 1996), whereas in the honey bee (*Apis mellifera*) and in the moth (*Manduca sexta*) there are exclusively data available that describe spiking local interneurons (Christensen et al. 1993; Sun et al. 1993). The cellular mechanisms that underlie these important intrinsic properties remain obscure, as relatively little is known about the physiological properties of antennal lobe interneurons. It has been shown that the properties of neurons are largely determined by the types of ion channel and the rate of channel expression for the different channel types (Baro et al. 1997). As a first step toward addressing this issue, in this study I have explored the electrophysiological properties of voltage activated calcium currents in antennal lobe interneurons in the brain of *Periplaneta americana*.

1.2 Variety of voltage gated calcium channels

Due to their different functions and tasks antennal lobe neurons do not only differ in their morphology and arborization patterns, but also in their basic physiological and neuronal properties. In this context calcium handling plays a critical role in the

control of a variety of neural processes such as synaptic release, membrane excitability, enzyme activation and activity dependent gene activation (Berridge 1998; Augustine et al. 2003). The spatial and temporal dynamics of these signals are determined by a variety of cellular parameters including: calcium influx, calcium buffering, calcium extrusion, geometry of the cell and locally changing diffusion coefficients (Neher and Augustine 1992; Helmchen 2005). A main source of cytoplasmic Ca^{2+} that contributes significantly to the dynamics of intracellular Ca^{2+} signals are voltage gated Ca^{2+} channels (VGCC). Multiple types of voltage-gated Ca^{2+} channels, characterized by different functional properties, are usually differentially distributed in functionally specialized subcellular compartments of the neuron and contribute to its whole cell Ca^{2+} current. Characterized by their physiological and biophysical phenotypes the following voltage gated Ca^{2+} channel types can be presently distinguished: Low-voltage activated (LVA) channels (T-type, $\text{Ca}_v3.1$ - $\text{Ca}_v3.3$) and high-voltage activated (HVA) channels (L-, N-, P/Q-, R-type, $\text{Ca}_v1.1$ - $\text{Ca}_v1.4$, $\text{Ca}_v2.1$ - $\text{Ca}_v2.3$).

In important structural aspects insect VGCCs seem to resemble the vertebrate VGCCs. For instance, the *Drosophila* genome contains genes, which are homologous to mammalian α_2 - subunits that underlie T-, L- and N-type currents as well as genes encoding β - and $\alpha_2\beta$ -subunits (Littleton and Ganetzky 2000). Despite the similarities of Ca^{2+} channel sequences in invertebrates and vertebrates, invertebrate channels greatly differ in their pharmacological profile. For instance, one of the characteristics of L-type channels in vertebrates is their sensitivity to 1,4-dihydropyridines (e.g. nifedipine), whereas most invertebrate channels with homologous 'L-type-like' sequences lack this feature (for reviews see Jeziorski et al. 2000; Wicher et al. 2001).

In the insect central nervous system, VGCCs can be separated electrophysiologically into low-voltage activated (LVA) or mid-low-voltage activated (M-LVA) and high-voltage-activated (HVA) calcium channels (Grolleau and Lapied 1996; Wicher and

Penzlin 1997). It has been demonstrated that the LVA current in dorsal unpaired median (DUM) neurons of *P. americana* could be further bisected into two components according to their sensitivity to Ni^{2+} ions: a transient (tLVA) and a sustained LVA current (mLVA; (Grolleau and Lapied 1996)). In DUM neurons, LVA currents start to activate at -80 mV, M-LVA at -50 mV and HVA currents at -40 mV. M-LVA and HVA currents were further characterized by their differential sensitivity to inorganic ions (Ni^{2+} , Cd^{2+}) and peptide toxins (conotoxins and agatoxins; Wicher and Penzlin 1997). Differential sensitivity of HVA currents in embryonic brain neurons from *P. americana* to peptide toxins suggests 2 current components resembling the vertebrate P/Q- and R-type channels (Benquet et al. 1999).

Because of the obvious importance of voltage activated calcium currents in olfactory information processing, the objective of this thesis was to characterize in detail I_{Ca} in identified interneurons of the insect antennal lobe.

1.3 Objectives of this thesis

The specific goals of this thesis were:

1. To characterize physiological and biophysical properties of voltage activated calcium currents in olfactory interneurons from the ALs of adult *Periplaneta americana* under controlled in vitro conditions.
2. To establish an in situ recording method that allows unequivocal identification of the recorded neurons and their stimulation with biologically relevant odors.
3. To characterize voltage activated calcium currents in identified olfactory interneuron types such as uniglomerular projection neurons and different types of local interneurons in an intact brain preparation.

2 Materials & Methods

2.1 Animals and materials

P. americana were reared in crowded colonies at 27 °C under a 13:11 h light/dark photoperiod regimen and reared on a diet of dry rodent food, oatmeal and water. All experiments were performed with adult animals, in situ preparations were done with adult males. Before dissection the animals were anesthetized by CO₂ or cooling (4 °C) for several minutes. For cell culture, they were then adhered in plastic tubes with adhesive tape and the heads were immobilized using dental modeling wax (S-U Modellierwachs, Schuler-Dental, Ulm, Germany) with a low solidification point (57 °C). For in situ experiments, the animals were placed in a custom built holder, and the caput was immobilized with tape (tesa ExtraPower Gewebeband, tesa AG, Hamburg, Germany). The antennae were immobilized on a removable plastic ring that was later used to transfer the brain with antennae to the recording chamber (for details see Figure 2.1).

All chemicals, unless stated otherwise, were obtained from Applichem (Darmstadt, Germany) or Sigma-Aldrich (Taufkirchen, Germany) with a purity grade of p.a. (per analysis).

2.2 Cell culture

2.2.1 Cell culture dissection

To examine the electrophysiological properties of isolated antennal lobe neurons, cells were dissociated and cultured using modified protocols reported previously (Grolleau and Laped 1996; Hayashi and Hildebrand 1990; Kirchhof and Mercer 1997). The head capsule was opened with razor blade pieces fixed in a knife holder and the antennal lobes were dissected with fine forceps. Typically, ALs from eight animals were pooled in sterile 'culture' saline (kept on ice) containing (in mM): 185 NaCl, 4 KCl, 6 CaCl₂, 2 MgCl₂, 35 D-glucose, 10 HEPES, 5% fetal bovine serum (S-10, c.c.pro, Neustadt, Germany), adjusted to pH 7.2 (with NaOH), which resulted in an osmolarity of 420 mOsm.

2.2.2 Dissociation of olfactory interneurons

For dissociation the ALs were transferred for 2 min at 37 °C into 500 µl Hanks' Ca²⁺ and Mg²⁺ free buffered salt solution (14170, GIBCO, Invitrogen, Karlsruhe, Germany) containing (in mM): 10 HEPES, 130 sucrose, 8 units ml⁻¹ collagenase (LS004194, Worthington, Lakewood, New Jersey, USA) and 0.7 units ml⁻¹ dispase (LS02100, Worthington), adjusted to pH 7.2 (with NaOH) and to 450 mOsm (with sucrose). Dissociation of neurons was aided by careful titration with a fire-polished Pasteur pipette for 3 - 5 min. Enzyme treatment was terminated by cooling and centrifuging the cells twice through 6 ml of culture medium (4 °C, 480 g, 5 min). The culture medium consisted of 5 parts Schneider's *Drosophila* medium (21720, GIBCO) and 4 parts Minimum Essential Medium (21575, GIBCO) to which was added (in mM): 10 HEPES, 15 glucose, 10 fructose, 60 sucrose, 5% fetal bovine serum adjusted to pH 7.5 (with NaOH) and 430 mOsm (with sucrose). After centrifugation, the cells were

resuspended in a small volume of culture medium (100 μl per dish, 6 dishes), and allowed to settle for 2 h to adhere to the surface of the culture dishes coated with concanavalin A (C-2010, Sigma, 0.7 mg ml^{-1} dissolved in H_2O). The cultures were placed in an incubator at 26 $^{\circ}\text{C}$, and used for electrophysiological experiments on the same day. For recordings the cells were visualized with an inverted microscope (IX71, Olympus, Hamburg, Germany) using a 40x objective (U-Apo/340, 40x/1.15, Olympus) and phase contrast optics.

2.3 Intact brain preparation

The intact brain preparation was based on an approach described by (Kloppenburger et al. 1999a; Kloppenburger et al. 1999b), in which the central olfactory network was left intact. Shortly before the experiment, the holder was filled with 'normal' saline (see below). The head capsule of the anesthetized animal was opened by cutting a window between the two compound eyes and the bases of the antennae. The brain with antennal nerves and antennae attached was dissected from the head capsule and transferred to the recording chamber using the plastic ring for stabilization. The brain was pinned with fine wire in a Sylgard-coated (Dow Corning Corp., Midland, Michigan, USA) recording chamber containing 'normal' saline (see below). To gain better access to the recording site and facilitate the penetration of pharmacological agents into the tissue, the brain was enzyme treated (papain, P4762, Sigma, 0.3 mg ml^{-1} and L-cysteine, 30090, Fluka/Sigma, 1 mg ml^{-1} dissolved in 'normal' saline) for ~ 3 minutes at room temperature before the AL was desheathed using fine forceps. The AL neurons were visualized with a fixed stage upright microscope (BX51WI, Olympus) using a 40x water-immersion objective and IR-DIC optics (Dodt and Zieglgänsberger 1994).

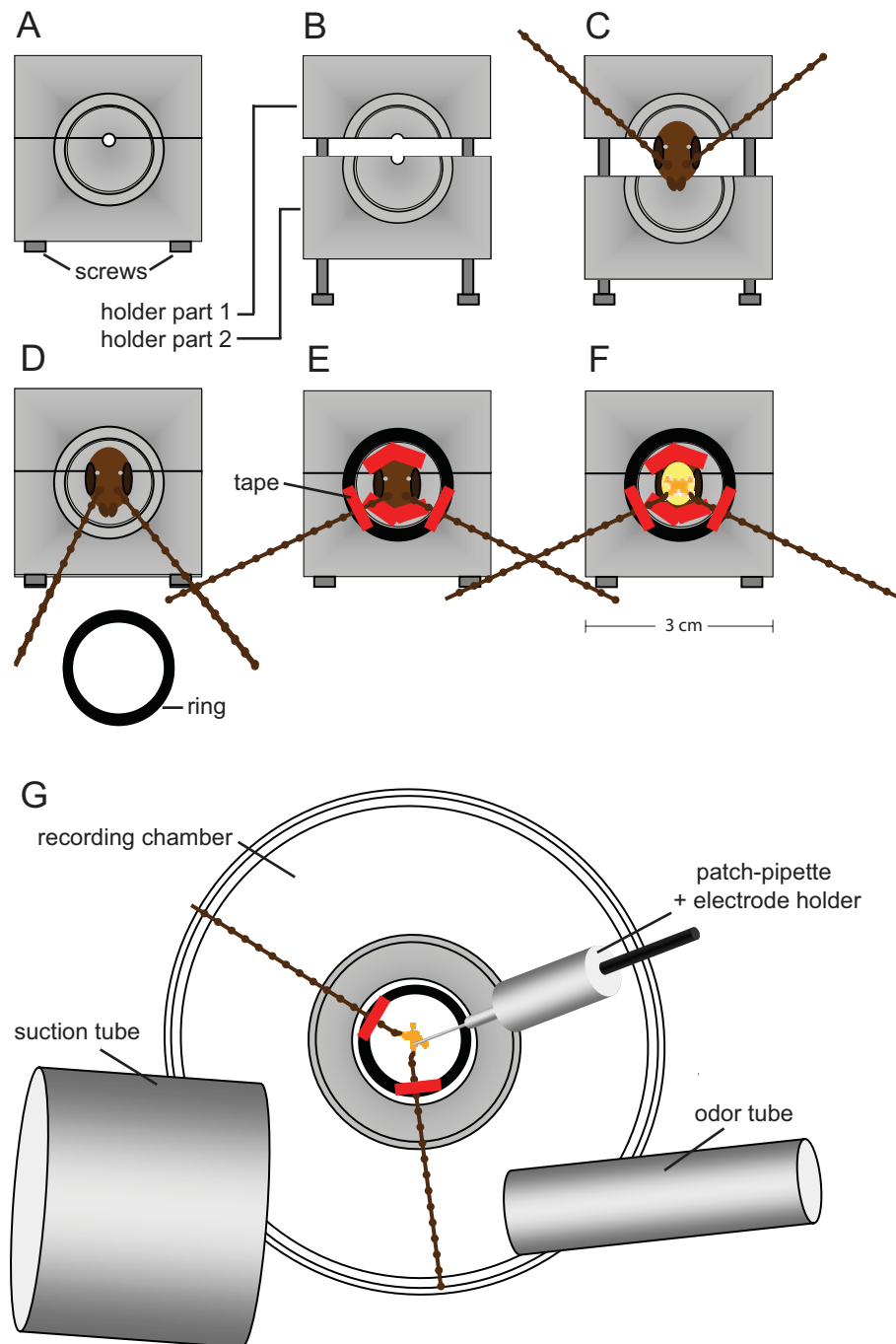


Figure 2.1. Schematic representation of the intact brain preparation

A and B: For the intact brain preparation a custom build holder was used, that could be closed (A) and opened (B) via two metal screws. C: The animal was placed inside the opened holder. D: To stabilize the animal and to avoid loss of saline during dissection, the two parts were pushed together tightly and sealed with vaseline. E: The caput was immobilized with tape stripes and the antennae were mounted on a plastic ring. F: The head capsule was opened and the brain was dissected with antennae and antennal nerves attached. G: The ring including the intact brain preparation was transferred to the recording chamber. It was possible to record from neurons under visual control and stimulate the antennae with physiologically relevant odors.

2.4 Electrophysiological recordings

2.4.1 Whole cell patch clamp recordings

Whole cell recordings were performed at 24 °C following the methods described by Hamill et al. (Hamill et al. 1981). Electrodes (tip resistance between 3-5 MΩ) were fashioned from borosilicate glass (GB150-8P, 0.86 × 1.5 × 80 mm, Science Products, Hofheim, Germany) with a temperature controlled pipette puller (PIP5, HEKA-Elektronik, Lambrecht, Germany) and filled with a solution containing (in mM): 190 K-Aspartate, 10 NaCl, 1 CaCl₂, 2 MgCl₂, 10 HEPES and 10 EGTA adjusted to pH 7.2 (with NaOH), resulting in an osmolarity of ~ 415 mOsm. During the experiments, if not stated otherwise, the cells were superfused constantly with 'normal' saline solution containing (in mM): 185 NaCl, 4 KCl, 6 CaCl₂, 2 MgCl₂, 10 HEPES, 35 D-glucose. The solution was adjusted to pH 7.2 (with NaOH) and to ~ 430 mOsm (with glucose).

To isolate the Ca²⁺ currents a combination of pharmacological blockers and ion substitution was used that has been shown to be effective in other insect preparations (Kloppenburger et al. 1999b; Kloppenburger and Hörner 1998; Schäfer et al. 1994). Transient voltage-gated sodium currents were blocked by tetrodotoxin (TTX, 10⁻⁷-10⁻⁴ M, T-550, Alomone, Jerusalem, Israel). 4-aminopyridine (4-AP, 4 × 10⁻⁴ M, A78403, Sigma) was used to block transient K⁺ currents and tetraethylammonium (TEA, 20 × 10⁻³ M, T2265, Sigma) blocked sustained K⁺ currents ($I_{K(V)}$) as well as Ca²⁺ activated K⁺ currents ($I_{K(Ca)}$). In addition the intracellular potassium was substituted with cesium. For calcium current isolation the following pipette solution (calcium saline) was used (in mM): 190 CsCl, 10 NaCl, 1 CaCl₂, 2 MgCl₂, 10 HEPES and 10 EGTA adjusted to pH 7.2 (with NaOH), resulting in an osmolarity of 415 mOsm.

2.4.2 Data acquisition

Whole cell voltage-clamp recordings were made with an EPC9 patch-clamp amplifier (HEKA-Elektronik) that was controlled by the program Pulse (version 8.63, HEKA-Elektronik) running under Windows. The electrophysiological data were sampled at intervals of 100 μ s (10 kHz), except the 5 ms tail current measurements were sampled at 20 kHz. The recordings were low pass filtered at 2 kHz with a 4-pole Bessel-Filter. Compensation of the offset potential and capacitance were performed using the 'automatic mode' of the EPC9 amplifier. The liquid junction potential between intracellular and extracellular solution of 15.4 mV for 'normal' saline and of 4.8 mV for 'calcium' saline (calculated with Patcher's-Power-Tools plug-in from <http://www.mpibpc.gwdg.de/abteilungen/140/software/index.html> for Igor Pro (Wavemetrics, Portland, Oregon, USA)) was also compensated (Neher 1992). To remove uncompensated leakage and capacitive currents, a p/6 protocol was used. Voltage errors due to series resistance (RS) were minimized using the RS-compensation of the EPC9. RS was compensated between 30% and 70% with a time constant (τ) of 2 μ s. Stimulus protocols used for each set of experiments are provided in the *Results*.

2.4.3 Data analysis

The data from the dose-response experiments were fit with a Hill equation of the form:

$$\frac{I}{I_{max}} = \frac{1}{1 + \left(\frac{IC_{50}}{[C]}\right)^{n_H}} \quad (\text{eq. 1}).$$

I is the peak amplitude of I_{Ca} at a -5 mV testpulse from $V_h = -60$ mV in the presence of different concentrations of drugs ($[C]$), and I_{max} is the peak amplitude of the control. IC_{50} is the concentration where half of I_{Ca} is blocked and n_H is the Hill coefficient.

Steady-state tail-current activation and steady-state inactivation data were fit using a first-order ($n = 1$) Boltzmann equation:

$$\frac{I}{I_{max}} = \frac{1}{(1 + e^{(V_{0.5} - V)/s})^n} \quad (\text{eq. 2}).$$

I_{max} is the maximal current, V is the voltage of the testpulse, I is the current at voltage V , s is the slope factor and $V_{0.5}$ is the voltage at which half-maximal activation occurs.

The peak conductance (g) was calculated using the equation:

$$g = \frac{I}{(V - V_{rev})} \quad (\text{eq. 3}).$$

I is the current density, V the test potential and V_{rev} is the Ca^{2+} equilibrium potential. To convert peak current density to peak conductance a reversal potential for calcium was calculated as $V_{rev} = 160$ mV.

To describe the time course of voltage activated calcium currents a sum of two exponential functions with two time constants was used:

$$I = A_1 \cdot e^{\frac{-t}{\tau_1}} + A_2 \cdot e^{\frac{-t}{\tau_2}} \quad (\text{eq. 4}).$$

$\tau_{1,2}$ are the different time constant, $A_{1,2}$ are the different current amplitudes at $t = 0$ and t is the time at which the current I occurs.

For analysis of electrophysiological data the software Pulse (version 8.63, HEKA-Elektronik), Igor Pro 4 (Wavemetrics, including the Patcher's PowerTools plug-in), and Sigma Stat (Systat Software GmbH, Erkrath, Germany) were used. All calculated values are expressed as mean \pm standard deviation (SD). Significance of differences between mean values were evaluated with Mann-Whitney Rank Sum tests or student's t-tests. Significance was accepted at $P \leq 0.05$.

2.5 Odor stimulation

Odors were delivered to the antennae using a custom-built and computer controlled olfactometer. Schematic diagram of the odor application system is shown in Fig. 2.2. A moistened and charcoal-filtered air stream (2 l/min) ventilated the antenna ipsilateral to the recorded antennal lobe through a glass tube (7 mm internal diameter). The glass tube ended \sim 2 cm from the antenna. The odor stimulus was added to the stream by opening a solenoid valve that was controlled by the EPC9 D/A-output triggered by Pulse software (Heka Electronics). Air was blown through an odor laden glass bottle for 500 ms into the continuous stream of air. An odor puff with a duration of 500 ms resulted in a volume of 22.5 ml odor saturated air.

Odorants used in the experiments were α -ionone, citronellal, citral and eugenol purchased from Sigma. Odorants were dissolved in mineral oil. In order to compensate for differences in vapor pressure, all odorants were 'normalized' to the odor with the lowest vapor pressure (eugenol). Dilutions were as follows: eugenol 100%, α -ionone 72,4 %, citral 14,6 %, citronellal 4,9 %. Five milliliters of diluted odorants were applied into odor application glass bottles equipped with filter papers (1 x 3 cm). Control stimulus consisted of filter paper with mineral oil only.

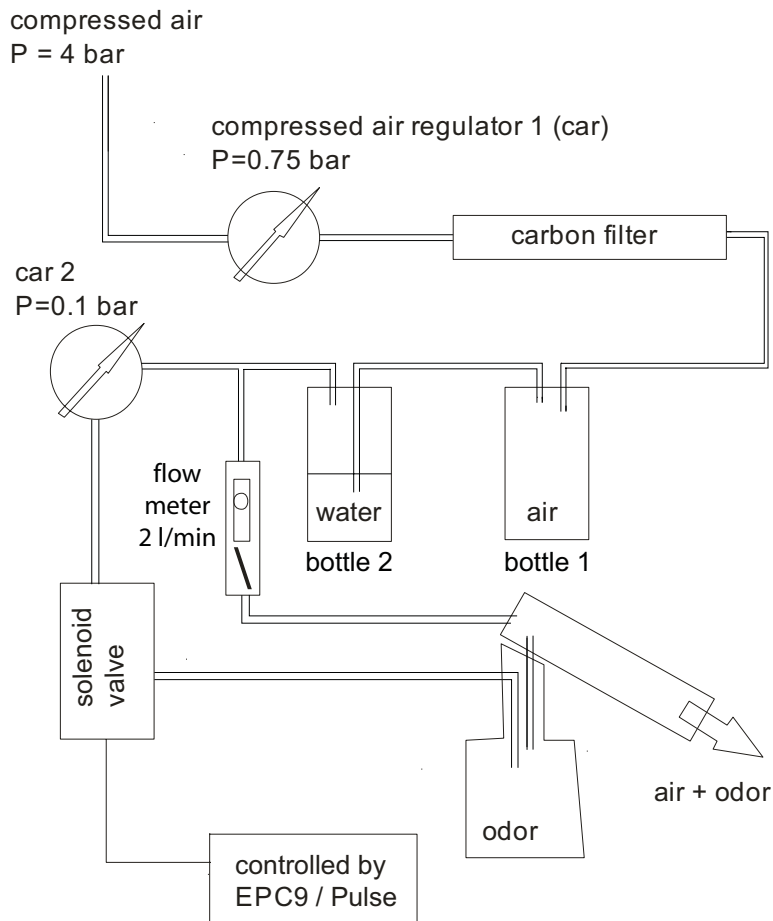


Figure 2.2. Odor application system

Schematic diagram of the odor application system. Compressed air (4 bar) was passed through an air regulator (car1, 0.75 bar; Festo AG & Co. KG, Esslingen, Germany), a carbon filter (Carbon-Cap 150, Whatman, Clifton, NJ), a dry and an aqua bidest.-filled bottle. The filtered and humidified stream of air was then divided into two streams, one leading to a flow meter (2 l/min; Cole Palmer, Vernon Hills, Il) and an odor application tube aimed at the ipsilateral antenna of the recording site, the other passing through a second air regulator (0.1 bar), a solenoid valve (controlled by Heka Software, connected to the EPC9 D/A-output) and a custom-built odor application tool (Pipettierovrrichtung, Karl Hecht KG, Sondheim, Germany) attached to a glass bottle (100 ml) bearing the stimulus on a piece of filter paper. The antenna to be stimulated was ventilated continually with a steady stream of air at a distance of ~ 2 cm, thus minimizing mechanical stimulus artefacts. By opening the solenoid activated valve, pressure was applied to the glass bottle, a puff of odor saturated air was injected into the continuous blank air stream.

2.6 Histology

2.6.1 Whole mount preparation of biocytin filled neurons

For single cell staining, 1% biocytin (Sigma) was added to the pipette solution. Immediately after the experiments, the brains were fixed in 4% paraformaldehyde (Merck, Darmstadt, Germany; in 0.2 M phosphate buffer; pH 7.4) overnight at 4 °C. After fixation the brains were rinsed (3 x 10 min) in 0.1 M Tris-HCl buffered solution (TBS; pH 7.4). To enhance the streptavidin penetration the preparations were treated with 1 mg ml⁻¹ collagenase-dispase (Roche Diagnostics GmbH, Mannheim, Germany) and 1 mg ml⁻¹ hyaluronidase (Sigma-Aldrich), for 20 min at 37 °C. The enzyme treatment was terminated in 4 °C cold TBS (3 x 10 min). To further increase streptavidin accessibility, the brains were subsequently incubated in 1% Triton X-100 (Serva, Heidelberg, Germany) diluted in TBS (at RT for 30 min). Afterwards, the brains were incubated in *Alexa Fluor 633 (Alexa 633)* conjugated streptavidin (1:600, Molecular Probes, Eugene, OR) for 1-2 days at 4 °C in TBS containing 10% Normal Goat Serum (Vector Labs, Burlingame, CA). Subsequently, brains were rinsed again in 4 °C cold TBS and dehydrated in an ascending ethanol series (50, 70, 90, 2 x 100%, 10 min each) before being cleared and mounted in methylsalicylate (Sigma-Aldrich). Overview confocal images were taken immediately.

2.6.2 Slice preparation of the stained neurons

Brains were viewed first as wholemounts to document the overall structure of the stained neurons. Subsequently, the brains were washed in 100% ethanol for 10 min to remove the methylsalicylate. Afterwards the brains were rehydrated in a descending ethanol series (2 x 100%, 90%, 70%, 50%), and washed in TBS three times for 10 min or they were stored in 70% ethanol until further processing. The brains were

embedded in agarose (4% in TBS, Serva, Heidelberg, Germany) and 100 μm frontohorizontal sections were obtained with a vibratome (Leica VT1000 S, Heidelberg, Germany) in 4° C cold TBS. The slices were washed in aqua bidest., dried on 0.05 % chrome-alum (Fluka) and 0.5% gelatin (Merck) coated slides, treated with xylene for 10 min and mounted in Permount (Fisher Scientific, Fair Lawn, NJ). This procedure provided the possibility of long lasting storage and enabled to view the stained neurons with high magnification objectives (e.g. 63x oil).

2.6.3 Confocal laser scanning microscopy

The fluorescence images of the wholemount and sections were captured with an LSM 510 and LSM 510 Meta scanner/detector system (Carl Zeiss MicroImaging GmbH, Göttingen, Germany) mounted on a fixed stage inverse microscope (Zeiss Axiovert 100M with Plan-Neofluar 10x/0.3 NA, Plan-Apochromat 20x/0.75 NA, Plan-Neofluar 40x/1.30 NA Oil and Plan-Apochromat 63x/1.4 NA Oil DIC objectives). Streptavidin-*Alexa 633* was excited with a helium neon laser at 633 nm. For the confocal scans the HFT 514/633 nm beam splitter (BS) and LP 650 nm long-pass emission filter of the detector unit were used. Digital fluorescence images were captured using the Zeiss LSM Software v3.5. If the wholemount was too large for an overview stack using the 10x objective, stacks of two overlapping tiles were captured and their respective projections were fitted using the photomerge function in Photoshop CS2 (Adobe Systems Incorporated, San Jose, CA). Calibration, noise reduction and z-projections were done using ImageJ v1.35d with the WCIF plugin bundle (www.uhnresearch.ca/facilities/wcif/).

3 Results

The goal of this thesis was the characterization of physiological and biophysical properties of voltage activated calcium currents in olfactory interneurons (projection neurons and local interneurons). First, I established a cell culture preparation to characterize voltage activated calcium currents in acutely dissociated cells in vitro. Advantages of experiments in cell culture are excellent accessibility for patch-clamp experiments and very good voltage control during whole cell voltage-clamp. Perfect control of extracellular drug concentrations justify in vitro measurements as the first step in understanding physiological characteristics of olfactory interneurons. However, in vitro data often raise concerns about their physiological relevance, because only the somata are available since the neurites have been lost as a consequence of the preparation method. Therefore in the second step an in situ preparation was established in which the olfactory network stayed intact. During an early stage of in situ recordings in nonidentified AL neurons, a high variability in physiological parameters of voltage activated calcium currents became apparent. To clarify the cause of the variability, in the following recordings were obtained from clearly identified olfactory neuron groups. Subsequently every recorded neuron was stained and the physiological parameters were set in context to its individual morphology. Physiological properties and voltage activated calcium current parameters could be described for one distinct group of projection neurons, the

uniglomerular projection neurons, and two strikingly different types of local interneurons: type I and type II LNs.

3.1 Voltage activated calcium currents in vitro and in situ

Whole cell voltage-clamp recordings were used to characterize voltage dependent Ca^{2+} currents in antennal lobe interneurons of *P. americana* in two conditions: in acutely dissociated cells (in vitro) and in an intact brain preparation (in situ). The recorded neurons were identified as antennal lobe interneurons by the position of their cell bodies within the antennal lobe. At this stage, they were not unequivocally classified as local interneurons or projection (output) neurons. If not stated otherwise, the membrane potential was clamped at -60 mV, which was in the range of the normal resting potential of these neurons (see also chapter 3.2.5 and Table 1).

3.1.1 Voltage activated inward currents

Current-clamp recordings from AL neurons in vitro and in situ are shown in Fig. 3.1A. The resting membrane potentials of the cultured AL neurons measured immediately after breaking into the cells ranged from -40 mV to -60 mV. However, because the pipette solution diffuses into the cell as soon as the membrane is ruptured (Pusch and Neher 1988) these values may differ slightly from the true resting potential. In many acutely dissociated cells current injection elicited AP like membrane potential oscillation (Fig. 3.1A1), depending on the amount of available voltage activated sodium currents and potassium currents within the total set of currents. Typically, in voltage-clamp recordings depolarizing voltage steps evoked a combination of inward and outward currents in AL neurons. In some acutely dissociated cells no voltage dependent sodium currents were found. Assuming these channels were located on the neurites, the loss of Na^+ currents can be explained by

the cell dissociation procedure. In most in situ preparations current injection elicited overshooting APs (Fig. 3.1A2). In voltage-clamp, depolarizing steps elicited a typical combination of inward and outward currents (Fig. 3.1B). The inward and outward currents are a combination of several ionic currents.

When voltage activated Na^+ , K^+ and H currents were reduced by ion substitution, pharmacological reagents and appropriate voltage protocols, inward currents were elicited that had the characteristics of typical Ca^{2+} currents (Hille 2001).

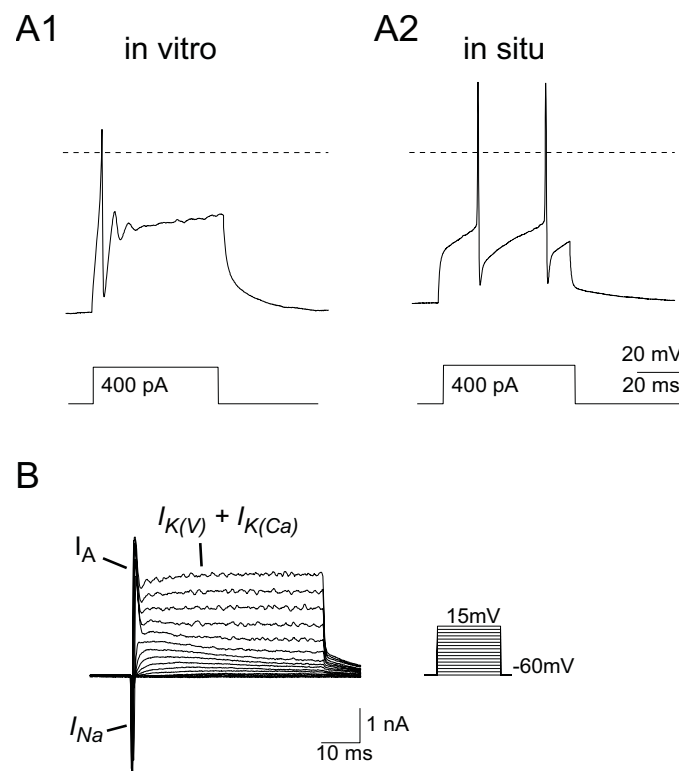


Figure 3.1. Action potentials and total current profiles

A: TTX sensitive action potentials were found in vitro (A1) and in situ (A2). B: In voltage-clamp, depolarizing steps elicited a fast transient inward current followed by a transient and a sustained outward current. Both the inward and outward currents are a combination of several ionic currents. The transient inward current was blocked with TTX and identified as a Na^+ current. K^+ was the major charge carrier of the outward currents. The fast activating, transient component (I_A) was blocked with 4-AP and the sustained, delayed rectifier like component was blocked by TEA.

To analyze I_{Ca} , outward currents were minimized by substituting K^+ in the pipette solution with Cs^+ and adding 3×10^{-2} M TEA and 4×10^{-3} M 4-AP to the extracellular

solution. The remaining inward current consisted of a transient very fast activating / inactivating component and a more slowly inactivating component (Fig.3.2A), that did not completely inactivate even after long (> 1 s) depolarizations (Fig. 3.2B). By using pharmacological blockers and ion substitution, the main charge carrier of both components could be separated and identified. The fast transient component was a TTX sensitive sodium current, whereas the other components of the inward current were identified as voltage activated Ca^{2+} conductances (see below). To measure I_{Ca} , the neurons were superfused with saline containing 10^{-7} M TTX, 4×10^{-3} M 4-AP, and 3×10^{-2} M TEA. In the pipette solution K^+ was replaced with Cs^+ .

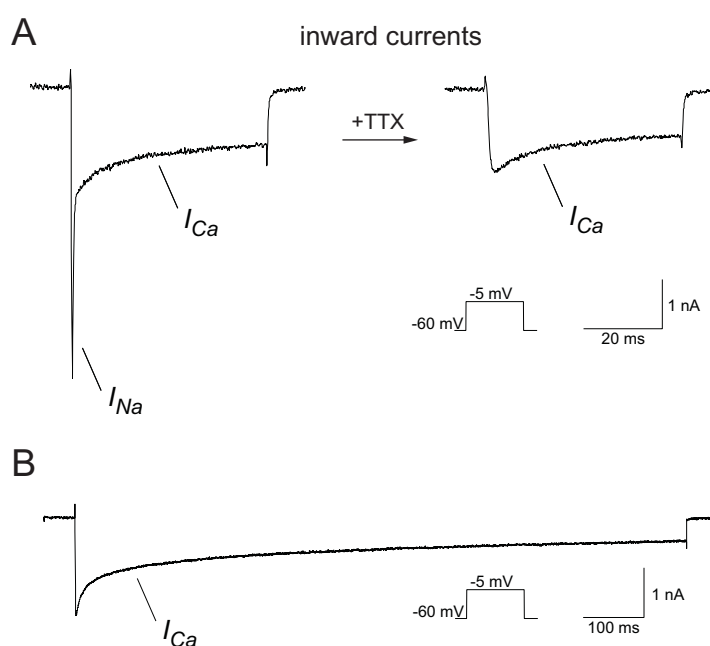


Figure 3.2. Whole cell recording of voltage activated inward currents.

Depolarizing voltage steps (50 ms) from a holding potential of -60 mV to -5 mV evoked a combination of inward and outward currents. Outward currents were blocked by substituting K^+ in the pipette solution with Cs^+ and adding 3×10^{-2} M TEA and 4×10^{-3} M 4-AP to the extracellular solution. The remaining inward current consisted of a transient very fast activating/inactivating component and a more slowly inactivating component. A: The fast transient component was a TTX sensitive Na^{2+} current, whereas the other components of the inward current were identified as voltage activated Ca^{2+} conductances, I_{Ca} (see Fig. 3.3 and Fig. 3.4). B: I_{Ca} consisted of an inactivating and sustained component, which did not completely inactivate even after long (1 s) depolarization.

3.1.2 Charge carrier

Experiments with varying extracellular Ca^{2+} concentrations confirmed that Ca^{2+} was the charge carrier of the investigated inward current. Low extracellular Ca^{2+} concentrations acted quickly to reduce the inward current reversibly ($n = 5$; Fig. 3.3). This reduction of I_{Ca} was concentration dependent. When EGTA containing Ca^{2+} free extracellular solution was applied, the inward current was completely abolished (data not shown).

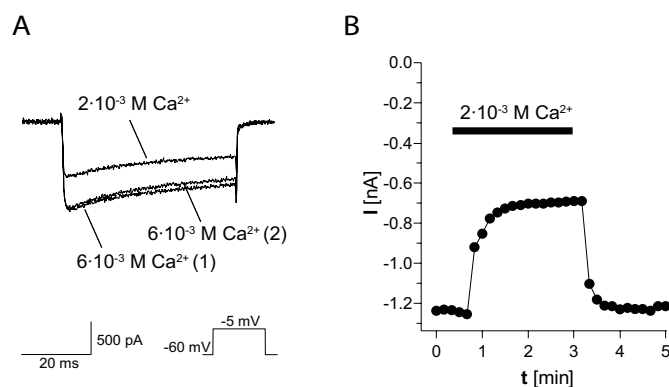


Figure 3.3. Inward currents variability caused by calcium concentration variation

Ca^{2+} is the charge carrier of the TTX insensitive voltage activated inward currents. In all experiments the cells were held at -60 mV . A: Experiments with varying extracellular Ca^{2+} concentrations indicated that Ca^{2+} was the main charge carrier of the investigated inward current. Inward currents elicited by 50 ms voltage steps to -5 mV were reduced reversibly by decreasing the extracellular Ca^{2+} concentration from $6 \times 10^{-3} \text{ M}$ to $2 \times 10^{-3} \text{ M}$ ($n = 5$). B: Time course of peak inward current during a decreased extracellular calcium concentration.

In a few experiments, I compared the inward currents using Ca^{2+} or Ba^{2+} as charge carriers. I did not routinely use Ba^{2+} saline as described in other preparations (Heidel and Pflüger 2006), because the Ba^{2+} current was often unstable and run down quickly. When extracellular Ca^{2+} was substituted with Ba^{2+} (Fig. 3.4), the maximal peak current was enhanced by approximately 20% (Fig. 3.4, A and C) indicating that the channels are more permeable to Ba^{2+} than to Ca^{2+} , as described for Ca^{2+} channels in other cell types (Hille 2001). Simultaneously the I/V relation shifted by $\sim 10 \text{ mV}$ ($n = 4$) to more hyperpolarized membrane potentials (Fig. 3.4C), which might result from changes in

the surface charge of the cell membrane (Fedulova et al. 1985). The resulting voltage dependent differences between I_{Ca} and I_{Ba} are demonstrated by steps to -20 mV and -5 mV in Fig. 3.4, B1 and B2, respectively. Furthermore, the amount of inactivation during a depolarizing voltage pulse was reduced, which became specially obvious during long lasting depolarizations (1 s; -5 mV; Fig. 3.4E). These results suggest that inactivation during a voltage step is, at least in part, a Ca^{2+} dependent mechanism.

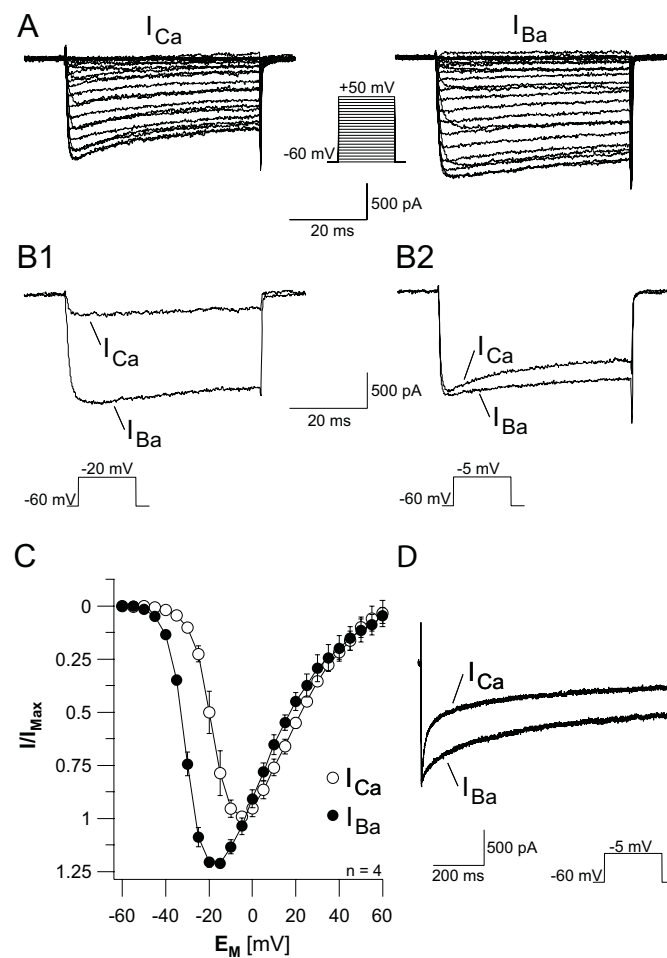


Figure 3.4. Substitution of extracellular calcium with barium

A: Voltage-activated inward currents with Ca^{2+} as the main charge carrier (I_{Ca}) and when Ca^{2+} was substituted with Ba^{2+} (I_{Ba}). Each series represents current responses to increasing voltage steps between -60 mV and 50 mV in 5 mV increments. When extracellular Ca^{2+} was substituted with Ba^{2+} the peak amplitude was enhanced by approximately 20%. B: Currents elicited by voltage steps to -20 mV (B1) and -5 mV (B2) demonstrate the difference between I_{Ca} and I_{Ba} at different command potentials. C: The I/V relation of I_{Ba} was shifted by ~ 10 mV to more hyperpolarized membrane potentials compared to I_{Ca} ($n = 4$). D: I_{Ca} and I_{Ba} during a long lasting depolarization (1 s; -5 mV) demonstrating decreased inactivation for I_{Ba} .

3.1.3 Calcium currents in vitro

The characteristics of I_{Ca} are shown in Fig. 3.5. The I/V relationship of the peak currents was determined by increasing voltage steps (50 ms, 5 mV) between -60 mV and 40 mV from a holding potential of -60 mV (Fig. 3.5A). The voltage dependence I_{Ca} activation was determined from tail currents that were evoked by 5 ms voltage steps from -80 mV holding potential to 40 mV in 10 mV increments (Fig. 3.5B). Steady state inactivation of I_{Ca} was measured from a holding potential of -60 mV. Prepulses (500 ms) were delivered in 5 mV increments from -95 mV to -5 mV, followed by a 50 ms testpulse to -5 mV, and the peak currents were determined (Fig. 3.5C). The I/V relations were fit to a first-order Boltzmann equation (eq. 2; Fig.3.5, G - I).

During a depolarizing voltage step I_{Ca} activated relatively quickly and decayed during a maintained voltage step (Fig. 3.5A). The current waveforms and I/V relations for activation were typical for I_{Ca} , but varied between cells (Fig. 3.5, D-F). In vitro, I_{Ca} started to activate with voltage steps more depolarized than -50 mV (Fig. 3.5D). The mean peak currents reached its maximum (I_{max}) of 1.7 ± 0.6 nA (Fig. 3.5D2) at -6.5 ± 3.8 mV ($n = 65$; Fig. 3.5E) and decreased during more positive testpulses as they approached the calcium equilibrium potential (Fig. 3.5D). Given a mean whole cell capacitance of 29.6 ± 10.6 pF ($n = 65$), this corresponds to a mean current density of 52.8 ± 18.1 pA/pF (Fig. 3.5F).

The activation and inactivation kinetics during a voltage step are voltage dependent (Fig. 3.5, A and B); the time to peak current and the time constant for the decay during a voltage pulse decreased when voltage steps of increasing amplitude were applied. These parameters, however, were not analyzed quantitatively. The tail currents that are independent of the changing driving force during the series of voltage pulses had a maximum of 1.9 ± 0.4 nA ($n = 21$). This corresponds to a mean maximal conductance (G_{max}) of 12.6 ± 2.7 nS (eq. 3) and a mean current density of 63.6 ± 13.8 pA/pF.

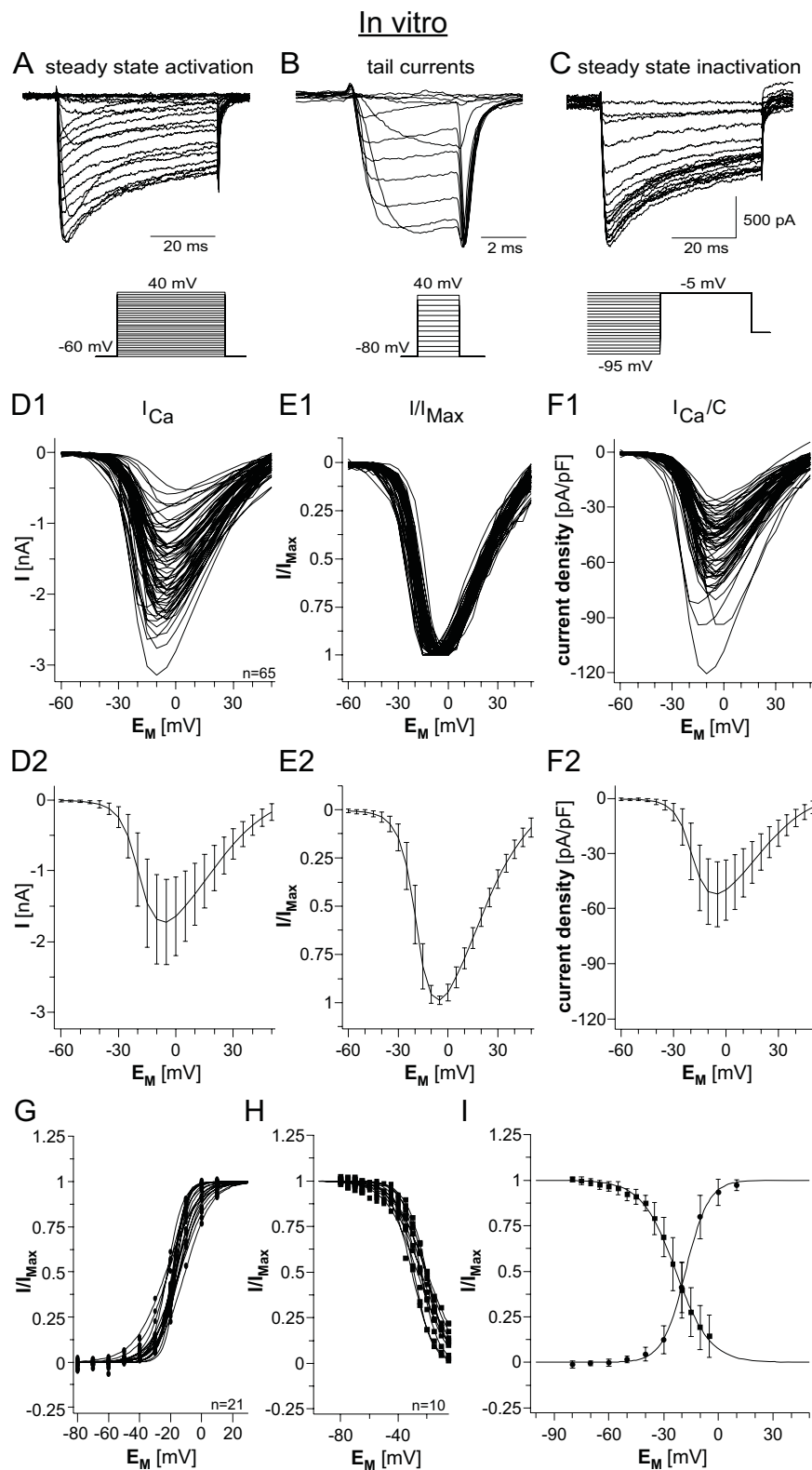


Figure 3.5. Calcium currents in acutely dissociated cells (in vitro)

Figure 3.5. A - C: Example current traces for steady state activation, steady state activation of tail currents, and steady state inactivation. A: Steady state activation. The holding potential was -60 mV and I_{Ca} was evoked by 50 ms voltage steps from -60 mV to 40 mV in 5 mV increments. B: Tail currents. The holding potential was -80 mV and tail currents were evoked by 5 ms voltage steps from -80 mV to 40 mV in 10 mV increments. C: Steady state inactivation. The holding potential was -60 mV. Testpulses to -5 mV (50 ms) were preceded by 500 ms pulses ranging from -95 mV to -5 mV in 5 mV increments. D: Voltage dependence of peak I_{Ca} from 65 neurons. D1 shows data from single neurons and D2 shows the averaged data. The mean peak amplitude (I_{max}) is 1.7 ± 0.6 nA. E: I/V relation of peak I_{Ca} normalized to the maximal current of each cell, I_{max} . E1 shows data from single neurons and E2 shows the averaged data. The current is activated at command potentials more depolarized than -50 mV with a maximum at $-6.5 \text{ mV} \pm 3.8 \text{ mV}$ ($n = 65$). F: Current density / voltage relation. Current density was calculated from the ratio of I_{Ca} and the cell's capacitance. F1 shows data from single neurons and F2 shows the averaged data. The mean maximal current density was 52.8 ± 18.1 pA/pF. G: I/V relation of tail currents normalized to the maximal tail current of each cell. Curves are fits to a first order Boltzmann relation (eq. 2). The mean maximal tail current is 1.9 ± 0.4 nA ($n = 21$). H: I/V relations for steady state inactivation of 10 neurons. Curves are fits to a first order Boltzmann relation. I: Mean I/V relations of steady state inactivation of peak I_{Ca} (filled squares) and tail current activation (filled circles). The curves are fits to first-order Boltzmann equations with the following parameters: Tail current activation: $V_{0.5(act)} = -17.8 \pm 3.3$ mV; $s_{act} = 6.0 \pm 2.2$; $n = 21$. Steady state inactivation: $V_{0.5(inact)} = -24.2 \pm 3.7$ mV; $s_{inact} = 8.7 \pm 2$; $n = 10$.

The I/V relation of the tail currents was well fitted by a first-order Boltzmann equation (eq. 2) with a mean voltage for half-maximal activation ($V_{0.5(act)}$) of -17.8 ± 3.3 mV ($s = 6.0 \pm 2.2$; $n = 21$; Fig. 3.5, G and I). Steady state inactivation started in vitro at prepulse potentials around -60 mV and increased with the amplitude of the depolarizing prepulse (Fig. 3.5, C,H,I). The I/V relationship was fit with a first order Boltzmann equation (eq. 2) with a voltage for half-maximal inactivation ($V_{0.5(inact)}$) of $-24.2 \text{ mV} \pm 3.7 \text{ mV}$ ($s = 8.7 \pm 2$; $n = 10$; Fig. 3.5, H and I).

3.1.4 Inorganic ions as calcium channel blockers

In a series of in vitro experiments our laboratory analyzed the effect of several inorganic ions and organic substances on I_{Ca} , which block voltage activated calcium currents in vertebrate and invertebrate preparations. During this thesis I studied the divalent inorganic blockers Cd^{2+} , Co^{2+} and Ni^{2+} . These results are described below and in Fig 3.6 and 3.7.

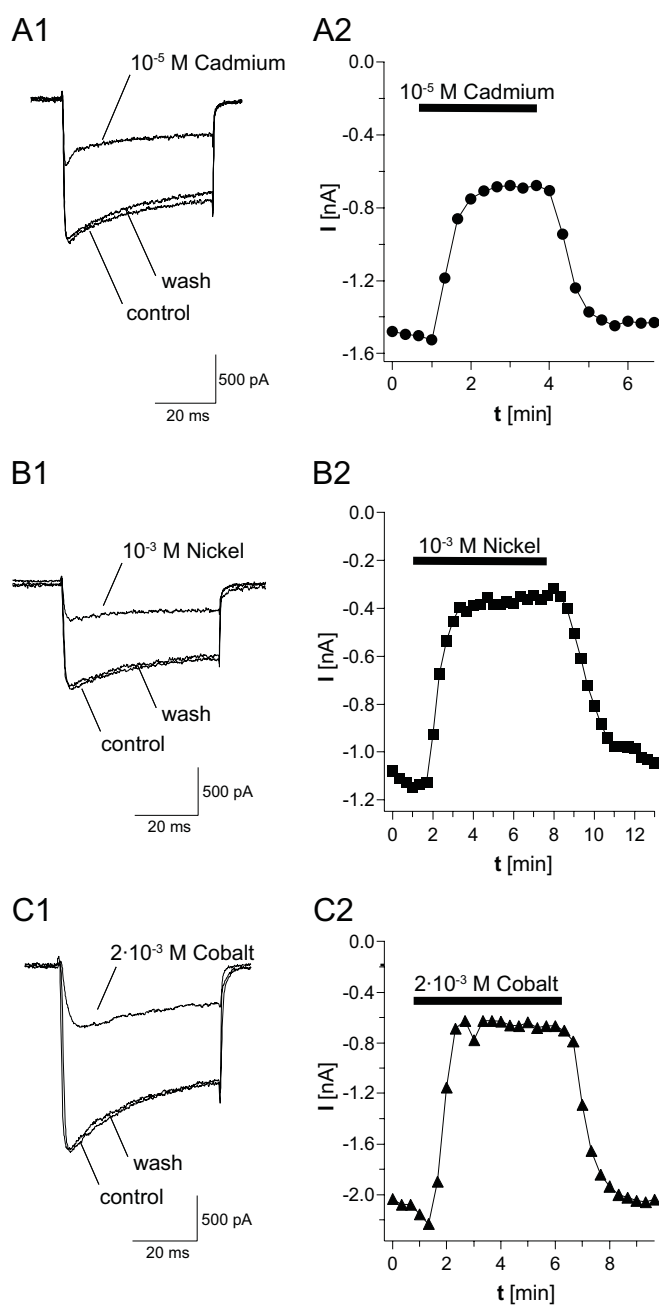


Figure 3.6. Calcium current block by inorganic ions

The divalent inorganic ions Cd^{2+} (A), Ni^{2+} (B) and Co^{2+} (D) reduce I_{Ca} in a concentration-dependent way. A: Effect of 10^{-5} M Cd^{2+} on I_{Ca} . A1: I_{Ca} evoked by a 50 ms voltage step to -5 mV from a holding potential of -60 mV before (control), during and after (wash) application of 10^{-5} M Cd^{2+} . A2: Time course of Cd^{2+} (10^{-5} M) induced reduction of peak I_{Ca} . The black bar indicates the time of Cd^{2+} application. B: Effect of 10^{-3} M Ni^{2+} on I_{Ca} . B1: I_{Ca} before (control), during and after (wash) application of 10^{-3} M Ni^{2+} . B2: Time course of Ni^{2+} (10^{-3} M) induced reduction of peak I_{Ca} . The black bar indicates the time of Ni^{2+} application. C: Effect of 2×10^{-3} M Co^{2+} on I_{Ca} . C1: I_{Ca} before (control), during and after (wash) application of 2×10^{-3} M Co^{2+} . C2: Time course of Co^{2+} (2×10^{-3} M) induced reduction of peak I_{Ca} . The black bar indicates the time of Co^{2+} application.

In collaboration with Simon Heß I also found that verapamil, diltiazem, and nifedipine, which all belong to different chemical classes (phenylalkalamine, benzothiazepine and 1,4-dihydropyridine) and are known to selectively block vertebrate L-type channels, differentially modify I_{Ca} . Amiloride (10^{-3} M), a T-type channel blocker, and (\pm) BAY K 8644 (10^{-4} M), a 1,4-dihydropyridine and L-type channel agonist, had no effect (data not shown). The detailed description of this analysis is described in (Husch et al., submitted).

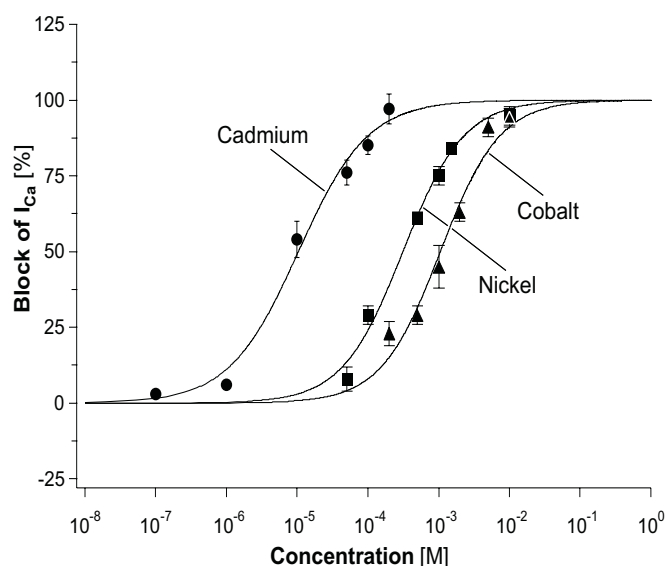


Figure 3.7. Dose response curves for cadmium, nickel and cobalt

Dose-response curves for the aforementioned blockers. Values are means \pm SD from at least 3 experiments. Cadmium was the most effective blocker, followed by nickel and cobalt. Data were fit with a Hill function (see eq. 1) with the following parameters: Cadmium: $IC_{50} = 10^{-5}$ M; $n_H = 0.87$; Nickel: $IC_{50} = 3.13 \times 10^{-4}$ M; $n_H = 1.01$; Cobalt: $IC_{50} = 1.06 \times 10^{-3}$ M; $n_H = 1.04$.

Cd^{2+} , Co^{2+} and Ni^{2+} blocked I_{Ca} in a dose dependent way. Figure 3.6, A-C, show single example experiments for each of the blockers and Fig. 3.7 presents the dose inhibition curves for all three cations. I_{Ca} was elicited by a 50 ms voltage pulse to -5 mV from a holding potential of -60 mV. The dose inhibition curves were well fit with a Hill equation (eq. 1). The most effective blocker was Cd^{2+} with a half-inactivating

concentration (IC_{50}) of 10^{-5} M (Hill coefficient $n_H = 0.87$) followed by Ni^{2+} ($IC_{50} = 3.13 \times 10^{-4}$ M; $n_H = 1.01$) and Co^{2+} ($IC_{50} = 1.06 \times 10^{-3}$ M; $n_H = 1.04$).

3.1.5 Calcium currents in situ

The in vitro results indicate that under the described pharmacological recording conditions, the isolated inward current in olfactory interneurons is mediated by calcium channels. To demonstrate the physiological relevance of the above mentioned results, the following recordings were done in intact neurons in a whole brain preparation.

Calcium currents (I_{Ca}) recorded in situ (Fig. 3.8) showed similar characteristics as in vitro. However, the I/V relationships had a larger variance and the means were shifted significantly to more depolarized membrane potentials. The mean voltage for activation of the maximal peak current was shifted by 14.4 mV ($P < 0.001$). The voltage for half-maximal tail current activation ($V_{0.5(act)}$) was shifted by 7.3 mV ($P < 0.001$). In situ, I_{Ca} started to activate at command potentials more depolarized than -40 mV (Fig. 3.8D). The mean peak currents reached a maximum (I_{max}) of 1.2 ± 0.4 nA ($n = 22$; Fig. 3.8D) at 8 ± 7.8 mV (Fig. 3.8E). Based on a mean whole cell capacitance of 28.8 ± 7.8 pF, this corresponds to a mean current density of 42.6 ± 14.3 pA/pF (Fig. 3.8F). The tail currents had a mean maximum of 1.8 ± 0.4 nA and a mean voltage for half-maximal activation ($V_{0.5(act)}$) of -10.5 ± 6 mV ($s = 7.5 \pm 1.8$; $n = 13$; Fig. 3.8, G and I). In situ steady state inactivation started at prepulse potentials around -60 mV and had a mean voltage for half-maximal inactivation ($V_{0.5(inact)}$) of -19.9 ± 6.7 mV ($s = 8.7 \pm 1.9$; $n = 8$; Fig. 3.8, H and I).

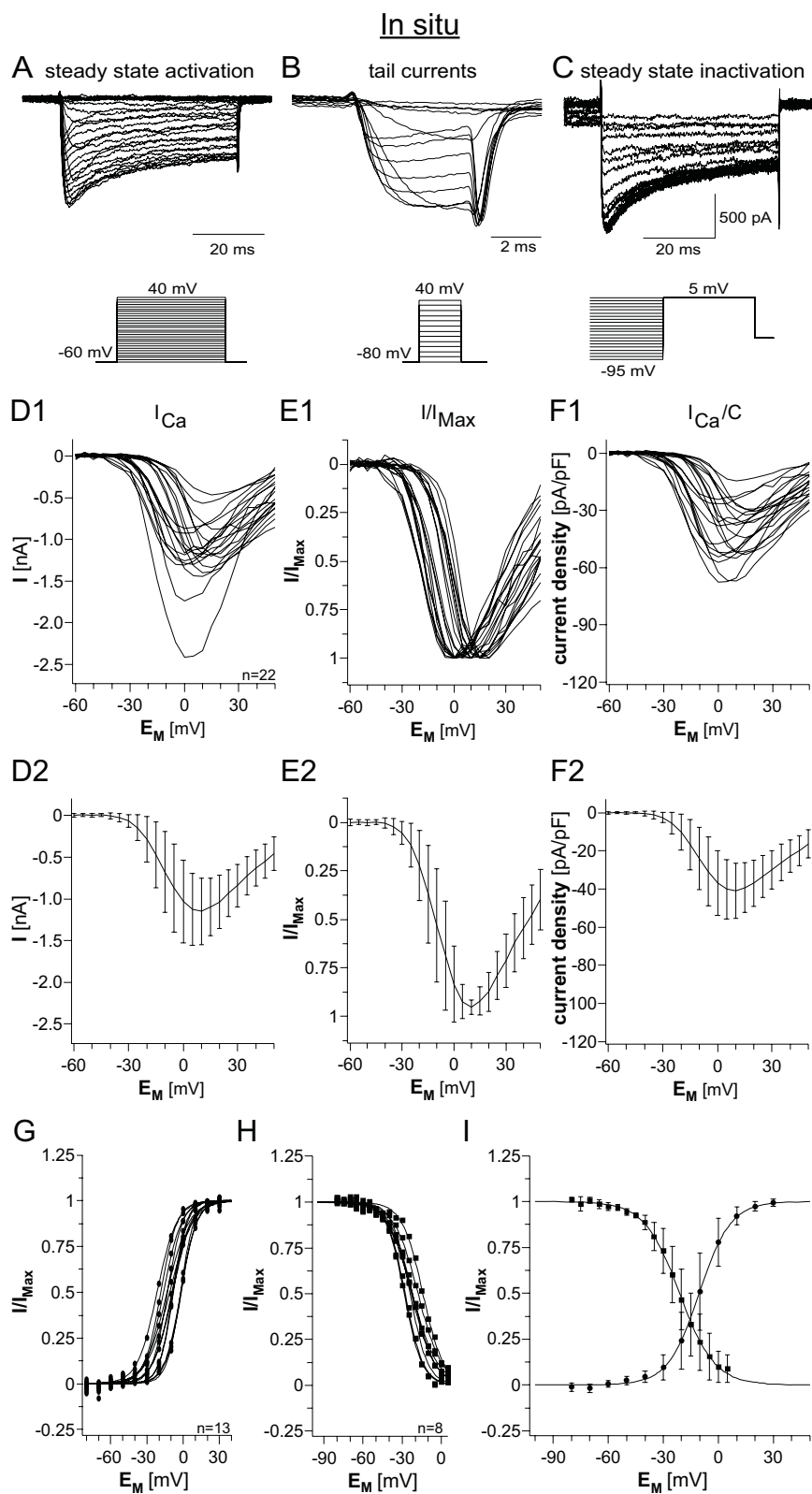


Figure 3.8. Calcium currents in the intact brain preparation (in situ)

Figure 3.8. For details see legend Fig. 3.5. A - C: Current traces for steady state activation, steady state activation of tail currents, and steady state inactivation, respectively. The voltage step for steady state inactivation was 5 mV. D: Voltage dependence of peak I_{Ca} . D1 shows data from single neurons and D2 shows the averaged data. The current is activated at command potentials more depolarized than -40 mV with a maximum around 8 ± 7.8 mV ($n = 22$). The mean peak amplitude (I_{max}) is 1.2 ± 0.4 nA. E: Current density / voltage relation. The mean maximal current density was 42.6 ± 14.3 pA/pF. F: I/V relation of peak I_{Ca} normalized to the maximal current of each cell, I_{max} . On average the mean maximal current (I_{max}) of 1.2 ± 0.4 nA is reached at a membrane potential (E_{max}) of 8 ± 7.8 mV. G: I/V relation of tail currents normalized to the maximal tail current of each cell. The mean maximal tail current is 1.8 ± 0.4 nA ($n = 13$). H: I/V relations for steady state inactivation. I: Mean I/V relations of steady state inactivation of peak I_{Ca} (filled squares) and tail current activation (filled circles). The Boltzmann fits have the following parameters: Tail current activation: $V_{0.5(act)} = -10.5 \pm 6$ mV; $s_{act} = 7.5 \pm 1.8$; $n = 13$. Steady state inactivation: $V_{0.5(inact)} = -19.9 \pm 6.7$ mV; $s_{inact} = 8.7 \pm 1.9$; $n = 8$.

The high variability in I_{Ca} activation curves illustrated in Fig. 3.8, D1, E1, F1 might suggest different I_{Ca} characteristics in different types of central olfactory neurons. To analyze this variability of voltage activated calcium currents in more detail, in the following data were obtained from clearly identified and biocytin-streptavidin stained olfactory interneurons.

3.2 Identification of different olfactory interneuron types

The previous part of this thesis dealt with the study of I_{Ca} in olfactory interneurons in vitro and in situ, but the neurons were not unequivocally identified as projection neurons or local interneurons. However, I presented averaged data from a large number of experiments to characterize the parameter space of I_{Ca} in AL interneurons. It was the first step to characterize I_{Ca} of adult AL interneurons in detail. The variance of the data should not be ignored. It might be due to differential expression of Ca^{2+} channel types in different cell types. This hypothesis was tested by electrophysiological characterization of neurons that are unequivocally identified by their morphology and physiology. Thus, in the following, all data were obtained from clearly identified olfactory interneurons, PNs and LNs. To identify the neurons it was necessary to establish an in situ recording method that allows stimulation with biologically relevant odors and subsequent morphological analysis of single labeled cells.

The intact brain preparation including antennae, antennal nerves and the brain was visualized under an upright microscope with DIC-optics. This method enables to record from olfactory interneurons under visual control. To get access to somata of formerly described projection neuron and local interneuron groups (Distler 1989; Malun et al. 1993), the antennal lobe was slightly twisted to the ventrolateral side in the antennal nerve axis (Fig. 3.9A). The ventrolateral cell cluster in the cockroach antennal lobe was used as a landmark to locate and record from identified cell clusters in individual preparations (Fig. 3.9A). Using this procedure it was possible to reproducibly record from three distinct olfactory interneuron types: uniglomerular projection neurons (uPNs) and two types of local interneurons (type I and type II LNs). The somata inside the ventrolateral group belonged to uniglomerular

projection neurons (uPN), that are well described in their morphology and physiology (Distler and Boeckh 1997a). Somata of local interneurons were located within a lateral cluster, dorsal to the cell bodies of the uPN group (Distler and Boeckh 1997b). Within this local interneuron cluster somata of variable soma sizes were located. Additionally, these local interneuron subgroups were characterized by significant differences in morphology and physiology as described in the following. At this stage the neurons with smaller somata are referred to as type I LNs, the neurons with larger somata are referred to as type II LNs. The parameters for the final classification are summarized in chapter 3.2.5. For this study 75 olfactory interneurons were recorded and filled with biocytin: 25 PNs, 21 type I LNs and 29 type II LNs.

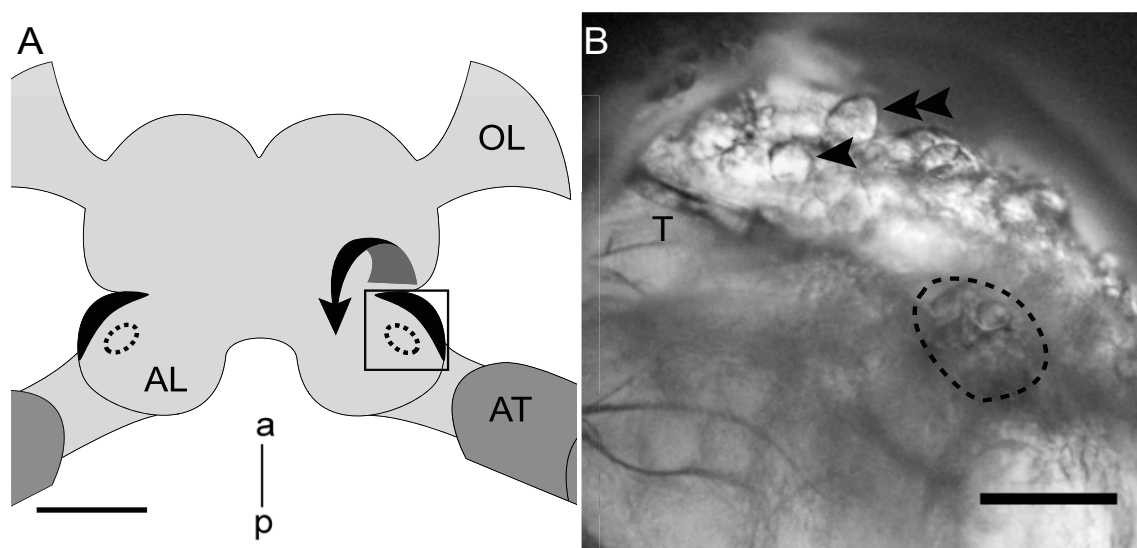


Figure 3.9. Overview of the intact brain preparation

A: Schematic representation of the cockroach brain. Areas outlined with a broken line indicate the location of the PN cell bodies in the recording situation. Filled black areas indicate the location of LN cell bodies. For recording the antennal lobes were slightly bent to the ventral side (curved arrow). The framed area marks the location shown in B. B: IR-DIC transmission images taken from different planes of focus of the recording site showing cell bodies of the different neuron types (Photoshop layer projection). PN cell bodies are outlined with a broken line. LN cell bodies were located more medio-dorsally, dorsal to a characteristic landmark trachea branch (T). Arrowheads indicate LN cell bodies and the size difference of cell bodies among LN cell bodies (arrowhead, double arrowheads). a: anterior; AL: antennal lobe; AT: antenna; OL: optic lobe; p: posterior; T: landmark trachea. Scale bar in A: 500 μm ; in B: 50 μm .

3.2.1 Odor responses

The initial characterization of different olfactory neuron types was started with recordings of electrophysiological responses to application of 4 single component odors: α -ionone, +/- citral, citronellal and eugenol (Fig. 3.10).

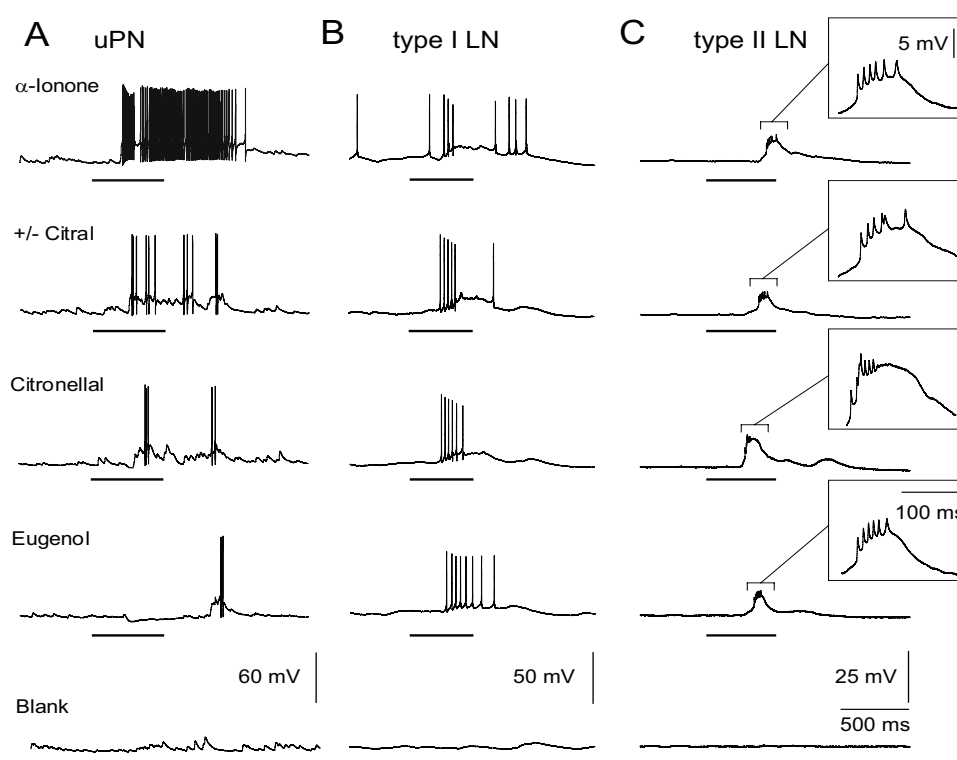


Figure 3.10. Typical responses to different odors in uPNs, type I and type II LNs

Whole cell patch-clamp recordings of uPN, type I and type II LNs during odor stimulation. Four odorants and a blank (mineral oil) were used. The bar beneath the recording indicates the opening of the solenoid valve of the stimulation unit (500 ms). A: Typical odor responses of an uPN. They respond to odorants of many different chemical types, often with elaborate patterns of spiking that could include periods of inhibition. B: Odor responses of a type I LN. Typically type I LNs responded to all presented odors. All odors evoked a depolarization and overshooting action potentials were elicited. C: Typical odor responses of a type II LN. Type II LNs typically reacted to all presented odors. In response to odor stimulation small depolarization in the range of 2 - 10 mV were recorded. Odor stimulation never evoked overshooting sodium driven action potentials. In some of the recorded neurons small (1 - 3 mV) transient depolarization events on top of the membrane depolarization were recorded (insets). During the blank stimulation no change in membrane potential was recorded.

A given uPN can respond to odorants of many different chemical classes, often with elaborate patterns of excitation and spiking that could also include periods of

inhibition (Fig. 3.10A). These spiking patterns can vary for different odorants. Blank stimulation (mineral oil) did not lead to detectable responses in any cell type, showing that the reactions were not elicited by mechanical stimulation. Typically, LNs responded to all tested odors, too. Interestingly type I and type II LNs showed completely different odor responses. At type I LN somata as well as at uPNs overshooting action potentials (APs) were measured. In contrast to this, in type II LNs odor stimulation never lead to overshooting action potentials in the somata. Nevertheless, in 80 % of the recorded type II LNs there was a membrane depolarization, in some cases with small (~ 2 mV) 'spikelets' riding on the long lasting depolarization events. Such an odor response is illustrated in Fig. 3.10C.

Repetitive odor stimulation revealed the odor response specificity in uPNs. Stimulating uPNs three times (1 minute intervals) with the same odor, the patterns of excitation and inhibition were highly reproducible. In the example of an uPN recording in Fig. 3.11A α -ionone elicited a series of action potentials, interrupted after about 100 ms and continuing with eliciting action potentials. This response was highly robust during all trials. Repetitive stimulation with eugenol resulted also in a very robust pattern. First the uPN was hyperpolarized for approximately 500 ms, followed by a depolarization with a number of overshooting action potentials (Fig. 3.11A). In type I LNs, repetitive stimulation also elicited similar odor responses, although they were not as stereotypic and odor specific as the responses in uPNs. The type I LN recording example in Fig. 3.11B showed that α -Ionone as well as eugenol stimulation elicited overshooting action potentials with variation in timing. Also in type II LNs repetitive odor responses were not as stereotypic as in uPNs. Beside response variations within one specific odor, the response to eugenol was remarkably longer than the response to α -ionone indicating a tendency for odor specificity (Fig. 3.11C).

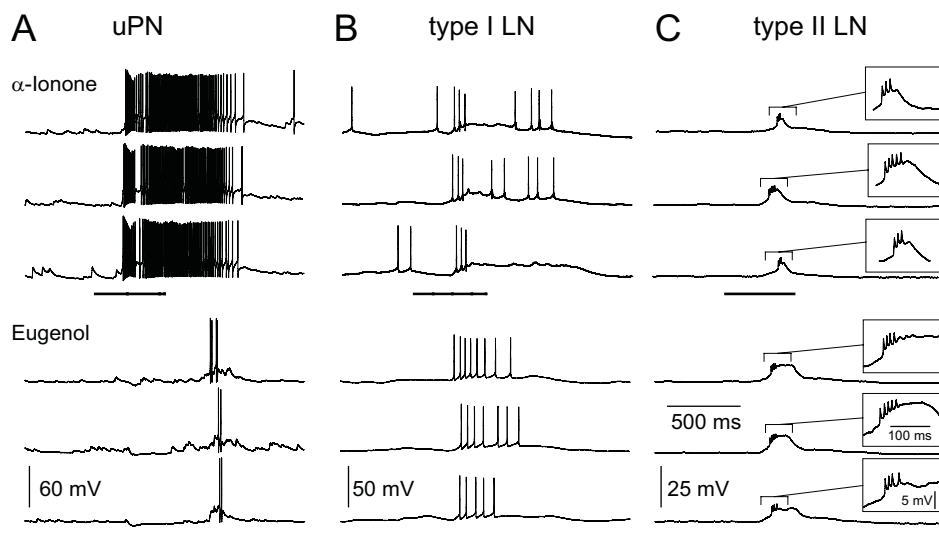


Figure 3.11. Repetitive odor stimulation in uPNs, type I and type II LNs

Whole cell patch-clamp recording of odor responses. Odor stimulation was applied three times with one minute intervals. The bar beneath the recording indicates the opening of the solenoid valve of the stimulation unit (500 ms). A: uPN showed odor specific and robust odor responses. Variation between trials of the same odor was minimal. The response to eugenol in this case is characterized by a hyperpolarization followed by a depolarization and APs. B: Type I LN show less stereotypic and odor specific responses compared to uPNs. The variation between trials is greater compared to the responses of the uPN. C: Typically type II LN show a less odor specific response compared to uPNs. For example response duration variation gets visible comparing the first and the second α -Ionone response.

3.2.2 Uniglomerular projection neurons (uPNs)

A typical example of a uPN is shown in Fig. 3.12. These neurons are typical spiking output neurons and will serve as 'reference' neurons in the following analysis of different types of LNs. They respond to physiological odor stimulation with overshooting action potentials (Fig. 3.12A). Also depolarizing current injection elicited overshooting action potentials (Fig. 3.12B). The EPSPs were only present when the antennal nerve was intact. Voltage-clamp steady state activation protocols from holding potential of -80 mV in 5 mV increasing voltage steps always evoked a combination of TTX sensitive sodium current and a TEA and 4-AP sensitive potassium current (Fig. 3.12C). Biocytin staining of each recorded neuron inside the

ventrolateral cluster showed that exclusively uniglomerular projection neurons were recorded in the ventrolateral cell cluster (Fig. 3.12D). They project their axons through the inner antennocerebral tract to the protocerebrum, innervating the mushroom body calyces and the lateral lobe of the protocerebrum (Fig. 3.12E).

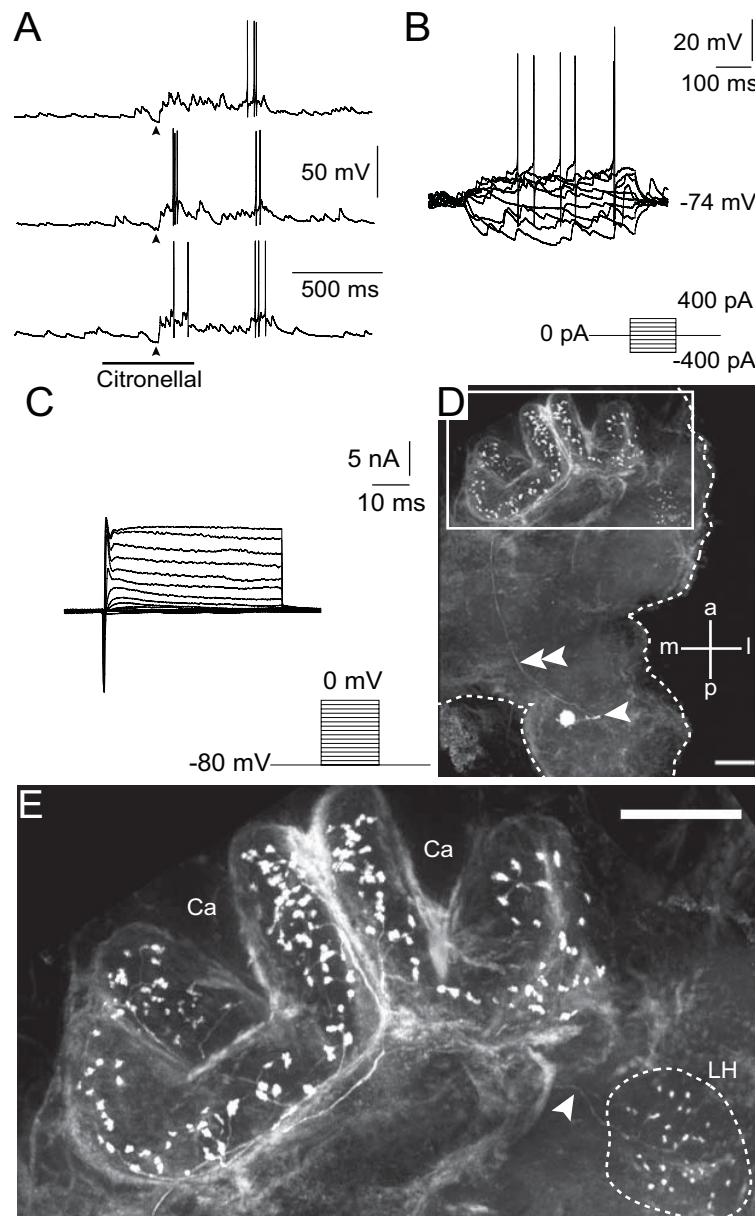


Figure 3.12. Electrophysiological and morphological characteristics of uPNs

Figure 3.12. *A: Odor stimulation in uPNs typically evoked responses consisting of depolarization and hyperpolarization periods, with an odor specific series of overshooting action potentials. In this particular experiment citronellal evoked a brief hyperpolarization (arrowhead). Membrane potential then depolarizes rapidly and two short bursts consisting of 2 - 3 action potentials were recorded. B: Depolarizing current injection elicited overshooting action potentials. Current was injected for 500 ms from -400 pA to 400 pA in 100 pA steps. C: Steady state voltage-clamp activation protocols for 50 ms from a holding potential of -80 mV to 0 mV in 5 mV increments elicited a transient inward current followed by an outward current with a transient and a sustained component. The transient fast inactivating current was identified as a TTX sensitive sodium current. The transient outward current component was blocked by 4-AP application. Its sustained component was eliminated by TEA. Outward currents were identified as potassium currents. D: Morphology of a streptavidin-Alexa 633 stained uPN. Maximum intensity projection of a confocal LSM image stack. The cell body was lost during processing (arrowhead). The neuron branches off to a single glomerular innervation and a neurite running along the inner antennocerebral tract (double arrowheads) to the mushroom body calyces and the lateral lobe of the protocerebrum (framed area). E: Detailed view of the framed area in D showing dense innervation of the mushroom body calyces and a neurite (arrowhead) innervating the lateral lobe of the protocerebrum (area outlined by dotted line). a: anterior; Ca: calyces of the mushroom bodies; l: lateral; LH: lateral lobe of the protocerebrum; m: medial; p: posterior; Scale bar in D and E: 100 μ m*

Mean membrane potential in uPNs was $U_M = -61.4 \pm 9.1$ mV ($n = 14$). Calculating the voltage step over its corresponding negative current injection resulted in a mean membrane resistance of $R_M = 89.6 \pm 39.2$ M Ω ($n = 11$). The values for capacity compensation lead to a value for mean whole cell membrane capacity of $C_M = 22.9 \pm 9.3$ pF ($n = 15$).

3.2.3 Type I local interneurons (type I LNs)

A typical example of a type I LN is shown in Fig. 3.13. In this neuron type, as in the uPNs, action potentials could be elicited by odor stimuli (Fig. 3.13A) and by depolarizing current injection (Fig. 3.13B). Accordingly a voltage-clamp activation protocol as described above (chapter 3.2.2) elicited sodium carried inward currents and transient and sustained outward currents carried by potassium. Complex structure and geometry of these interneurons lead to multiple inward and outward current peaks (Fig. 3.13C). In contrast to uPNs the arborizations of the LNs remain within the antennal lobe. The type I LNs innervate many but not all glomeruli

(multiglomerular), the intraglomerular innervation was homogeneous, with interglomerular differences in the innervation density (intraglomerular homogeneous and interglomerular heterogeneous innervation) (Fig. 3.13D, *inset*). Mean membrane potential in type I LNs was measured as $U_M = -53.0 \pm 7.4$ mV ($n = 16$). Calculating the voltage step over negative current injection lead to a mean membrane resistance $R_M = 50.6 \pm 22.3$ M Ω ($n = 13$). The somata of the type I LNs were larger than uPNs with a whole cell capacitance of $C_M = 36.8 \pm 16.3$ pF ($n = 19$).

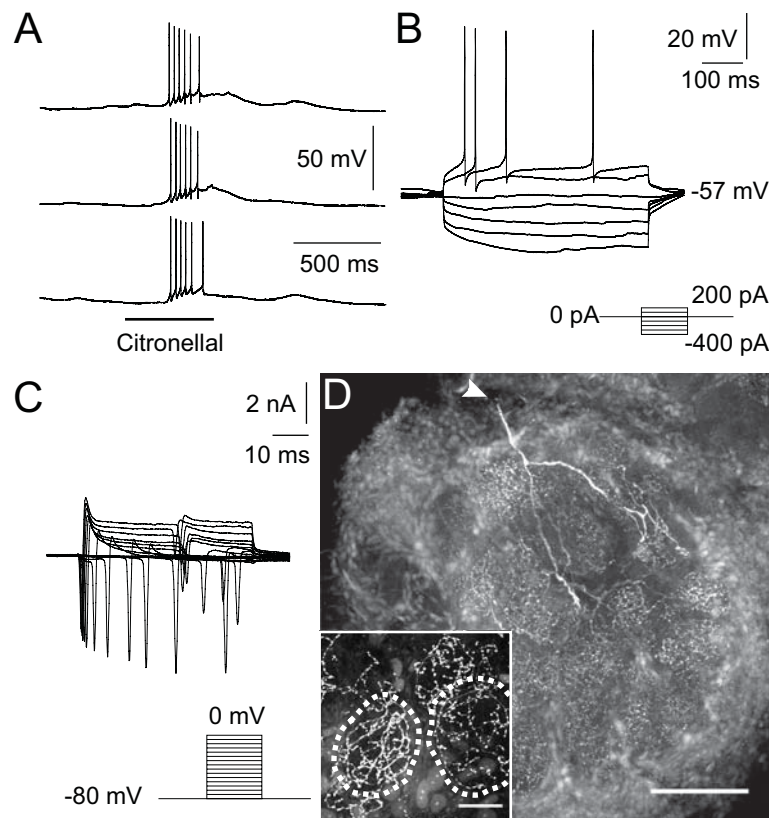


Figure 3.13. Electrophysiological and morphological characteristics of type I LNs

For details see legend of figure 3.12 A: Whole cell patch-clamp recording from a type I LN during odor stimulation with a 500 ms puff of citronellal. Overshooting action potentials were elicited B: Depolarizing current injection elicited overshooting action potentials. C: Voltage-clamp activation protocols elicited transient sodium carried inward currents followed by an outward currents with a transient and sustained component. D: Morphology of a Streptavidin-Alexa 633 stained type I LN in fixed wholemount tissue. Maximum intensity projection of a confocal LSM image stack. Multiglomerular innervation, with variance in density in individual glomeruli (*inset*). The cell body was lost during processing (*arrowhead*). Scale bar in D: 100 μ m; D *inset*: 20 μ m.

3.2.4 Type II local interneurons (type II LNs)

A completely different physiological and morphological phenotype was found in type II LNs. Figure 3.14 shows a typical example of a type II LN. In contrast to the uPNs and the type I LNs, in these neurons sodium action potentials could not be elicited, neither with odor stimulation (Fig. 3.14A) nor with current injection (Fig. 3.14B).

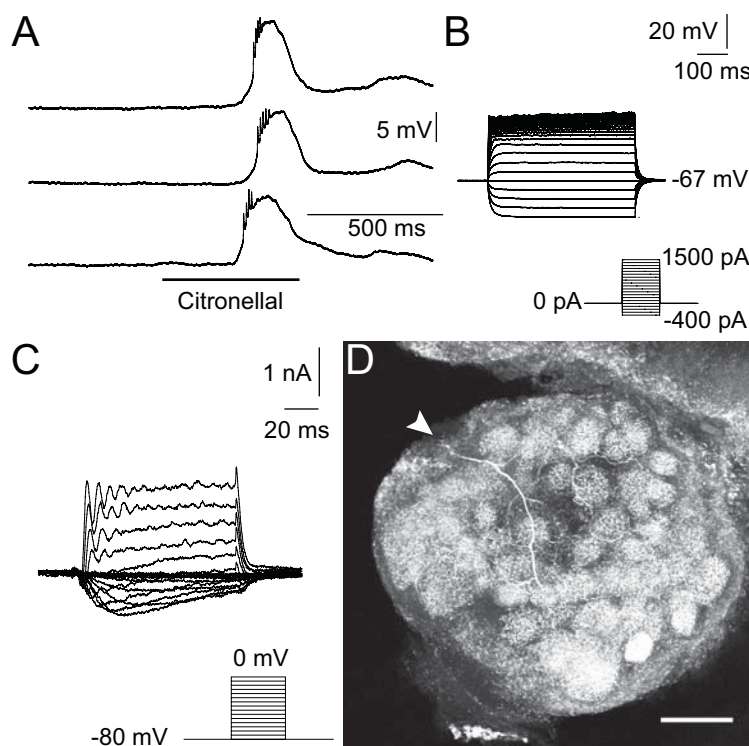


Figure 3.14. Electrophysiological and morphological characteristics of type II LN

A: Whole cell patch-clamp current-clamp recording during repetitive odor stimulation of the antenna with citronellal. Typically for this neuron type odors evoked ~ 10 mV depolarization, no sodium driven action potentials as in uPNs or type II LNs were elicited. In some experiments small 'spikelets' riding on the depolarization were recorded. B: Current-clamp recording during injection of 500 ms current pulses from -400 pA to 1500 pA in 100 pA steps. The type II LNs never generated spikes when depolarized even with large current amplitudes, but showed strong rectification during injection of depolarizing currents. C: Voltage-clamp activation; the neuron was depolarized for 50 ms from a holding potential of -80 mV to 0 mV in 5 mV increments. A sustained inward current followed by an outward current with a transient and a sustained component were elicited. Typically no sodium currents were elicited D: Morphology of a streptavidin-Alexa 633 stained type II LN. Maximum intensity projection of a confocal LSM image stack. The cell body was lost during processing (arrowhead). Typical for type II LNs all glomeruli were similarly innervated. Scale bar in D: 100 μ m

As mentioned above, odors that elicited overshooting action potentials in uPNs and type I LNs, only elicited slow depolarization in type II LNs, in some cases with 'spikelets' riding on top of these events (Fig. 3.14A). In voltage-clamp activation protocols at the type II LN soma, no transient inward currents were activated. However, it is remarkable, that in the unblocked state there is a sustained inward current (Fig. 3.14C). Inward currents were similar to voltage activated calcium currents recorded previously in dissociated AL neurons. Usually voltage activated calcium currents are masked by large voltage activated potassium currents. In contrast to type I LNs, the type II LNs innervate all glomeruli (omniglomerular) and the glomeruli were similarly innervated, in some type II LNs the innervation was locally restricted within glomeri (interglomerular and intraglomerular homogeneous innervation) (Fig. 3.14D; see also Fig. 3.21, C - F). Mean membrane potential was in between the values for uPN and type I LN (type II $U_M = -56.9 \pm 11.3$ mV; $n = 24$). The mean membrane resistance was calculated as $R_M = 37.6 \pm 14.9$ M Ω ($n = 22$). The large soma sizes were causing large membrane capacity values of $C_M = 87.7 \pm 38.7$ pF ($n = 29$).

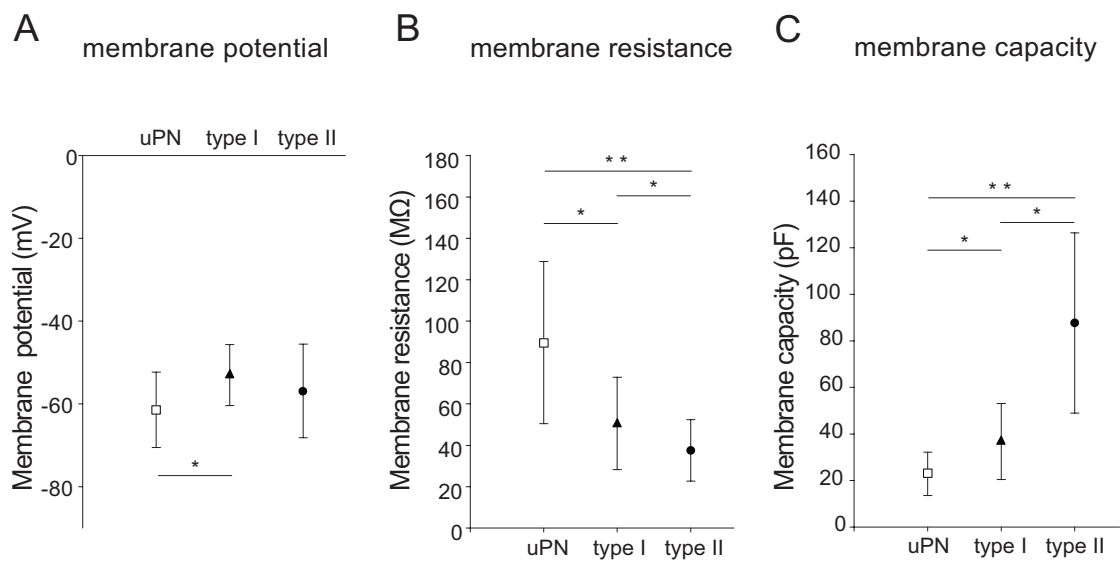
3.2.5 Comparison between uPNs, type I LNs and type II LNs

In summary it is now possible to differentiate three types of central olfactory interneurons by their morphological and physiological properties: uPNs, type I LNs and type II LNs. uPNs innervate one glomerulus, their somata are located in the ventrolateral cluster, and they project to the mushroom bodies and to the lateral lobe of the protocerebrum. Type I LNs innervate many glomeruli (multiglomerular) and the innervation pattern inside each glomerulus is homogeneous, but some glomeruli are more innervated and some are less innervated (interglomerular heterogeneous). Type II LNs innervate all glomeruli (omniglomerular) in a similar way, whereas differentiation between 2 subtypes was possible: type IIa LNs innervate the glomeruli

intraglomerular homogeneous, type IIb LNs show local innervation of each glomerulus (Fig. 3.21, C - F). The basic physiological parameters, such as U_M , R_M , C_M are summarized in Table 1. The comparison of mean values are illustrated in Fig. 3.9. Odor stimulation as well as depolarizing current injection elicited sodium carried overshooting action potentials in uPNs and type I LNs, whereas type II LNs never reacted with overshooting action potentials. Confirming the physiological relevance of these findings, in the unblocked state the voltage activated currents in type I and type II LNs were completely different. Again, the uPNs, as known 'reference' neuron groups, showed up typical combination of sodium carried inward current and potassium carried - transient and sustained - outward currents. Whereas in type I LNs similar current components were present, in type II LNs the current profile was completely different. Transient inward currents were not detectable, but a sustained inward current was activated (Fig. 3.14C). This voltage activated current reminded of voltage activated calcium currents as measured in vitro and in situ before (Fig. 3.5 and Fig. 3.8). Usually voltage activated potassium currents cover the voltage activated calcium currents in the unblocked state. Two explanations for this result were possible. First, in this LN subpopulation potassium currents were smaller than in other preparations and/or second, the voltage activated calcium currents were relatively larger compared to data formerly described in olfactory interneurons. In the following voltage activated calcium currents were isolated in identified neuron types to clarify the differences in physiological behavior during odor stimulation, current clamp and voltage clamp activation protocols.

Table 1: Summary of physiological parameters in uPN, type I LN and type II LN.

	uPN	type I LN	type II LN
odor responses	+	+	+
sodium APs	+	+	-
C_{slow} (pF)	22.9 ± 9.3 $n = 15$	36.8 ± 16.3 $n = 19$	87.7 ± 38.7 $n = 29$
U_M (mV)	-61.4 ± 9.1 $n = 14$	-53.0 ± 7.4 $n = 16$	-56.9 ± 11.3 $n = 24$
R_M (M Ω)	89.6 ± 39.2 $n = 11$	50.6 ± 22.3 $n = 13$	37.6 ± 14.9 $n = 22$
glomerular innervation	uni-glomerular	multi-glomerular	omni-glomerular

**Figure 3.15. Membrane-potential, -resistance and -capacity in uPN, type I and type II LNs**

For details see also Table 1. A: uPN and type I LN had different mean membrane potential, the different local interneuron groups had similar membrane potentials; B: uPNs had the largest membrane resistance, followed by type I LNs and type II LNs. C: The three olfactory interneuron types had significantly different soma sizes reflected in their significantly different membrane capacity values. Asterisks mark the level of significance: (*) $p \leq 0.05$, (**) $p < 0.001$.

3.3 Voltage activated calcium currents in identified neuron groups

Unblocked whole cell currents and the differences in physiological properties suggested differences in voltage activated calcium currents in different types of olfactory interneurons. Whole cell voltage-clamp recordings were used to characterize voltage activated Ca^{2+} currents in identified olfactory interneurons in the antennal lobe of *P. americana*. For final identification and characterization, each recorded neuron was filled with biocytin, stained with streptavidin-*Alexa 633* and scanned under a confocal microscope, to confirm the neuroanatomical and morphological classification.

To analyze I_{Ca} , the intact brain preparation was superfused with saline containing 10^{-7} M TTX, 4×10^{-3} M 4-AP, and 3×10^{-2} M TEA. In the pipette solution K^+ was replaced by Cs^+ (for more details see also chapter 2.4.).

3.3.1 I/V-relationship of calcium current activation

The characteristics of I_{Ca} are shown in Fig. 3.16. - 3.20. The I/V relationship of the peak currents was determined by increasing voltage steps (50 ms, 5 mV) between -80 mV and 40 mV from a holding potential of -80 mV (Fig. 3.16A). During a depolarizing voltage step I_{Ca} activated relatively quickly and decayed during a maintained voltage step (Fig. 3.16A). In uPNs I_{Ca} started to activate with voltage steps more depolarized than -40 mV (Fig. 3.16B). The mean peak currents reached its maximum (I_{max}) of 1.4 ± 0.4 nA (Fig. 3.16B) at 5.8 ± 4.9 mV ($n = 12$) and decreased during more positive test pulses as they approached the calcium equilibrium potential. The mean peak current density was 54.9 ± 16.5 pA/pF (Fig. 3.16C). A similar I/V-relationship was observed in type I LNs. I_{Ca} started to activate with voltage steps more depolarized than -40 mV (Fig. 3.16B). The mean peak currents reached its maximum (I_{max}) of 1.0 ± 0.3 nA (Fig. 3.16B) at 9.0 ± 6.1 mV ($n = 10$), with a mean current density of 30.4 ± 14.8 pA/pF

(Fig. 3.16C). In type II LNs I_{Ca} started to activate with voltage steps more depolarized than -55 mV (Fig. 3.16B). The mean peak currents reached its maximum (I_{max}) of 3.0 ± 1.0 nA (Fig. 3.16B) at -7.5 ± 7.2 mV ($n = 12$) and decreased during more positive test pulses as they approached the calcium equilibrium potential. Calculating the mean current amplitude over the whole cell capacitance put the large difference of I_{Ca} amplitudes in perspective. Type II LNs had a mean current density of 31.9 ± 9.7 pA/pF (Fig. 3.16C).

The parameters for maximum tail current, maximum tail current densities and the voltage for maximum tail current activation are summarized in Table 2. The comparison of mean values is illustrated in Fig. 3.17. Type II LNs showed a significantly larger maximum current compared to the uPNs and type I LNs (Fig. 3.17A). In relation to each cell capacitance uPNs were set up with the largest current densities (I_{dens} uPN vs. I_{dens} type I LN: $P < 0.001$; t-test; I_{dens} uPN vs. I_{dens} type II LN: $P < 0.001$; t-test) caused by their relatively small soma size (C_M uPN: 22.9 ± 9.3 pF) but the current densities inside different local interneuron subpopulations were in the same range (see Fig. 3.17B). The mean voltage at maximum current ($E_{I_{max}}$) in uPNs and type I LNs in contrast to type II LNs were significantly different ($E_{I_{max}}$ uPN = 5.77 ± 4.94 mV; $E_{I_{max}}$ type I LN = 9 ± 6.15 mV; $E_{I_{max}}$ type II LN = -7.5 ± 7.23 mV; $E_{I_{max}}$ uPN vs. $E_{I_{max}}$ type II LN: $P < 0.001$; t-test; $E_{I_{max}}$ type I LN vs. $E_{I_{max}}$ type II LN: $P < 0.001$; t-test; Fig. 3.17C). This difference in voltage dependence is analyzed in more detail in the tail current analysis.

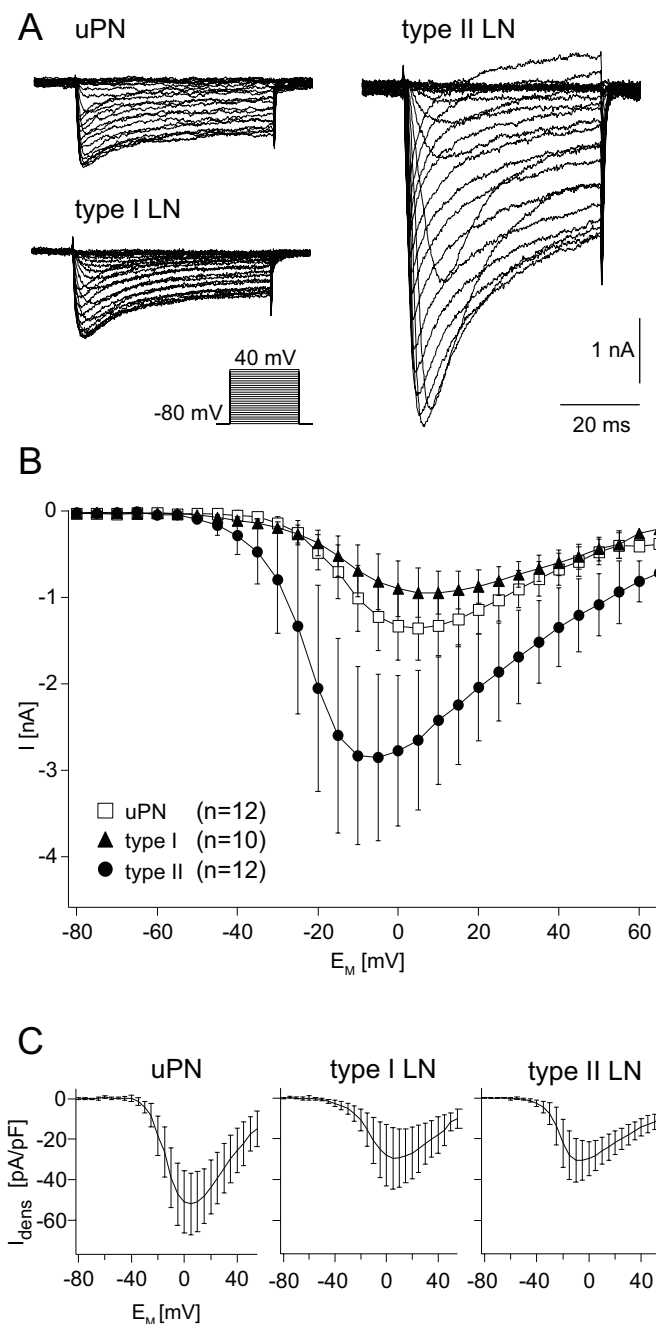
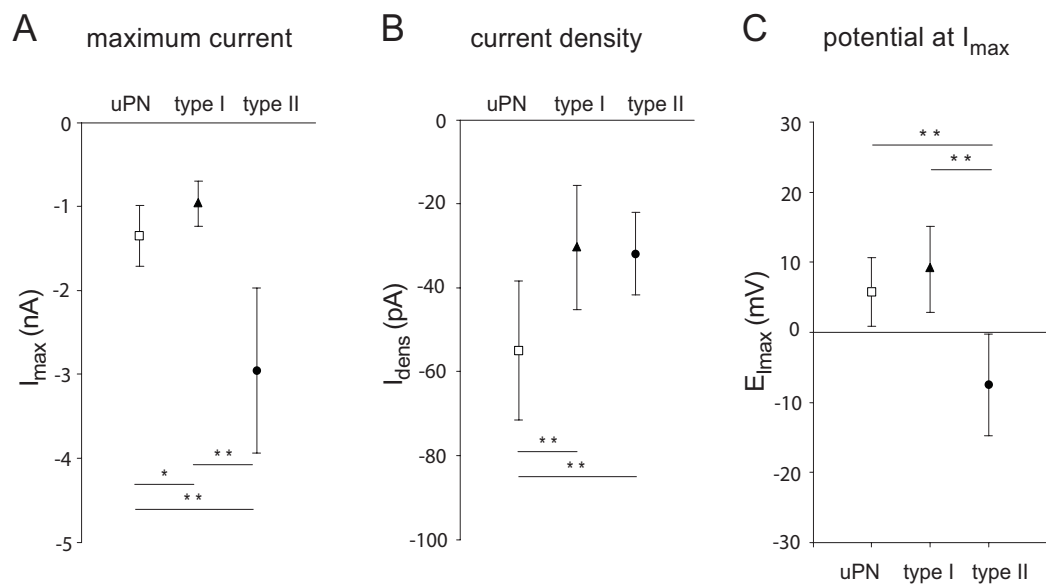


Figure 3.16. Steady state activation of calcium currents in uPNs, type I and type II LNs

A: Calcium currents from an uPN, a type I and a type II LN. The neurons were depolarized for 50 ms from a holding potential of -80 mV to 40 mV in 5 mV increments. Calcium currents were isolated by blocking voltage activated sodium and potassium currents. Notice that the absolute current amplitude is much greater in type II LN than in uPN or type I LN. *B:* I/V relation of calcium currents recorded from uPN, type I and type II LN. Mean absolute maximum current amplitudes: I_{max} uPN = 1.35 ± 0.37 nA; I_{max} type I LN = 0.96 ± 0.27 nA; I_{max} type II LN = 2.95 ± 0.99 nA. *C:* Current density over voltage relation of calcium currents recorded from uPN, type I and type II LN. Mean current density I/C_M uPN = 54.91 ± 16.54 pA/pF; I/C_M type I LN = 30.45 ± 14.81 pA/pF; I/C_M type II LN = 31.86 ± 9.77 pA/pF.

Table 2: Summary of voltage activated calcium steady state activation.

	uPN	type I LN	type II LN
Maximum current (nA)	1.35 ± 0.37 $n = 12$	0.96 ± 0.27 $n = 10$	2.95 ± 0.99 $n = 12$
Current density (pA/pF)	54.9 ± 16.5 $n = 12$	30.4 ± 14.8 $n = 10$	31.9 ± 9.7 $n = 12$
Potential at maximum current (mV)	5.8 ± 4.9 $n = 12$	9.0 ± 6.1 $n = 10$	-7.5 ± 7.2 $n = 12$

**Figure 3.17. Overview of calcium steady state activation parameters**

For details see Table 2; A: Type II LNs had significantly larger calcium currents compared to type I LNs and uPNs. B: Calculating the peak currents over the corresponding whole cell capacitance put the large difference of I_{Ca} amplitude in perspective. uPNs had the largest current densities, whereas LN subtypes had similar current density values. C: Type II LNs showed a hyperpolarized potential for maximum current activation, compared to uPNs and type I LNs. Asterisks mark the level of significance: (*) $p \leq 0.05$, (**) $p < 0.001$.

3.3.2 Tail current analysis

The voltage dependence of activation of I_{Ca} was determined in detail from tail currents that are independent of the changing driving force during the series of voltage pulses. Tail currents were evoked by 5 ms voltage steps from -80 mV holding potential to 50 mV in 10 mV increments (Fig. 3.18A). The I/V relations were fit to a first-order Boltzmann equation (eq. 2; Fig. 3.18B). In uPNs, the tail currents had a maximum of 2.1 ± 0.6 nA ($n = 12$). This corresponds to a mean current density of 89.0 ± 33.7 pA/pF. The mean voltage for half-maximal activation ($V_{0.5(act)}$) was calculated as $V_{0.5(act)} = -10.6 \pm 3.4$ mV ($s = 8.5 \pm 1.8$; $n = 12$; Fig. 3.18B).

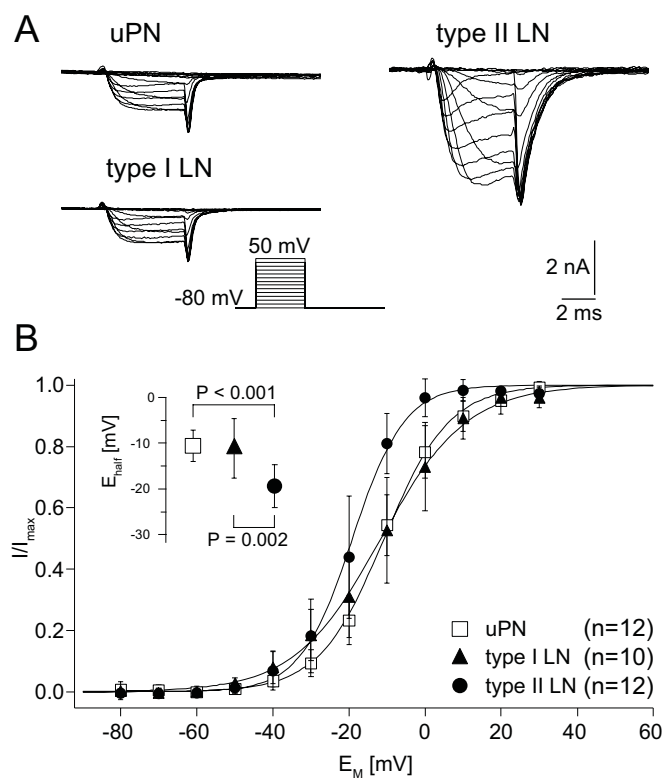


Figure 3.18. Quantification of half-maximal calcium tail current activation

A: Tail currents of uPN, type I and type II LN. Tail currents were elicited with 5 ms long voltage pulses from -80 mV to 50 mV in 10 mV increments. B: I/V -plot of normalized tail currents. The tail currents were normalized to their maximum current (I_{max}) and plotted against the voltage of the command potential. The plot was fit with the Boltzmann equation (eq. 2). The half-maximal activation potentials in uPN and type I LN were significantly different compared to type II LN.

In type I LNs the tail currents had a maximum of 1.4 ± 0.6 nA ($n = 10$), with a mean current density of 45.8 ± 22.3 pA/pF. The I/V relation of the tail currents was fit by a first-order Boltzmann equation with a mean voltage for half-maximal activation ($V_{0.5(act)}$) of -11.1 ± 6.5 mV ($s = 10.0 \pm 2.3$; $n = 10$; Fig. 3.18B). In type II LNs the tail currents had a maximum of 3.3 ± 1.2 nA ($n = 12$), with a mean current density of 35.7 ± 11.0 pA/pF. The I/V relation of the tail currents was fit by a first-order Boltzmann equation with a mean voltage for half-maximal activation ($V_{0.5(act)}$) of -19.4 ± 4.7 mV ($s = 6.4 \pm 2.3$; $n = 12$; Fig. 3.18B). The tail current activation parameters, such as maximum tail current, current densities, half maximal activation and slope factor are summarized in Table 3 and the comparison of the mean values are illustrated in Fig. 3.19. Type II LNs again had the largest absolute current amplitude with 3.3 ± 1.2 nA. In relation to their large capacity values the current density was again in the same range as in type I LNs (tail current density type II LNs 35.7 pA/pF; type I vs. type II: $P = 0.186$). Differences in voltage dependence become obvious comparing the Boltzmann equation parameters. Whereas calcium currents in uPNs and type I LNs had a similar potential at half-maximal tail current (see Table 3), in type II LNs the potential for half-maximal tail current activation was significantly shifted to more negative potentials.

Table 3: Summary of tail current parameters

	uPN	type I LN	type II LN
Maximum tail current (nA)	2.1 ± 0.6 $n = 12$	1.4 ± 0.6 $n = 10$	3.3 ± 1.2 $n = 12$
Tail current density (pA/pF)	89.0 ± 33.7 $n = 12$	45.8 ± 22.3 $n = 10$	35.7 ± 11.0 $n = 12$
Potential at half-maximal tail current (mV)	-10.6 ± 3.4 $n = 12$	-11.1 ± 6.5 $n = 10$	-19.4 ± 4.7 $n = 12$
Tail current slope factor s	8.5 ± 1.8 $n = 12$	10.0 ± 2.3 $n = 10$	6.4 ± 2.3 $n = 12$

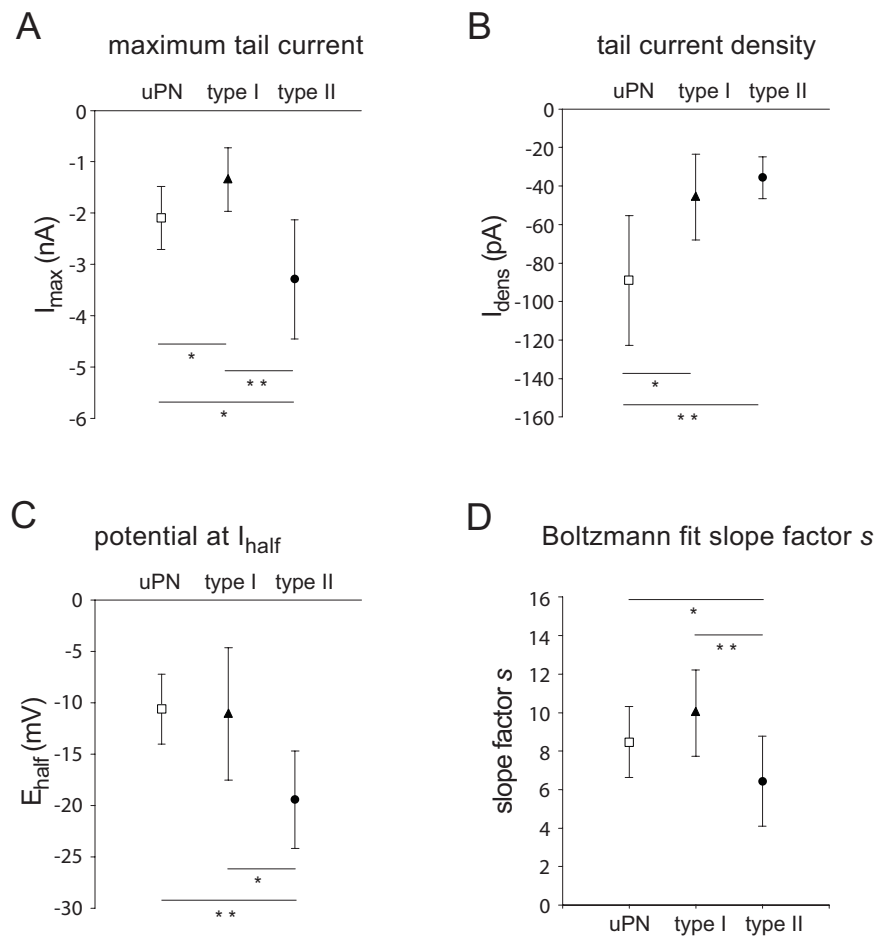


Figure 3.19. Parameters for tail current activation in uPN, type I and type II LNs

For details see Table 3. A: type II LNs had the largest tail currents, followed by uPNs and type I LNs; B: PNs were equipped with the largest current density. C: type II LNs had a significantly more hyperpolarized potentials for half-maximal activation. D: Boltzmann fit slope factor s was also significantly different in type II LNs compared to uPNs and type I LNs. Asterisks mark the level of significance: (*) $p \leq 0.05$, (**) $p < 0.001$.

3.3.3 Steady state inactivation

Steady state inactivation of I_{Ca} was measured from a holding potential of -80 mV. Prepulses (500 ms) were delivered in 5 mV increments from -95 mV to -5 mV, followed by a 50 ms test-pulse to -5 mV (Fig. 3.20A). The peak current amplitudes during testpulses were determined and were plotted against the testpulse potentials

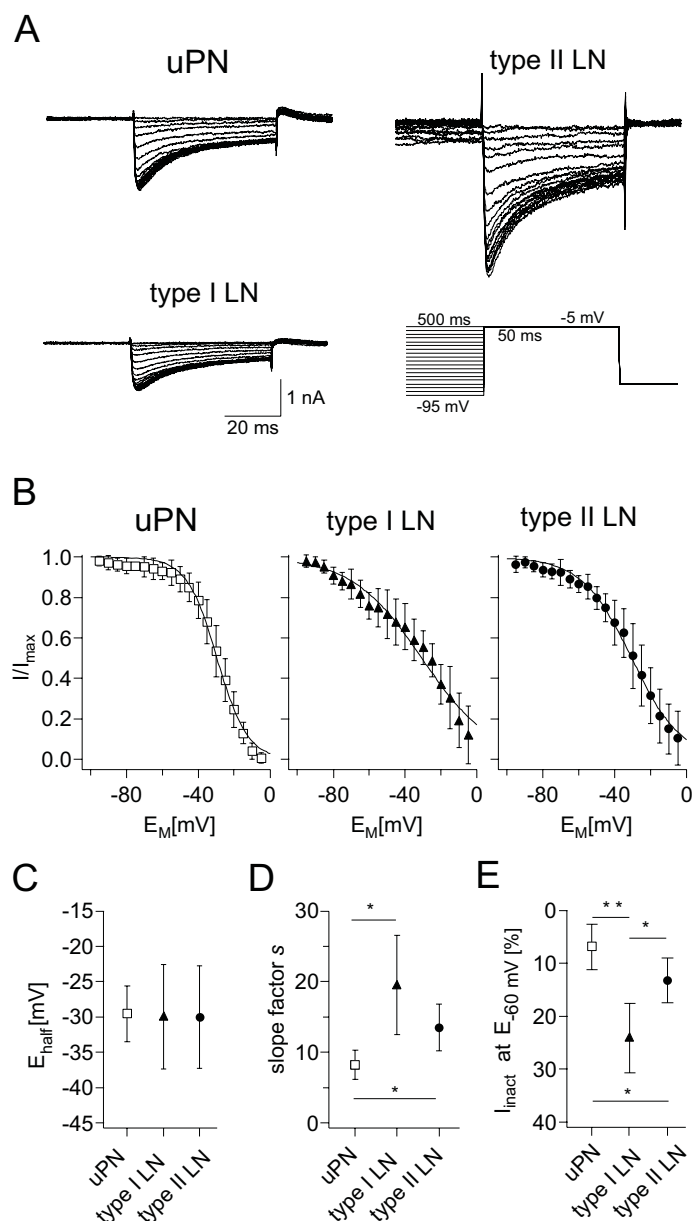


Figure 3.20. Steady state inactivation of voltage activated calcium currents

A: Calcium currents were elicited during a 50 ms testpulse to -5 mV, increasing the prepulsepotential in 5 mV steps from -95 mV to -5 mV. Prepulse duration was 500 ms. *B:* Mean I/V relations of steady state inactivation of peak I_{Ca} . The curves are fits to first-order Boltzmann equations (eq. 2), the parameters E_{half} and inactivation rate are plotted in C and D. *C:* Potential for halfmaximal inactivation was very similar in all investigated neuron types *D:* Inactivation rate: The differences in the slope factor s of the Boltzmann fits indicated the different inactivation kinetics. *E:* Amount of steady state inactivation at -60 mV demonstrated that the LNs inactivated at more hyperpolarized prepulse potentials compared to uPNs. For details see Table 4. Asterisks mark the level of significance: (*) $p \leq 0.05$, (**) $p < 0.001$.

(Fig. 3.20B). In uPNs steady state inactivation started around prepulse potentials more positive than -60 mV and increased with the amplitude of the depolarizing prepulse (Fig. 3.20, A and B). The peak current over prepulse potential relationship was fit with a first order Boltzmann equation (eq. 2) with a voltage for half-maximal inactivation ($V_{0.5(inact)}$) of -29.6 ± 4.0 mV ($s = 8.5 \pm 1.8$; $n = 12$; Fig. 3.20, B-D). In type I LNs steady state inactivation started with prepulse potentials around -80 mV (Fig. 3.20, A and B). The I/V relationship was also fit with a first order Boltzmann equation (eq. 2) with a voltage for half-maximal inactivation ($V_{0.5(inact)}$) of -30.0 ± 7.4 mV ($s = 10.0 \pm 2.3$; $n = 10$; Fig. 3.20, B-D). In type II LNs steady state inactivation started with prepulse potentials around -70 mV (Fig. 3.20, A and B). The parameters for steady state inactivation were $V_{0.5(inact)} = -30.0 \pm 7.2$ mV and $s = 6.4 \pm 2.3$ ($n = 12$; Fig. 3.20, B-D). The calcium current inactivation parameters are summarized in Table 4 and the comparison of the values are illustrated in Fig. 3.20, C-E.

Table 4: Summary of inactivation parameters

	uPN	type I LN	type II LN
Potential at half-maximal inactivation (mV)	-29.6 ± 4.0 $n = 12$	-30.0 ± 7.4 $n = 10$	-30.0 ± 7.2 $n = 12$
Steady state inactivation slope factor s	8.5 ± 1.8 $n = 12$	10.0 ± 2.3 $n = 10$	6.4 ± 2.3 $n = 12$
Inactivation at prepulse potential -60 mV (%)	6.9 ± 4.3 $n = 12$	24.1 ± 6.6 $n = 10$	13.3 ± 4.2 $n = 12$

Mean values for half-maximal inactivation were not significantly different, but the slope factor s indicated the different inactivation characteristics [uPN vs. type I LN: $P < 0.001$ (MWRS-test); uPN vs. type II LN: $P = 0.003$ (MWRS-test)]. Comparing the percentage of inactivation at prepulse potential -60 mV (Fig. 3.20E) indicates the different inactivation kinetics. In contrast to the LN types uPNs inactivate relatively

late, at the prepulse potential of -60 mV only $6.9 \pm 4.3\%$ ($n = 12$) of the previously measured maximum current was inactivated. LNs inactivate relatively early, for instance at the prepulse potential of -60 mV there is $24.1 \pm 6.6\%$ ($n = 10$) of the previously measured I_{max} inactivated and in type II LNs there was $13.3 \pm 4.2\%$ ($n = 12$) inactivated.

3.3.4 Characterization of calcium currents in type II LN subpopulations

Type II LNs are mainly characterized by their physiological and morphological properties: the omniglomerular innervation and the lack of voltage activated sodium currents (Fig. 3.14). As indicated earlier, the type II LNs can be further differentiated by their intraglomerular innervation: type IIa LNs show a homogeneous intraglomerular innervation (Fig. 3.21, C and D), whereas type IIb LNs innervate the glomeruli locally restricted (Fig. 3.21, E and F).

A careful electrophysiological analysis of these morphologically different types revealed also physiological differences in these types. The recordings suggest that the type IIa LNs showed slow depolarizations as a reaction to odor stimulation, sometimes with 'spikelets' riding on top of it (as shown in Fig. 3.14A), whereas type IIb LNs only showed slow depolarizations without any 'spikelets' (data not shown). These response properties also correlate to differences in cellular properties in detail described as follows.

For this study electrophysiological parameters from 18 type IIa and 11 type IIb LNs were analyzed and summarized in Table 5. The comparison of the mean values is illustrated in Fig. 3.22. Focusing on the mean membrane potentials of the different LN types it became apparent that type IIa LNs were more positive than the type IIb LNs (U_M type IIa LNs = -52.1 ± 9.2 mV; $n = 16$; U_M type IIb LNs = -66.4 ± 9.2 mV; $n = 8$; $P = 0.002$; t -test; Fig. 3.22A).

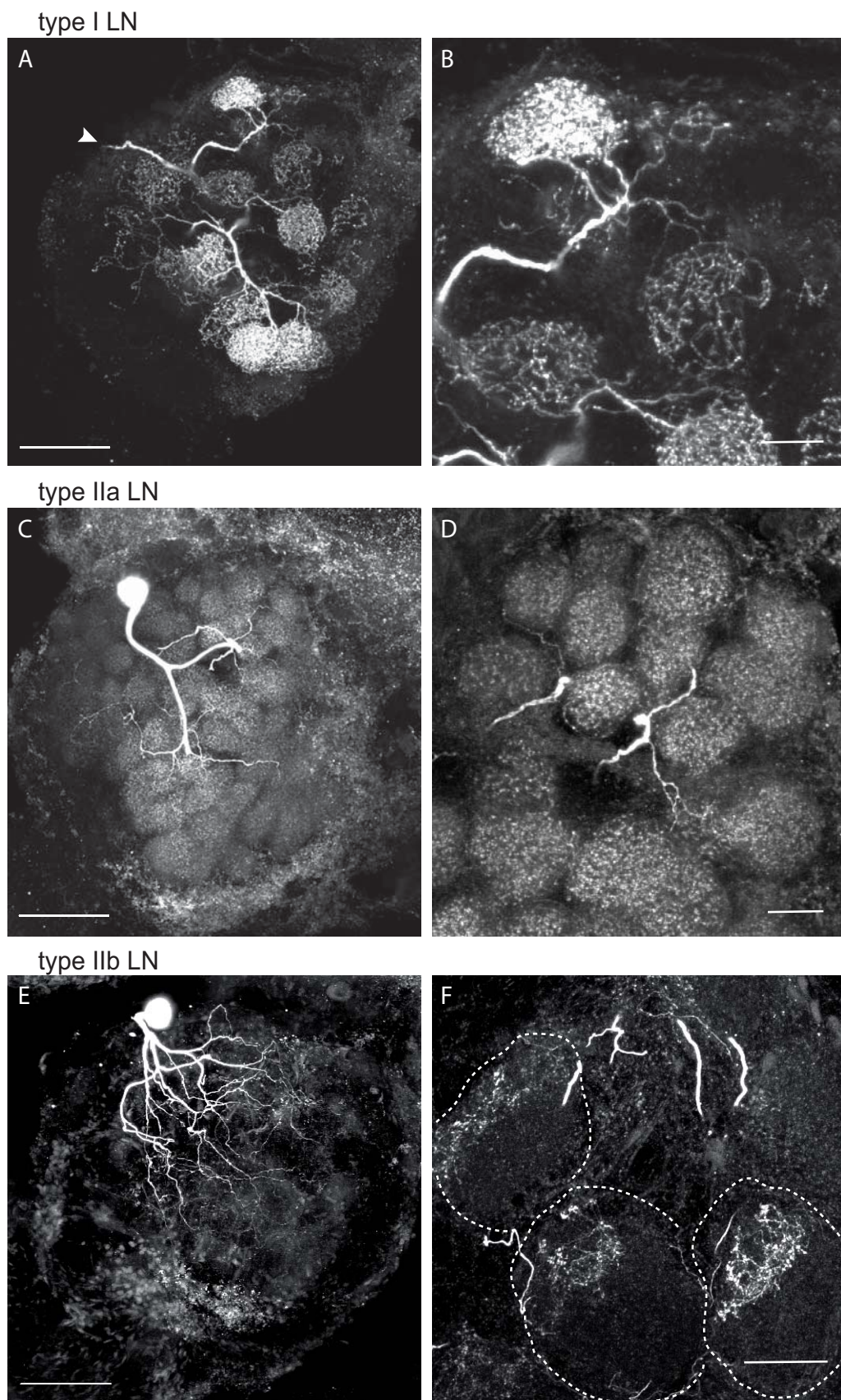


Figure 3.21. Morphological subtypes of LNs

Figure 3.21. A: type I LN: Projection of a confocal stack through a streptavidin/biocytin stained type I LN. Many but not all glomeruli are innervated (multiglomerular). B: Glomeruli are heterogeneously dense innervated; C: Projection of a confocal stack through a streptavidin/biocytin stained type IIa LN. D: Glomeruli are homogeneously innervated. E: Projection of a confocal stack through a streptavidin/biocytin stained type IIb LN. F: Glomeruli are locally restricted innervated. Scale bars left: 20 μm ; right: 100 μm .

Table 5: Summary of physiological parameters in type IIa and type IIb LNs

	type IIa LN	type IIb LN
Membrane Potential (mV)	-52.1 ± 9.2 $n = 16$	-66.4 ± 9.2 $n = 8$
Membrane Resistance (M Ω)	35.2 ± 15.0 $n = 14$	41.8 ± 14.5 $n = 8$
Membrane Capacitance (pF)	96.4 ± 45.3 $n = 18$	73.4 ± 18.4 $n = 11$

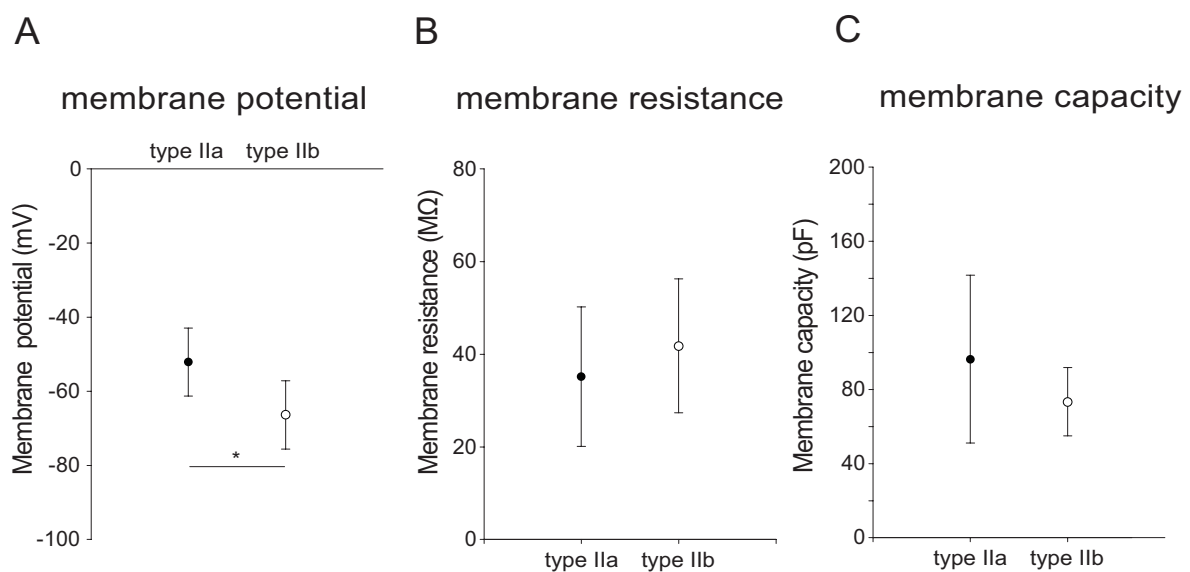


Figure 3.22. Membrane-potential, -resistance and -capacity, in type II LN subtypes

For details see Table 5. Mean membrane capacity and mean membrane resistance in type IIa and type IIb LNs were in the same range. A: Mean membrane potential in type IIa LNs was significantly more positive compared to mean membrane potential in type IIb LNs. B-C: membrane resistance and whole cell membrane capacitance were not significantly different. Asterisks mark the level of significance: (*) $p \leq 0.05$.

The mean membrane resistances in these neurontypes were not significantly different (R_M type IIa LNs = 35.2 ± 15.0 M Ω ; R_M type IIb LNs = 41.8 ± 14.5 M Ω ; $P = 0.324$; t-test;

Fig. 3.22B). According to their large soma sizes, their membrane capacity values were also similar (C_M type IIa LNs = 96.4 ± 45.3 pF, $n = 14$; C_M type IIb LNs = 73.4 ± 18.4 pF, $n = 8$; $P = 0.144$; MWRS-test; Fig. 3.22C).

Voltage activated calcium currents in type IIa and type IIb LNs

The fact that type II LNs don't show any voltage activated sodium currents lead to the assumption that the variability in their odor response can be caused by differences in voltage activated calcium currents. Beside their significantly different membrane potentials and their different glomeruli innervation, analyzing I_{Ca} activation discovered significant differences in calcium current activation characteristics.

The characteristics of I_{Ca} are shown in Fig. 3.23. The I/V relationship of the peak currents was determined by increasing voltage steps (50 ms, 5 mV) between -80 mV and 40 mV from a holding potential of -80 mV (Fig. 3.23A). During a depolarizing voltage step I_{Ca} in type IIa LNs activated relatively quickly and decayed fast during a maintained voltage step. I_{Ca} started to activate with voltage steps more depolarized than -60 mV. The mean peak currents reached its maximum (I_{max}) of 3.5 ± 0.9 nA (Fig. 3.23B) at -8.3 ± 8.2 mV ($n = 6$) and decreased during more positive test pulses as they approached the calcium equilibrium potential. The mean current density was 30.9 ± 7.1 pA/pF (Fig. 3.23B).

In type IIb LNs I_{Ca} activated quickly, but decayed relatively slow during a maintained voltage step (Fig. 3.23A). I_{Ca} started to activate with voltage steps more depolarized than -50 mV. The mean peak currents reached its maximum (I_{max}) of 2.4 ± 0.7 nA at -6.6 ± 6.8 mV ($n = 6$) with a mean current density of 32.8 ± 12.5 pA/pF (Fig. 3.23B).

The parameters for calcium I/V -relation are summarized in Table 6. A comparison of mean values is illustrated in Fig. 3.24.

While there were no differences in current density amplitudes and potentials at maximum currents, there were differences in voltage dependence of activation. To quantify the amount of current activation at a relatively negative testpulse potential, currents at testpulse potential of -35 mV were analyzed in more detail (Table 7). A comparison of peak current amplitude, current density and normalized currents over maximum currents at -35 mV are illustrated in Fig. 3.25.

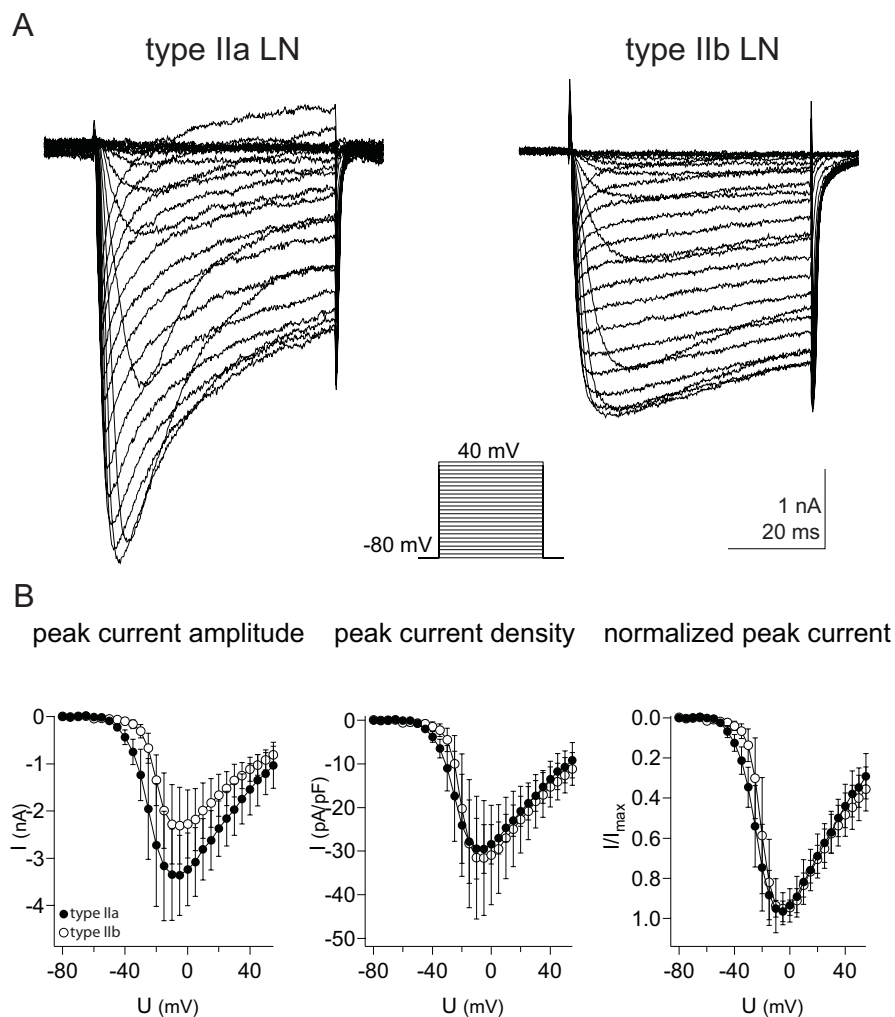
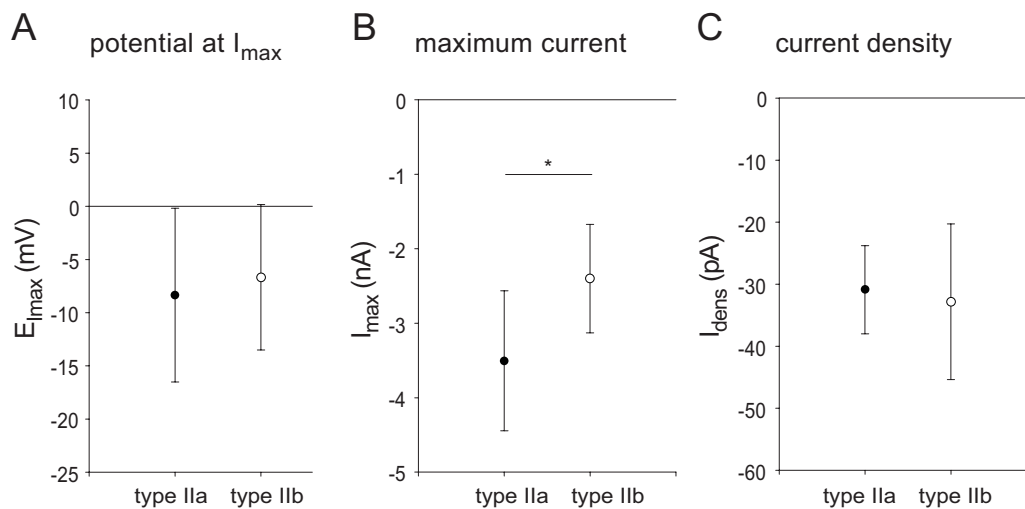


Figure 3.23. Steady state activation of calcium currents in type IIa and type IIb LNs

A: The cells were held at -80 mV. Voltage activated calcium currents were evoked by 50 ms voltage steps from -80 mV to 40 mV in 5 mV steps. (B) Peak current amplitude in type IIa LNs was significantly larger ($P = 0.046$). According to their membrane capacitance values, the maximum peak current densities were in the same range ($P = 0.746$). Potential at I_{max} was also in the same range ($P = 0.709$, t -test). However, normalizing the peak currents over I_{max} indicate, that type IIa LNs activate at more positive testpulse potentials than type IIb LNs.

Table 6: Summary of VGCC steady state activation parameters in type IIa and type IIb LNs

	type IIa LN	type IIb LN
Maximum current (nA)	3.50 ± 0.94 $n = 6$	2.40 ± 0.73 $n = 6$
Current density (pA/pF)	30.9 ± 7.1 $n = 6$	32.8 ± 12.5 $n = 6$
Potential at maximum current (mV)	-8.3 ± 8.2 $n = 6$	-6.6 ± 6.8 $n = 6$

**Figure 3.24. Parameters for steady state calcium activation in type II LN subtypes**

For details see Table 6. A: Mean membrane potentials at I_{max} were not significantly different. B: Type IIa LNs reached larger peak currents compared to type II LNs. C: According to their different membrane capacitance values the mean current densities were not significantly different. Asterisks mark the level of significance: (*) $p \leq 0.05$.

Not only the absolute peak current amplitudes of type IIa LNs (Fig. 3.25A; $P < 0.001$), but also the current densities at -35 mV are significantly larger compared to type IIb LNs (Fig. 3.25B; $P = 0.003$). Whereas the maximum peak current densities of the two types were very similar (see Table 6), at testpulse potentials of -35 mV type IIa LNs reached a more than two times higher mean current density than type IIb LNs and even a more than three times higher mean percentage of the maximum current (Fig. 3.25C; $P < 0.001$). While type IIa LNs reached more than 20 % of their

maximum currents at -35 mV (type IIa LN $I_{-35 \text{ mV}}/I_{\text{max}} = 21.3 \pm 6.8 \%$; $n = 6$), calcium currents in type II LNs were only activated less than 10% (type IIb LN $I_{-35 \text{ mV}}/I_{\text{max}} = 6.7 \pm 3.6 \%$; $n = 6$).

Table 7: Summary of I/V relationship parameters at testpulse potential -35 mV

	type IIa LN	type IIb LN
Maximum current at -35 mV (nA)	0.75 ± 0.16 $n = 6$	0.27 ± 0.09 $n = 6$
Current density at -35 mV (pA/pF)	6.52 ± 2.18 $n = 6$	2.32 ± 1.49 $n = 6$
Percentage of I_{max} at -35 mV (%)	21.3 ± 6.8 $n = 6$	6.7 ± 3.6 $n = 6$

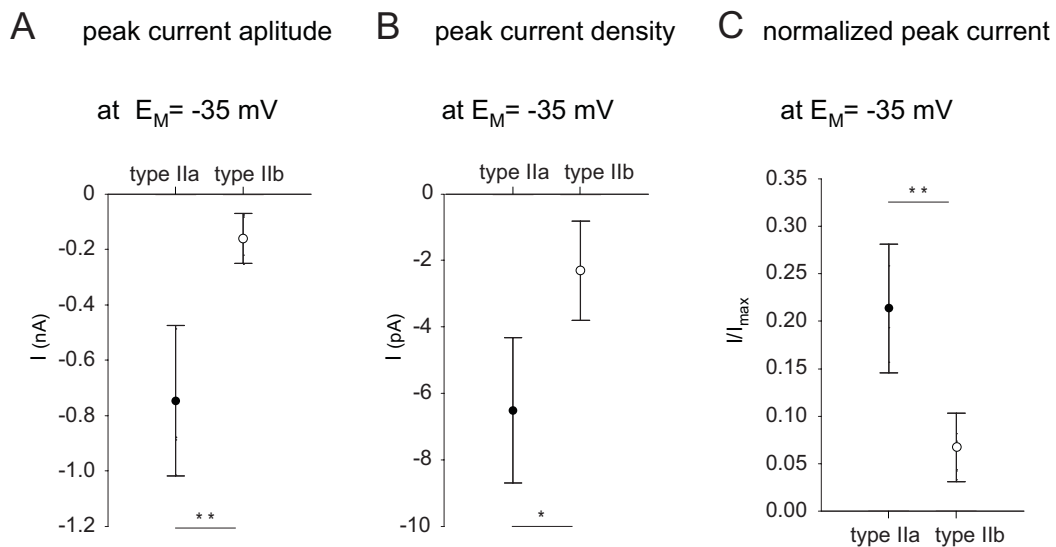


Figure 3.25.: Comparison of VGCC steady state activation parameters at -35 mV

Focusing on early activation at testpulse potential -35 mV mean values are significantly different. For details see Table 7. *P*-values for significance tests were: I_{max} at -35 mV: $P < 0.001$; I_{dens} at -35 mV: $P = 0.03$; I/I_{max} at -35 mV: $P < 0.001$ (*t*-test).

To analyze the difference in voltage dependence in the two subgroups of type II LNs in more detail, a tail current analysis was performed. The I/V relations were fit to a first order Boltzmann equation (eq. 2). However, halfmaximal activation of tail

current activation in the type II LN subgroups was not significantly different ($P = 0.095$; t-test). In type IIa LNs the parameters were given as: $V_{0.5(act)} = -21.7 \pm 5$ mV, $s = 8.2 \pm 2.1$; $n = 6$. In type IIb LNs fits to first-order Boltzmann equations (eq. 2) delivered the following parameters: $V_{0.5(act)} = -17.1 \pm 3.5$ mV $s = 4.8 \pm 5.1$; $n = 6$. The difference in the slope factor s indicated differences in I_{Ca} characteristics. The tail current analysis is not illustrated in this thesis, but the current decays over time are analyzed in the following to point out the apparent differences in I_{Ca} characteristics.

Inactivation over time

As indicated in Fig 3.23A time dependent inactivation seemed to be a different. While type IIa LNs showed a fast inactivating component, I_{Ca} in type IIb LNs inactivated less over time. To quantify the difference, decay time constants τ of exponential fits through the current decays were calculated (eq. 4). Because the 50 ms activation pulses were too short to fit the decay properly, long lasting depolarizations were analyzed in more detail. Type II LNs were voltage-clamped from a holding potential of -80 mV to testpulse potentials of -5 mV for 550 ms. Although the complex geometry of these large interneurons lead to space clamp problems, especially over long lasting depolarizing voltage steps, it was possible to analyze decay time constants of current amplitude decreases over time in 3 type IIa LNs and in 3 type IIb LNs. It was obvious that type IIa LNs had a faster inactivating calcium current component. The current time courses were well fitable with a double exponential fit (see eq. 2). Mean decay time constants τ_1 was significantly shorter in type IIa LNs than in type IIb LNs, reflecting the faster inactivating calcium current component in type IIa LNs. (Table 8; $P = 0.004$; t-test). Mean values for the decay time constants τ_1 and τ_2 are summarized in table 8. Comparison of the parameters for decay time constants is illustrated in Fig. 3.26. The analysis of steady state activation and current decay fits delivered data to conclude the differences in I_{Ca} in the type II subtypes.

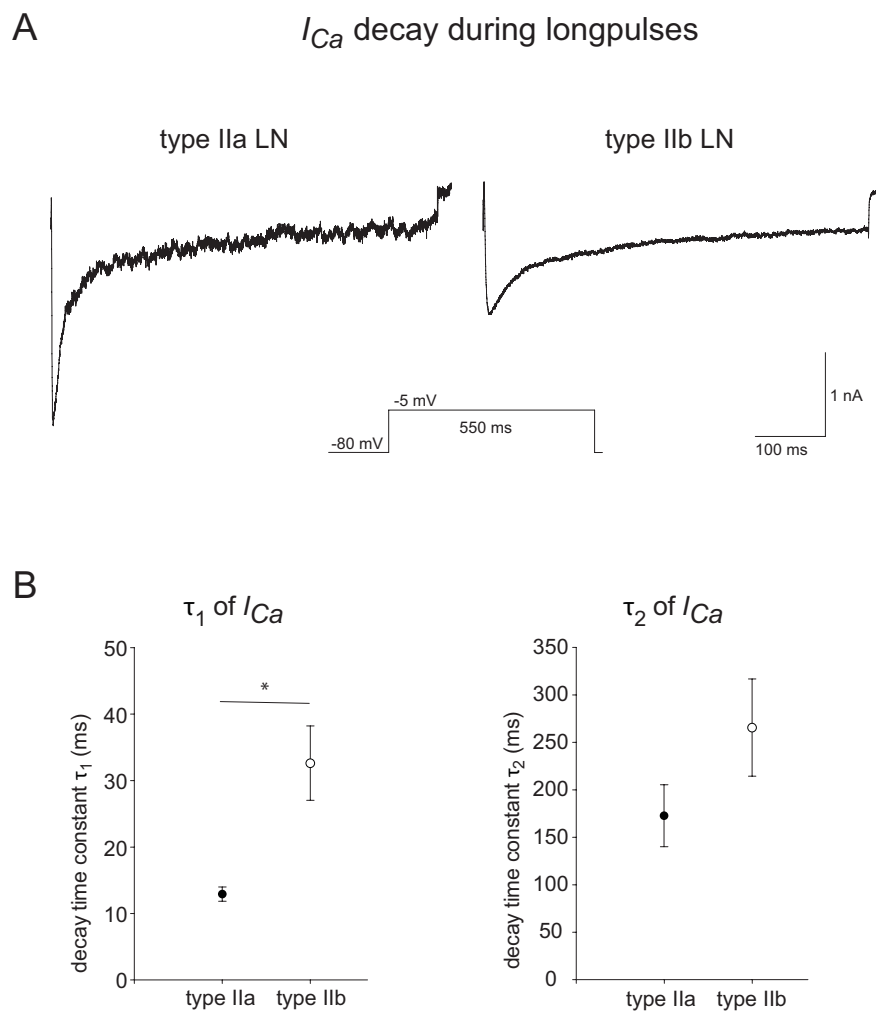


Figure 3.26. Comparison of decay time constants of long pulse activated calcium currents
A: Calcium currents evoked by a 550 ms voltage step from -80 mV to -5 mV. B: The current decay was fit with a double exponential fit (eq. 4). Decay time constant τ_1 is significantly shorter in type IIa LNs compared to the mean values in type IIb LNs. For details see Table 8. Asterisks mark the level of significance: () $p \leq 0.05$.*

Table 8: Summary of decay time constant parameters in different type II LNs

	type IIa LN	type IIb LN
Decay time constant τ_1 (ms)	12.9 ± 1.1 $n = 3$	32.6 ± 5.6 $n = 3$
Decay time constant τ_2 (ms)	173.0 ± 32.7 $n = 3$	266.0 ± 51.1 $n = 3$

4 Discussion

The insect AL serves as an important model for olfactory information processing at the network level (Hildebrand and Shepherd 1997; Laurent 1999; Strausfeld and Hildebrand 1999; Wilson and Mainen 2006), however, comparatively little is known about the biophysical properties of olfactory interneurons. In this study, whole cell patch-clamp recordings were used to examine the voltage activated calcium currents of antennal lobe interneurons of the cockroach *Periplaneta americana*. After characterizing the parameter space of I_{Ca} in acutely dissociated AL interneurons under controlled conditions (in vitro), an intact brain preparation was established to confirm the physiological relevance of the in vitro results in an in situ preparation, where the neurons were in their native environment and their synaptic contacts were still intact. Subsequently, a preparation was established, which enabled the unequivocal identification of central olfactory interneuron types. Finally, voltage activated calcium currents were analyzed in uniglomerular projection neurons and in two morphologically and physiologically different local interneuron subtypes.

4.1 Voltage activated calcium currents in vitro and in situ

Antennal lobe interneurons were examined both in vitro as well as in an intact brain preparation. During the first stage of this thesis the objective was to explore the basic membrane properties of the olfactory interneurons, especially the parameter space of

biophysical properties of voltage activated calcium currents. In vitro recordings of acutely dissociated cells provided many advantages, such as: (1) controlled recording conditions. During in vitro experiments the concentrations of extracellular as well as intracellular substances are well defined by the composition of extracellular and intracellular solution. Direct accessibility for blockers and other pharmacological agents allows a detailed analysis of biophysical and chemical properties. (2) Close to perfect voltage control. Simple spherical geometry of acutely dissociated cells provides an almost perfect voltage control over the whole membrane. Although cells in vitro are particularly amenable to voltage clamp and can be studied under controlled conditions, extrapolating these results to conditions in vivo often raises doubt about its physiological relevance, as cells in vitro are removed from their natural environment and are synaptically disconnected. To confirm the physiological relevance of the in vitro data, an intact brain preparation was established that allows to record from unequivocally identified olfactory interneurons. In addition, the intact brain preparation provided the possibility of stimulating the recorded neurons with biologically relevant odors, and to characterize physiological relevant responses and providing the possibility to classify their potential role in olfactory information processing.

This combined in vitro/in situ approach enabled me to take advantage of the easy access and controlled conditions provided by in vitro studies, and to demonstrate the biological relevance of these results by examining unequivocally identified cells in their native environment, with their neurites, arborizations and synaptic connections largely intact.

4.1.1 General parameters of voltage activated calcium currents

I_{Ca} recorded in vitro from isolated somata of adult AL olfactory interneurons activated at membrane potentials above ~ -40 mV with a maximum current around -5

mV. I_{Ca} consisted of a relatively fast activating/inactivating and a non-inactivating component. In situ the I/V relation for steady state activation/inactivation was shifted to more depolarized membrane potentials. Interestingly, in a similar study of honeybee antennal motoneurons, differences between in vitro and in situ recordings were not observed (Kloppenburg et al. 1999b). However, taking into account the different experimental conditions between in vitro and in situ experiments, such a shift of parameters was not unexpected. The reasons might be imperfect voltage control across the whole neuron in the intact brain preparations, in which the neuronal arborizations are still intact, and/or differences in voltage dependence of calcium channels that are localized in distal regions of the neurons. Nevertheless, both the in vitro and in situ parameters of I_{Ca} are well within the range of Ca^{2+} currents described in other insect preparations including *Drosophila* neurons (Byerly and Leung 1988; Saito and Wu 1991), honey bee Kenyon cells (Grünewald 2003; Schäfer et al. 1994) and antennal motoneurons (Kloppenburg et al. 1999b), *Manduca* motor neurons (Hayashi and Levine 1992), embryonic cockroach neurons (Benquet et al. 1999), cockroach DUM neurons (Heidel and Pflüger 2006), cockroach motor neurons (Mills and Pitman 1997), locust thoracic neurons (Laurent et al. 1993; Pearson et al. 1993), cricket giant interneurons (Kloppenburg and Hörner 1998). In vitro the average current density of ~ 50 pA/pF was in the same range as found in vitro in honeybee projection neurons (Grünewald 2003) and cockroach DUM neurons (Heidel and Pflüger 2006).

In this study, the inactivation kinetics of I_{Ca} were very variable between recordings. The reason for this variability is unclear, but could be due to differential expression of different Ca^{2+} channel types, or the presence of residual currents carried by ions others than calcium. Substituting calcium with barium increased the maximum amplitude of the I_{Ca} , indicating that the investigated channels are more permeable to Ba^{2+} than to Ca^{2+} , as described for voltage gated Ca^{2+} channels in other cell types

(Hille 2001). Furthermore the amount of inactivation during a depolarizing voltage pulse was reduced, which became specially obvious during long lasting depolarizations. These results suggest that inactivation during a voltage step is, at least in part, a Ca^{2+} dependent mechanism.

In vertebrates, Ca^{2+} currents are usually classified into low-voltage activated (LVA or T-type, with activation starting above ~ -70 mV) and high-voltage activated (HVA, activation starting above ~ -30 mV) classes. Subtypes such as L-, P/Q-, N-, and R-type are defined by biophysical and pharmacological properties (Ertel et al. 2000; Hille 2001; Triggle 2006). In accordance with other studies, Husch et al. (submitted) found that the pharmacological classification of vertebrate calcium currents is difficult to transfer to I_{Ca} of insects (for review see King 2007). The I_{Ca} in AL interneurons exhibit some characteristics that are typical for some HVA channel types: Ba^{2+} is a better charge carrier than Ca^{2+} , inactivation is Ca^{2+} dependent and relatively slow compared with LVA channels, I_{Ca} is more sensitive to Cd^{2+} than Ni^{2+} , and I_{Ca} is reduced by the L-type blockers verapamil, diltiazem, and nifedipine (Husch et al., submitted). However, the activation range of I_{Ca} is more hyperpolarized than traditional HVA channels and thus resemble currents with L-type properties that have more mid-voltage activated ranges (Johnson et al. 2003; Wicher and Penzlin 1997). Despite these 'L-type' like characteristics (\pm)-BAY K 8644 did not modify I_{Ca} , indicating that calcium channels in AL interneurons differs from vertebrate L-type calcium channels pharmacologically. Amiloride, a vertebrate T-type channel blocker, did not affect I_{Ca} (Husch et al., submitted), while amiloride does inhibit calcium currents in different *Drosophila* preparations (embryonic central neurons (Baines and Bate 1998); larval muscles (Gielow et al. 1995)). Though Husch et al. (submitted) used comparatively high organic blocker concentrations, they still found substance specific effects. In previous studies, it has been argued that the I_{Ca} blocker concentrations, which are needed to inhibit calcium currents in insect neurons, are too high to achieve any

specific effects on calcium channel subtypes (Benquet et al. 2002). While often the organic Ca^{2+} channel blockers act more potently on vertebrate cells than on invertebrate neurons (Hille 2001), the results from Husch et al. (submitted) indicate that they still can have specific effects, and thus be useful as tools for physiological experiments, as it is true for other ion channel types. For instance, 4-AP is regarded as a relative specific blocker for transient potassium currents (I_A) in invertebrate and vertebrate preparations at a concentration of ~ 5 mM for complete block of I_A , and TEA is used to specifically block $I_{K(V)}$ and $I_{K(Ca)}$.

4.1.2 Rundown during whole cell voltage-clamp recordings

In some experiments, after a recording time of ~ 15 minutes, I_{Ca} started to show a considerable 'rundown'. Therefore, application of blockers was started immediately when the control recording was stable (Fig. 3.6). It has been reported in some cell types that the rundown is slower when Ca^{2+} is replaced with Ba^{2+} , indicating a Ca^{2+} -dependent effect on I_{Ca} (e.g. Schäfer et al. 1994). In my experiments, barium substitution did not change the probability for 'rundown' occurrence. The observed 'rundown' appeared to be accelerated with increasingly positive voltage pulses. The Ca^{2+} influx, however, did not increase further, but started to decrease at membrane potentials more positive than approximately -10 mV owing to the equilibrium potential of Ca^{2+} . This observation suggests that at least part of the observed 'rundown' was voltage-dependent.

Another reason for rundown can be washout of second messenger such as ATP and GTP. Experiments in our lab have shown that adding 3 mM ATP and 0.3 mM GTP to the intracellular solution, stabilize the recordings for times more than 20 minutes (personal communication, Simon Heß). Perforated patch recordings is another method to minimize rundown by washout (Horn and Marty 1988). In this variation of patch-clamp recording a gigaohm seal is established and the intracellular access is

achieved by pore forming agents such as Amphotericin-B or Nystatin. These artificial pores are permeable for small ions, but not for larger molecules, such as ATP, glucose or divalent ions. The advantage is reduced dialysis of cytoplasmic components of the cell compared to whole cell recordings. A series of experiments in our lab have shown that the rundown is at least in part caused by the whole cell configuration dependent washout of cytoplasmic components (personal communication, Heike Demmer) and could be reduced by perforated patch recordings as previously demonstrated in other preparations (Falke et al. 1989; Korn and Horn 1989; Kurachi et al. 1989). Beside the described advantages perforated patch recordings might lead to other recording difficulties. The access resistance is higher, which might result in decreased current resolution and voltage control. Additionally, the membrane under the electrode tip is weakened by the pores and tends to rupture. When the patch ruptures, the recording is essentially in whole-cell mode with pore former inside the cell (Korn et al. 1991).

4.2 Identification of olfactory interneurons

In the antennal lobe there is a large variety of central olfactory interneurons. The main groups are the projection neurons and the local interneurons. Within these main types there are several subtypes of neurons. In this study, I focused on one type of projection neurons, the uniglomerular projection neurons (uPNs). Additionally I characterized two subtypes of local interneurons, that were referred as type I LNs and the type II LNs. This is the first study in an insect olfactory system in which physiological parameters of two completely different local interneuron types were examined.

The cell bodies of the olfactory interneurons were detected in situ using an upright microscope, revealing the ventrolateral somagroup of the antennal lobe described

previously (Distler and Boeckh 1996; Distler et al. 1998). The topography and neuroanatomy of the fibers connecting the deutocerebrum to the protocerebrum are well described in *P. americana* (Malun et al. 1993). The projection neurons are a group of neurons with a lot of different subtypes. They are classified on one hand by the fibers they innervate on their way to the protocerebrum and on the other hand by number and nature of the glomeruli they innervate. Within the projection neurons the uPNs form a relative homogeneous and well defined group. Physiology and morphology of uniglomerular projection neurons, innervating the inner antenno-cerebral tract (IACT uPN) are well described in the cockroach (Malun 1991a; Malun 1991b). As 'normal' output neurons they elicited common overshooting action potentials and during steady state activation a typical current profile was elicited, with transient sodium carried inward current and transient and sustained potassium outward currents. The odor reactions in uPNs are already well described. It was not surprising that odor stimulation evoked overshooting action potentials mediating the information transfer from the antennal lobe to the protocerebrum (Abel et al. 2001). In contrast to the uPNs, less information is available about the physiology and morphology of local interneurons.

In the second stage of this study the ultimate identification of the neurontypes was done by biocytin-streptavidin-Alexa 633 single cell staining of each recorded neuron. The combination of visual selection of identifiable soma clusters and subsequently the identification with a confocal laser scanning microscope of the neurons enabled me to record repetitively from two distinct local interneuron types. These two types were characterized by completely different physiological and morphological properties. In type I LNs odor stimulation evoked overshooting action potentials and during voltage clamp activation a common pattern of sodium and potassium current activation occurred that was similar to the findings in uPNs. Spiking local

interneurons with similar properties were found in other olfactory systems (Christensen et al. 1993; Sun et al. 1993; Wilson et al. 2004).

The type II LNs described in this thesis never generated any sodium driven APs, neither by odor stimulation nor when depolarized even with large current amplitudes. Voltage-clamp activation protocols never elicited voltage activated sodium currents, which is in contrast to the uPNs as well as to the spiking type I LNs. Non-spiking local interneurons were already described in other preparations, for instance in the locust (Laurent et al. 1996). Until now there was no insect olfactory system described, in which both types, spiking and non-spiking local interneurons, were found. Interestingly, the type II LNs generated large calcium currents. To further investigate their remarkable voltage activated current composition the voltage activated calcium currents in uPNs, type I LNs and type II LNs were isolated and analyzed.

4.3 Diversity of voltage activated calcium currents in identified neuron types

In the first part of this thesis, averaged data from a large number of experiments were analyzed to characterize the parameter space of I_{Ca} in AL interneurons. It was the first step to characterize I_{Ca} of adult AL interneurons in detail and to get pharmacological tools to manipulate I_{Ca} . The data were obtained from unidentified neurons. The variance of the data might be caused by differential expression of Ca^{2+} channel types in different cell types. This hypotheses was tested by recordings from neurons that were unequivocally identified by single cell labeling.

4.3.1 Analysis of calcium currents in identified neurons

The unequivocal identification of distinct neurontypes such as the uPNs, the multiglomerular type I LNs and the omniglomerular type II LNs enables to analyze voltage activated calcium currents in identified neuron groups. As indicated by the whole cell current profiles, the voltage activated calcium currents in type II LNs were significantly larger compared to I_{Ca} measured in type I LNs and uPNs. Although there is a striking difference in I_{Ca} amplitude, inside the LN subtypes the current densities are in the same range, whereas the uPNs had significantly higher current densities. Comparing the data from identified neurons to the in vitro results, it seemed to be that most neurons recorded in cell culture were uPNs, because current densities in uPNs and in in vitro data were very similar. In the in situ recordings without cell type identification presumably a mixture of both were measured. The mean current density in situ was in between uPNs and LNs. It should be noted that the channel distribution is not uniform in the neuron, so that comparison between dissociated somata and intact neurons is problematic. It has been shown in the stomatogastric system that calcium influx can be highly localized (Kloppenburg et al. 2000), suggesting that the current densities are variable at different locations of the membrane.

Another biophysical parameter, that is even better to quantify, is the voltage for half maximal activation of I_{Ca} . Already during the steady state activation highly significant differences in activation kinetics were quantified. In agreement with their similar basic physiological properties such as their ability to generate sodium driven APs, in uPNs and type I LNs, the mean values for half maximal activation were not different. In contrast, the type II LNs had their half-maximal current at significantly more hyperpolarized potentials. Voltage clamp investigations in DUM neurons have revealed the occurrence of at least two types of voltage dependent Ca^{2+} currents (Wicher and Penzlin 1994; Wicher and Penzlin 1997): M-LVA activated and HVA

activated currents. The values for half maximal activation voltages indicate, that the uPNs and type I LNs exhibit more HVA-calcium currents, whereas type II LNs type II LNs seemed to have more M-LVA calcium currents. These findings correspond to the previously presented physiological properties of type II LNs. They cannot elicit sodium driven action potentials and have no voltage activated sodium currents. Instead they express Ca^{2+} currents in the low voltage range. These findings suggest that the odor response in type II LNs is mainly driven by M-LVA calcium channels. Analyzing the type II LNs in more detail, two significantly different subtypes were found. Type IIa LNs started to depolarize at more hyperpolarized potentials and the inactivation over time was significantly faster, indicating a higher amount of M-LVA calcium channels. Interestingly they reacted to odor stimulations in some experiments with small 'spikelets'. It can be speculated that the odor evoked 'spikelets' in type IIa LNs are calcium driven.

4.3.2 Functional significance of voltage activated calcium currents

The results of this thesis provide an overview of physiological and morphological differences in olfactory interneurons. As mentioned above, this is the first study, in which spiking neurons and neurons without sodium spikes are found together in an insect olfactory system. Immunocytochemistry by Debora Fusca (Fusca 2007) demonstrated that type I LNs were GABAergic. This result is consistent with earlier work in *Periplaneta americana* (Distler et al. 1998), that has described the majority of local neurons as inhibitory GABAergic neurons. In contrast to these findings, Fusca has shown that the majority of type II LNs were not GABA-immunoreactive. These results strongly demonstrate that only the spiking neurons are inhibitory. While the type I LNs have a large I_{Na} , it is lacking completely in type II LNs. However, they have a large calcium current, that activates at relatively low voltage potentials. These results suggest that type I neurons trigger GABA release with overshooting APs. In

contrast, the physiology of the type II LNs suggest graded nonspike evoked transmitter (or neuromodulator) release, as also suggested for nonspiking local interneurons in the thoracic nervous system of the locust (Laurent et al. 1993). The calcium currents underlying graded transmission in invertebrates have been most extensively studied in leech heart interneurons (Angstadt and Calabrese 1991; Ivanov and Calabrese 2000; Ivanov and Calabrese 2006; Lu et al. 1997). These currents resemble LVA-type currents: similar to the type II LNs, they have very hyperpolarized activation ranges (e.g. compared to uPNs) and they are blockable with Nickel. Interestingly, the calcium currents in the STG that mediate graded release lack the sensitivity to Nickel and there is even an increase of graded transmission by nickel reported (Zirpel et al. 1993). These results suggest that the currents measured in type II LNs might be similar to the currents that underlying leech graded transmission, but differ from the I_{Ca} controlling pyloric graded chemical transmission. In its activation range and relatively low sensitivity to nifedipine, the I_{Ca} in pyloric neurons more closely resembles the L-type current mediating graded transmitter release from cochlear hair cells (Spassova et al. 2001) and vertebrate retinal neurons (Berntson et al. 2003; Taylor and Morgans 1998).

Beside graded chemical release, the early activating calcium currents in these olfactory interneurons could contribute to plateau potential properties as described in in developing antennal-lobe neurons of the moth, *Manduca sexta* (Mercer et al. 2005) and other small neuronal circuits like the stomatogastric ganglion (Russell and Hartline 1982). For instance, plateau potentials in the gastric DG neurons are supported by calcium currents with a similar activation range as the LNs measured here (Zhang et al. 1995; Zhang and Harris-Warrick 1995).

4.4 Diversity of other voltage activated ion currents

It is important to keep in mind that the present study gives only a small insight into the biophysical properties of antennal lobe interneurons. During this study, I have gathered evidence for the existence of several other currents not described in detail here. For example, different kinds of potassium and sodium conductances. Most obvious is the lack of voltage activated sodium currents in type II LNs. Because of the complex geometry of the cells, it is difficult to determine whether or not there are voltage activated sodium currents at any location of these geometrically complex local interneurons. TTX incubation did not lead to a change of the total current profile during voltage clamp steady state activation. To examine the role of voltage activated sodium currents during odor responses in type II LNs incubation with TTX would also block the action potentials inside the olfactory receptor neurons, resulting in a complete silencing of the olfactory system. One possible opportunity to analyze sodium currents exclusively in the type II LNs are sodium channel blockers, that act from intracellular, e.g. QX 314 (Yeh 1978). Thus, effects on the odor evoked depolarization could be observed over time with increase of intracellular diffusion. A better application form would be the exchange of the intracellular solution during the experiments by patch pipette perfusion or double patch clamp recording with two electrodes at one soma. These experiments are complex, but they would contribute to the question whether or not the type II LNs are 'real' non-spiking neurons with definitely no voltage activated sodium currents.

Comparing Fig. 3.12 C, Fig. 3.13C, and Fig 3.14C it becomes obvious, that the outward current profiles consist at least of two components: (1) a transient (I_A) and (2) a sustained current ($I_{K(V)}$). Note the differences of the total profile in the examined neuron types, e.g. the different ratios of I_A to $I_{K(V)}$ in uPNs and type I LNs. The transient potassium current in uPNs has a faster inactivation decay time constant,

indicating the existence of sodium dependent potassium currents. Although I have not been searching systematically for ionsensitive ionic currents, I observed a reduction in amplitude and change in the form of the outward currents in experiments during which Ca^{2+} or Na^+ currents were blocked, suggesting the presence of Ca^{2+} - and Na^+ -sensitive K^+ currents. Ca^{2+} - dependent (Schäfer et al. 1994 (honeybee); Thomas 1984 (cockroach)) and Na^+ -dependent K^+ currents have also been found in vertebrates and invertebrates (Bader et al. 1985; Dale 1993; Grolleau and Lapied 1994; Hartung 1985).

4.5 Conclusions

In this thesis biophysical parameters of three identified central olfactory neuron groups were analyzed. Results in uPNs were as expected. Sodium driven action potentials were elicited with odor stimulation and current injection. In voltage clamp activation protocols an inward sodium current and an outward potassium current was present. In the group of local interneurons I have found at least two subtypes with very different physiological and biophysical properties: type I LNs responded to odor stimulation with sodium driven action potentials, whereas in type II LNs odor stimulation evoked depolarizations, but no action potentials. Additionally the different types were morphologically distinguishable: type I LNs innervated many glomeruli with variation in innervation density, whereas type II LNs were innervating all glomeruli in an evenly and homogeneous way. While currently the transmitter from these neurons is not known, it can be speculated, that at least some of these neurons might have acetylcholine as an excitatory neurotransmitter, as supported by a recent work in *Drosophila* (Shang et al. 2007).

Further work is needed to clarify the functional role of the I_{Ca} in synaptic transmission between different neuron types. There is a lot of electron microscopical

data available in the cockroach (Distler and Boeckh 1997a; Distler and Boeckh 1997b; Distler and Boeckh 1998) but electrophysiological data are still rare. First double patch-clamp recordings in the intact brain preparation have shown the feasibility of recording of synaptic transmission, but a systematically quantification of synaptic strength between projection neurons and local interneurons has still to be done.

List of Figures

Figure 2.1. Schematic representation of the intact brain preparation.....	19
Figure 2.2. Odor application system.....	24
Figure 3.1. Action potentials and total current profiles.....	29
Figure 3.2. Whole cell recording of voltage activated inward currents.....	30
Figure 3.3. Inward currents variability caused by calcium concentration variation.....	31
Figure 3.4. Substitution of extracellular calcium with barium.....	32
Figure 3.5. Calcium currents in acutely dissociated cells (in vitro).....	34
Figure 3.6. Calcium current block by inorganic ions.....	36
Figure 3.7. Dose response curves for cadmium, nickel and cobalt.....	37
Figure 3.8. Calcium currents in the intact brain preparation (in situ).....	39
Figure 3.9. Overview of the intact brain preparation.....	42
Figure 3.10. Typical responses to different odors in uPNs, type I and type II LNs.....	43
Figure 3.11. Repetitive odor stimulation in uPNs, type I and type II LNs.....	45
Figure 3.12. Electrophysiological and morphological characteristics of uPNs.....	46
Figure 3.13. Electrophysiological and morphological characteristics of type I LNs.....	48
Figure 3.14. Electrophysiological and morphological characteristics of type II LN.....	49
Figure 3.15. Membrane-potential, -resistance and -capacity in uPN, type I and type II LNs. .	52
Figure 3.16. Steady state activation of calcium currents in uPNs, type I and type II LNs.....	55
Figure 3.17. Overview of calcium steady state activation parameters.....	56
Figure 3.18. Quantification of half-maximal calcium tail current activation.....	57
Figure 3.19. Parameters for tail current activation in uPN, type I and type II LNs.....	59
Figure 3.20. Steady state inactivation of voltage activated calcium currents.....	60
Figure 3.21. Morphological subtypes of LNs.....	63
Figure 3.22. Membrane-potential, -resistance and -capacity, in type II LN subtypes.....	64
Figure 3.23. Steady state activation of calcium currents in type IIa and type IIb LNs.....	66

Figure 3.24. Parameters for steady state calcium activation in type II LN subtypes.....67

Figure 3.25.: Comparison of VGCC steady state activation parameters at -35 mV68

Figure 3.26. Comparison of decay time constants of long pulse activated calcium currents. 70

References

- Abel R, Rybak J and Menzel R** (2001) Structure and response patterns of olfactory interneurons in the honeybee, *apis mellifera*. *J Comp Neurol* 437: 363-383.
- Angstadt JD and Calabrese RL** (1991) Calcium currents and graded synaptic transmission between heart interneurons of the leech. *J Neurosci* 11: 746-759.
- Augustine GJ, Santamaria F and Tanaka K** (2003) Local calcium signaling in neurons. *Neuron* 40: 331-346.
- Bader CR, Bernheim L and Bertrand D** (1985) Sodium-activated potassium current in cultured avian neurones. *Nature* 317: 540-542.
- Baines R and Bate M** (1998) Electrophysiological development of central neurons in the *Drosophila* embryo. *J Neurosci* 18: 4673-4683.
- Baro DJ, Levini RM, Kim MT, Willms AR, Lanning CC, Rodriguez HE and Harris-Warrick RM** (1997) Quantitative single-cell-reverse transcription-pcr demonstrates that a-current magnitude varies as a linear function of shal gene expression in identified stomatogastric neurons. *J Neurosci* 17: 6597-6610.
- Benquet P, Le Guen J, Dayanithi G, Pichon Y and Tiaho F** (1999) Omega-agaiva-sensitive (p/q-type) and -resistant (r-type) high-voltage-activated Ba²⁺ currents in embryonic cockroach brain neurons. *J Neurophysiol* 82: 2284-2293.
- Benquet P, Le Guen J, Pichon Y and Tiaho F** (2002) Differential involvement of Ca²⁺ channels in survival and neurite outgrowth of cultured embryonic cockroach brain neurons. *J Neurophysiol* 88: 1475-1490.
- Berg BG, Schachtner J, Utz S and Homberg U** (2007) Distribution of neuropeptides in the primary olfactory center of the heliothine moth *heliiothis virescens*. *Cell and Tissue Research* 327: 385-398.
- Berntson A, Taylor WR and Morgans CW** (2003) Molecular identity, synaptic localization, and physiology of calcium channels in retinal bipolar cells. *J Neurosci Res* 71: 146-151.
- Berridge MJ** (1998) Neuronal calcium signaling. *Neuron* 21: 13-26.
- Boeckh J and Tolbert LP** (1993) Synaptic organization and development of the antennal lobe in insects. *Microsc Res Tech* 24: 260-280.
- Byerly L and Leung HT** (1988) Ionic currents of *Drosophila* neurons in embryonic

cultures. *J Neurosci* 8: 4379-4393.

Christensen TA, Waldrop BR, Harrow ID and Hildebrand JG (1993) Local interneurons and information processing in the olfactory glomeruli of the moth *Manduca sexta*. *J Comp Physiol [A]* 173: 385-399.

Dale N (1993) A large, sustained Na⁺- and voltage-dependent K⁺ current in spinal neurons of the frog embryo. *J Physiol* 462: 349-372.

Distler P (1990) Gaba-immunohistochemistry as a label for identifying types of local interneurons and their synaptic contacts in the antennal lobes of the american cockroach. *Histochemistry* 93: 617-626.

Distler P (1989) Histochemical demonstration of GABA-like immunoreactivity in cobalt labeled neuron individuals in the insect olfactory pathway. *Histochemistry* 91: 245-249.

Distler PG and Boeckh J (1998) An improved model of the synaptic organization of insect olfactory glomeruli. *Ann N Y Acad Sci* 855: 508-510.

Distler PG and Boeckh J (1996) Synaptic connection between olfactory receptor cells and uniglomerular projection neurons in the antennal lobe of the american cockroach, *Periplaneta americana*. *J Comp Neurol* 370: 35-46.

Distler PG and Boeckh J (1997a) Synaptic connections between identified neuron types in the antennal lobe glomeruli of the cockroach, *Periplaneta americana*: I. Uniglomerular projection neurons. *J Comp Neurol* 378: 307-319.

Distler PG and Boeckh J (1997b) Synaptic connections between identified neuron types in the antennal lobe glomeruli of the cockroach, *Periplaneta americana*: II. Local multiglomerular interneurons. *J Comp Neurol* 383: 529-540.

Distler PG, Gruber C and Boeckh J (1998) Synaptic connections between GABA-immunoreactive neurons and uniglomerular projection neurons within the antennal lobe of the cockroach, *Periplaneta americana*. *Synapse* 29: 1-13.

Dodt H and Zieglgänsberger W (1994) Infrared videomicroscopy: a new look at neuronal structure and function. *Trends Neurosci* 17: 453-458.

Eisthen HL (2002) Why are olfactory systems of different animals so similar?. *Brain Behavior and Evolution* 59: 273-293.

Ertel E, Campbell K, Harpold M, Hofmann F, Mori Y, Perez-Reyes E, Schwartz A, Snutch T, Tanabe T, Birnbaumer L, Tsien R and Catterall W (2000) Nomenclature

- of voltage-gated calcium channels. *Neuron* 25: 533-535.
- Falke LC, Gillis KD, Pressel DM and Misler S** (1989) 'Perforated patch recording' allows long-term monitoring of metabolite-induced electrical activity and voltage-dependent Ca^{2+} currents in pancreatic islet β cells. *FEBS Lett* 251: 167-172.
- Fedulova SA, Kostyuk PG and Veselovsky NS** (1985) Two types of calcium channels in the somatic membrane of new-born rat dorsal root ganglion neurones. *J Physiol* 359: 431-446.
- Fonta C, Sun XJ and Masson C** (1993) Morphology and spatial-distribution of bee antennal lobe interneurons responsive to odors. *Chemical Senses* 18: 101-119.
- Fusca D** (2007) Gaba-like immunoreactivity in the antennal lobe of *Periplaneta americana* - a study on identified local interneurons. *Diplomarbeit*. Zoologisches Institut, Universität zu Köln.
- Gebhardt S and Homberg U** (2004) Immunocytochemistry of histamine in the brain of the locust *Schistocerca gregaria*. *Cell Tissue Res* 317: 195-205.
- Gielow M, Gu G and Singh S** (1995) Resolution and pharmacological analysis of the voltage-dependent calcium channels of *Drosophila* larval muscles. *J Neurosci* 15: 6085-6093.
- Grolleau F and Lapied B** (1994) Transient Na^+ -activated K^+ current in beating pacemaker-isolated adult insect neurosecretory cells (DUM neurones). *Neurosci Lett* 167: 46-50.
- Grolleau F and Lapied B** (1996) Two distinct low-voltage-activated Ca^{2+} currents contribute to the pacemaker mechanism in cockroach dorsal unpaired median neurons. *J Neurophysiol* 76: 963-976.
- Grünewald B** (2003) Differential expression of voltage-sensitive K^+ and Ca^{2+} currents in neurons of the honeybee olfactory pathway. *J Exp Biol* 206: 117-129.
- Hamill OP, Marty A, Neher E, Sakmann B and Sigworth FJ** (1981) Improved patch-clamp techniques for high-resolution current recording from cells and cell-free membrane patches. *Pflügers Arch* 391: 85-100.
- Hartung K** (1985) Potentiation of a transient outward current by Na^+ influx in crayfish neurones. *Pflügers Arch* 404: 41-44.
- Hayashi JH and Hildebrand JG** (1990) Insect olfactory neurons in vitro: morphological and physiological characterization of cells from the developing

- antennal lobes of *Manduca sexta*. *J Neurosci* 10: 848-859.
- Hayashi JH and Levine RB** (1992) Calcium and potassium currents in leg motoneurons during postembryonic development in the hawkmoth *Manduca sexta*. *J Exp Biol* 171: 15-42.
- Heidel E and Pflüger H** (2006) Ion currents and spiking properties of identified subtypes of locust octopaminergic dorsal unpaired median neurons. *Eur J Neurosci* 23: 1189-1206.
- Helmchen F and Tank DW** (2005) A single-compartment model of calcium dynamics in nerve terminals and dendrites. In: *Imaging in neuroscience and development*. edited by Yuste R & Konnerth A.: Cold Spring Harbor Laboratory Press, Cold Spring Harbor, New York, p. 265-275.
- Hildebrand JG and Shepherd GM** (1997) Mechanisms of olfactory discrimination: converging evidence for common principles across phyla. *Annual Review of Neuroscience* 20: 595-631.
- Hille B.** (2001) *Ion channels of excitable membranes*. Sinauer Associates, Inc, Sunderland, Massachusetts, USA.
- Horn R and Marty A** (1988) Muscarinic activation of ionic currents measured by a new whole-cell recording method. *J Gen Physiol* 92: 145-159.
- Husch A, Hess S and Kloppenburg P** (2007) Functional parameters of voltage activated Ca^{2+} currents from olfactory interneurons in the antennal lobe of *Periplaneta americana*. submitted in *J Neurophysiol*.
- Ivanov AI and Calabrese RL** (2006) Graded inhibitory synaptic transmission between leech interneurons: assessing the roles of two kinetically distinct low-threshold Ca^{2+} currents. *J Neurophysiol* 96: 218-234.
- Ivanov AI and Calabrese RL** (2000) Intracellular Ca^{2+} dynamics during spontaneous and evoked activity of leech heart interneurons: low-threshold Ca^{2+} currents and graded synaptic transmission. *J Neurosci* 20: 4930-4943.
- Jeziorski M, Greenberg R and Anderson P** (2000) The molecular biology of invertebrate voltage-gated Ca^{2+} channels. *J Exp Biol* 203: 841-856.
- Johnson BR, Kloppenburg P and Harris-Warrick RM** (2003) Dopamine modulation of calcium currents in pyloric neurons of the lobster stomatogastric ganglion. *J Neurophysiol* 90: 631-643.

- Keene AC and Waddell S** (2007) *Drosophila* olfactory memory: single genes to complex neural circuits. *Nat Rev Neurosci* 8: 341-354.
- King GF** (2007) Modulation of insect Ca²⁺ channels by peptidic spider toxins. *Toxicon* 49: 513-530.
- Kirchhof BS and Mercer AR** (1997) Antennal lobe neurons of the honey bee, *Apis mellifera*, express a d2-like dopamine receptor in vitro. *J Comp Neurol* 383: 189-198.
- Kloppenburg P and Hörner M** (1998) Voltage-activated currents in identified giant interneurons isolated from adult crickets *Gryllus bimaculatus*. *J Exp Biol* 201 : 2529-2541.
- Kloppenburg P, Ferns D and Mercer AR** (1999a) Serotonin enhances central olfactory neuron responses to female sex pheromone in the male sphinx moth *Manduca sexta*. *J Neuroscience* 19: 8172-8181.
- Kloppenburg P, Kirchhof BS and Mercer AR** (1999b) Voltage-activated currents from adult honeybee (*Apis mellifera*) antennal motor neurons recorded in vitro and in situ. *J Neurophysiol* 81: 39-48.
- Kloppenburg P, Zipfel WR, Webb WW and Harris-Warrick RM** (2000) Highly localized Ca²⁺ accumulation revealed by multiphoton microscopy in an identified motoneuron and its modulation by dopamine. *J Neuroscience* 20: 2523-2533.
- Korn SJ and Horn R** (1989) Influence of sodium-calcium exchange on calcium current rundown and the duration of calcium-dependent chloride currents in pituitary cells, studied with whole cell and perforated patch recording. *J Gen Physiol* 94: 789-812.
- Korn SJ and Marty A, Connor JA and Horn R** (1991) Perforated patch recording. *Methods Neurosci* 4: 364-373.
- Kurachi Y, Asano Y, Takikawa R and Sugimoto T** (1989) Cardiac Ca²⁺ current does not run down and is very sensitive to isoprenaline in the nystatin-method of whole cell recording. *Naunyn Schmiedebergs Arch Pharmacol* 340: 219-222.
- Laurent G** (1999) A systems perspective on early olfactory coding. *Science* 286: 723-728.
- Laurent G, Seymour-Laurent K and Johnson K** (1993) Dendritic excitability and a voltage-gated calcium current in locust nonspiking local interneurons. *J Neurophysiol* 69: 1484-1498.

- Littleton J and Ganetzky B** (2000) Ion channels and synaptic organization: analysis of the *Drosophila* genome. *Neuron* 26: 35-43.
- Loesel R and Homberg U** (1999) Histamine-immunoreactive neurons in the brain of the cockroach *leucophaea maderae*. *Brain Res* 842: 408-418.
- Lu J, Dalton JFT, Stokes DR and Calabrese RL** (1997) Functional role of Ca²⁺ currents in graded and spike-mediated synaptic transmission between leech heart interneurons. *J Neurophysiol* 77: 1779-1794.
- MacLeod K and Laurent G** (1996) Distinct mechanisms for synchronization and temporal patterning of odor-encoding neural assemblies. *Science* 274: 976-979.
- Malun D** (1991a) Inventory and distribution of synapses of identified uniglomerular projection neurons in the antennal lobe of *Periplaneta americana*. *J Comp Neurol* 305: 348-360.
- Malun D** (1991b) Synaptic relationships between GABA-immunoreactive neurons and an identified uniglomerular projection neuron in the antennal lobe of *Periplaneta americana*: a double-labeling electron microscopic study. *Histochemistry* 96: 197-207.
- Malun D, Waldow U, Kraus D and Boeckh J** (1993) Connections between the deutocerebrum and the protocerebrum, and neuroanatomy of several classes of deutocerebral projection neurons in the brain of male *Periplaneta americana*. *J Comp Neurol* 329: 143-162.
- Mercer AR, Kloppenburg P and Hildebrand JG** (2005) Plateau potentials in developing antennal-lobe neurons of the moth, *Manduca sexta*. *J Neurophysiol* 93: 1949-1958.
- Mills J and Pitman R** (1997) Electrical properties of a cockroach motor neuron soma depend on different characteristics of individual Ca components. *J Neurophysiol* 78: 2455-2466.
- Nässel DR** (1999) Histamine in the brain of insects: a review. *Microscopy Research and Technique* 44: 121-136.
- Neher E** (1992) Correction for liquid junction potentials in patch clamp experiments. *Methods Enzymol* 207: 123-131.
- Neher E and Augustine GJ** (1992) Calcium gradients and buffers in bovine chromaffin cells. *J Physiol* 450: 273-301.

- Ng M, Roorda RD, Lima SQ, Zemelman BV, Morcillo P and Miesenbock G** (2002) Transmission of olfactory information between three populations of neurons in the antennal lobe of the fly. *Neuron* 36: 463-474.
- Pearson H, Lees G and Wray D** (1993) Calcium-channel currents in neurons from locust (*Schistocerca gregaria*) thoracic ganglia. *J Experiment Biol* 177: 201-221.
- Pusch M and Neher E** (1988) Rates of diffusional exchange between small cells and a measuring patch pipette. *Pflügers Arch* 411: 204-211.
- Russell DF and Hartline DK** (1982) Slow active potentials and bursting motor patterns in pyloric network of the lobster, *Panulirus interruptus*. *J Neurophysiol* 48: 914-937.
- Saito M and Wu CF** (1991) Expression of ion channels and mutational effects in giant *Drosophila* neurons differentiated from cell division-arrested embryonic neuroblasts. *J Neurosci* 11: 2135-2150.
- Schäfer S, Rosenboom H and Menzel R** (1994) Ionic currents of Kenyon cells from the mushroom body of the honeybee. *J Neurosci* 14: 4600-4612.
- Shang Y, Claridge-Chang A, Sjulson L, Pypaert M and Miesenböck G** (2007) Excitatory local circuits and their implications for olfactory processing in the fly antennal lobe. *Cell* 128: 601-612.
- Spassova M, Eisen MD, Saunders JC and Parsons TD** (2001) Chick cochlear hair cell exocytosis mediated by dihydropyridine-sensitive calcium channels. *J Physiol* 535: 689-696.
- Stopfer M** (2005) Olfactory coding: inhibition reshapes odor responses. *Curr Biol* 15: R996-8.
- Strausfeld NJ and Hildebrand JG** (1999) Olfactory systems: common design, uncommon origins?. *Curr Neurobiol* 9: 634-639.
- Suh GS, Wong AM, Hergarden AC, Wang JW, Simon AF, Benzer S, Axel R and Anderson DJ** (2004) A single population of olfactory sensory neurons mediates an innate avoidance behaviour in *Drosophila*. *Nature* 431: 854-859.
- Sun XJ, Fonta C and Masson C** (1993) Odor quality processing by bee antennal lobe interneurons. *Chemical Senses* 18: 355-377.
- Taylor WR and Morgans C** (1998) Localization and properties of voltage-gated calcium channels in cone photoreceptors of tupaia belangeri. *Vis Neurosci* 15: 541-

- Thomas MV** (1984) Voltage-clamp analysis of a calcium-mediated potassium conductance in cockroach (*Periplaneta americana*) central neurones. *J Physiol* 350: 159-178.
- Triggle D** (2006) L-type calcium channels. *Curr Pharm Des* 12: 443-457.
- Vosshall LB and Stocker RF** (2007) Molecular architecture of smell and taste in *Drosophila*. *Annu Rev Neurosci* 30: 505-533.
- Waldrop B, Christensen TA and Hildebrand JG** (1987) Gaba-mediated synaptic inhibition of projection neurons in the antennal lobes of the sphinx moth, *Manduca sexta*. *J Comp Physiol [A]* 161: 23-32.
- Wang JW, Wong AM, Flores J, Vosshall LB and Axel R** (2003) Two-photon calcium imaging reveals an odor-evoked map of activity in the fly brain. *Cell* 112: 271-282.
- Wicher D and Penzlin H** (1997) Ca²⁺ currents in central insect neurons: electrophysiological and pharmacological properties. *Journal of Neurophysiology* 77: 186-199.
- Wicher D and Penzlin H** (1994) Ca²⁺ currents in cockroach neurones: properties and modulation by neurohormone d. *Neuroreport* 5: 1023-1026.
- Wicher D, Walther C and Wicher C** (2001) Non-synaptic ion channels in insects-- basic properties of currents and their modulation in neurons and skeletal muscles. *Prog Neurobiol* 64: 431-525.
- Wilson RI and Laurent G** (2005) Role of GABAergic inhibition in shaping odor-evoked spatiotemporal patterns in the *Drosophila* antennal lobe. *J Neurosci* 25: 9069-9079.
- Wilson RI and Mainen ZF** (2006) Early events in olfactory processing. *Annu Rev Neurosci* 29: 163-201.
- Wilson RI, Turner GC and Laurent G** (2004) Transformation of olfactory representations in the *Drosophila* antennal lobe. *Science* 303: 366-370.
- Yeh JZ** (1978) Sodium inactivation mechanism modulates qx-314 block of sodium channels in squid axons. *Biophys J* 24: 569-574.
- Zhang B and Harris-Warrick RM** (1995) Calcium-dependent plateau potentials in a crab stomatogastric ganglion motor neuron. I. Calcium current and its modulation

by serotonin. *J Neurophysiol* 74: 1929-1937.

Zhang B, Wootton JF and Harris-Warrick RM (1995) Calcium-dependent plateau potentials in a crab stomatogastric ganglion motor neuron. II. Calcium-activated slow inward current. *J Neurophysiol* 74: 1938-1946.

Zirpel L, Baldwin D, Graubard K (1993) Nickel induces oscillatory behavior and enhanced synaptic and electronic transmission between stomatogastric neurons of *Panulirus interruptus*. *Brain Res* 617: 205-213.

Acknowledgments

Ich danke allen, die mir bei der Durchführung dieser Arbeit behilflich waren, insbesondere:

Prof. Dr. Peter Kloppenburg, für die exzellente Betreuung und Ermöglichung dieser Arbeit. Seiner Unterstützung und Förderung verdanke ich u.a. die Teilnahme an verschiedensten neurowissenschaftlichen Kongressen weltweit, die Teilnahme am Sommer Kurs "Neural Systems and Behavior" am Marine Biological Laboratory in Woods Hole, sowie viele produktive und - ab und an - ausufernde abendliche Sitzungen vor der Kaffemaschine, zu denen nicht immer nur Kaffee getrunken wurde.

PD Dr. Jochen Schmidt, für die Bereitschaft zur Erstellung des Zweitgutachtens. Des weiteren danke ich ihm für die alljährliche wunderbare Zusammenarbeit im neurobiologischen Blutegelkurs.

Helmut Wratil, nicht nur für die perfekte technische Assistenz im Labor, ohne die diese Arbeit nicht möglich gewesen wäre, sondern auch für seine Kollegialität und Freude am Genuss.

Michael Dübbert und Michael Schöngen, für zuverlässige Unterstützung bezüglich Lösung Computer- und messtechnischer Problemstellungen.

Simon Heß, Moritz Pähler und Andreas Pippow, für die exzellente Zusammenarbeit, für viel Geduld und Durchhaltevermögen, sowie für die sorgfältige Durchsicht dieser Arbeit.

Für das sorgfältige Korrekturlesen dieser Arbeit bedanke ich mich besonders bei Heike Demmer, Simon Hess, Nicole Lindemann, Moritz Pähler und Andreas Pippow.

Holger Thiel, für die Einführung in die Patch Technik und eine gute Zeit.

Allen aktiven und ehemaligen Mitgliedern der AG Kloppenburg, für eine stets angenehme Arbeitsatmosphäre, viel Spaß und eine gute Zeit.

Meinen Freunden in Bonn und Köln, die jederzeit das Gästebett für mich bereithielten und damit ein erfolgreiches Abschließen dieser Arbeit unterstützt haben. In diesem Zusammenhang danke ich ebenfalls dem Zoologischen Institut Köln, dass ich jederzeit das 'Gästelabor' nutzen durfte.

Den Dynaminds, für eine gute Zeit und viel Spaß und vor allem einen wichtigen und effektiven Ausgleich zur Arbeit. "*... we ain't nothing but sophisticated slaves ...*"

Meiner Schwester Sandra und Ihrer Familie, Gerd, Annika und Marie.

Meinen Eltern Klara und Wilhelm Husch, dafür, dass Sie immer für mich da waren, an mich geglaubt haben (auch wenn es Grund zum Zweifel gab...), und mich in jeglicher Hinsicht unterstützt haben.

Ganz besonderer Dank gilt meinen Liebsten, Natalie und Katharina. In der kleinen Hoffnung, dass wir irgendwann zurückschauen können und mit einem Glas Rotwein in der Hand sinnierend feststellen können, dass sich die Anstrengungen und Entbehrungen doch gelohnt haben.

Vielen Dank!

Erklärung

Ich versichere, dass ich die von mir vorgelegte Dissertation selbständig angefertigt, die benutzten Quellen und Hilfsmittel vollständig angegeben und die Stellen der Arbeit – einschließlich Tabellen, Karten und Abbildungen –, die anderen Werke im Wortlaut oder dem Sinn nach entnommen sind, in jedem Einzelfall als Entlehnung kenntlich gemacht habe; dass diese Dissertation noch keiner anderen Fakultät oder Universität zur Prüfung vorgelegen hat; dass sie – abgesehen von unten angegebenen Teilpublikationen – noch nicht veröffentlicht worden ist sowie, dass ich eine solche Veröffentlichung vor Abschluss des Promotionsverfahrens nicht vornehmen werde. Die Bestimmungen dieser Promotionsordnung sind mir bekannt. Die von mir vorgelegte Dissertation ist von Prof. Dr. Peter Kloppenburg betreut worden.

Köln, den 16.10.2007

Teilpublikationen

Article

Der erste Teil dieser Promotion ist zur Publikation eingereicht worden:

- **Husch A, Hess S and Kloppenburg P** (2007) Functional Parameters of Voltage Activated Ca²⁺ Currents from Olfactory Interneurons in the Antenal Lobe of *Periplaneta Americana*. (submitted in *Journal of Neurophysiology*)

Poster and Abstracts

Husch A, Paehler M and Kloppenburg P (2007)

Electrophysiological and Morphological Characterization of Spiking and Nonspiking Local Interneurons in the Antennal Lobe of *Periplaneta Americana*. *Proceedings of the 31th Göttingen Neurobiology Conference and the 7th Meeting of the German Neuroscience Society*.

Hess S, Husch A and Kloppenburg P (2007)

Pharmacological Characterization of Voltage-gated Calcium Currents in Olfactory Interneurons of *Periplaneta Americana*. *Proceedings of the 31th Göttingen Neurobiology Conference and the 7th Meeting of the German Neuroscience Society*.

Husch A, Paehler M and Kloppenburg P (2006)

Structural and Functional Properties of Olfactory Interneurons in the Insect Antennal Lobe. *Neurovisionen: Perspektiven in NRW, Düsseldorf, Germany.*

Husch A, Demmer H, Lauinger I, Wratil H and Kloppenburg P (2005)

Voltage-Activated Calcium-Currents in Olfactory Interneurons of Insects Recorded in Vitro and in Situ. *Proceedings of the 30th Göttingen Neurobiology Conference and the 6th Meeting of the German Neuroscience Society.*

Husch A, Pippow A, Wratil H and Kloppenburg P (2004) Calcium Handling in Insect Olfactory Interneurons. *Annual Meeting of the Society for Neuroscience (SfN) Program No. 414.17. Abstract, Washington, DC.*

Husch A, Pippow A and Kloppenburg P (2004) Parameters that Determine Ca²⁺ Dynamics in Insect Olfactory Interneurons. *Program and abstracts, page 108, PO112, International Congress for Neuroethology, Nyborg, Denmark.*

Curriculum vitae

Dipl. Biol. Andreas Husch

CAMPUS ADDRESS:

University of Cologne, Institute for Zoology/Physiology
Molecular and Cellular Neurophysiology
Weyertal 119, 50923 Cologne, Germany
E-mail: andreas.husch@uni-koeln.de;
Phone: +(49)-21-470-5828

Date/ Place of Birth :01/10/76 in Pruem
Citizenship: German

Education

- Jun.-Aug. 2005: Participation at the summer course „Neural Systems & Behavior“ at Marine Biological Laboratory in Woods Hole, USA.
- 2003 - 2007 University of Cologne, Institute for Zoology/Physiology
PhD thesis in zoology in the Lab of Prof. Dr. P. Kloppenburg: “Diversity of Voltage Activated Calcium Currents in Identified Olfactory Interneurons”
- 1998 - 2003 University of Bonn, Institute for Zoology
- 2003 Diploma in biology (equivalent to masters) with majors in zoology, cell biology and physics; thesis: Influence of afferent information on the rhythmogenesis in the stomatogastric ganglion of *Cherax destructor*
- 2000 Pre-degree in biology (equivalent to bachelor)
- 1996 – 1998 Professional training as Emergency Medical Technician (EMT)

Professional Experiences

- 2003 – present University of Cologne, Institute for Zoology/Physiology
- 2000 – 2003 University of Bonn, Institute for Zoology

Honors

- 2005 Boehringer Ingelheim Travel Allowance for participation in the course 'Neural Systems and Behavior' at the Marine Biological Laboratory (Woods Hole, USA).

Lebenslauf

Dipl. Biol. Andreas Husch

CAMPUS ADRESSE:

Universität Köln, Zoologisches Institut
Molecular and Cellular Neurophysiology
Weyertal 119, D-50923 Köln
E-mail: andreas.husch@uni-koeln.de;
Phone: +(49)-21-470-5828

Geburtsdatum/ -ort :01.10.1976 in Prüm
Staatsangehörigkeit: deutsch

Ausbildung

- Jun.-Aug. 2005: Teilnahme am Sommerkurs „Neural Systems & Behavior“ am Marine Biological Laboratory in Woods Hole, USA.
- 2003 - 2007 Universität Köln, Zoologisches Institut / Tierphysiologie
Doktorarbeit im Fach Zoologie im Labor von Prof. Dr. P. Kloppenburg mit dem Thema: „Diversity of Voltage Activated Calcium Currents in Identified Olfactory Interneurons“.
- 1997 - 2003 Universität Bonn, Zoologisches Institut / Neurobiologie
2003 Diplomarbeit im Fach Zoologie im Labor von Prof. Dr. H.-G. Heinzel mit dem Thema: „Untersuchung zum Einfluss afferenter Informationen auf die Rhythmuserzeugung im stomatogastrischen Ganglion von *Cherax destructor albidus*“.
- 2000 Vordiplom in den Hauptfächern Zoologie, Botanik, Zellbiologie, Genetik und in den Nebenfächern Chemie und Physik.
- 1996 – 1997 Zivildienst DRK Eifel-Mosel-Hunsrück RettungsdienstGmbH
- 1987 – 1996 Regio-Gymnasium, Prüm. Erwerb der allgemeinen Hochschulreife (Abitur).

Berufliche Tätigkeiten

- 2005 – 2007 Wissenschaftlicher Mitarbeiter im Labor von Prof. Dr. P. Kloppenburg
- 2003 – 2005 Studentische Hilfskraft im Labor von Prof. Dr. P. Kloppenburg
- 2000 – 2003 Studentische Hilfskraft im Labor von Prof. Dr. H.-G. Heinzel

Köln, den 16.10.2007 _____